CATALYTIC DEPOLYMERIZATION OF CELLULOSE TO NANOCELLULOSE USING HETEROPOLY ACID

SITI KHADIJAH BINTI ZAIN

INSTITUTE OF GRADUATE STUDIES
UNIVERSITY OF MALAYA
KUALA LUMPUR

2015

CATALYTIC DEPOLYMERIZATION OF CELLULOSE TO NANOCELLULOSE USING HETEROPOLY ACID

SITI KHADIJAH BINTI ZAIN

DISSERTATION SUBMITTED IN FULFILMENT OF THE REQUIREMENT FOR THE DEGREE OF MASTER OF PHILOSOPHY

NANOTECHNOLOGY AND CATALYSIS RESEARCH CENTRE
INSTITUTE OF GRADUATE STUDIES
UNIVERSITY OF MALAYA
KUALA LUMPUR

2015

UNIVERSITY OF MALAYA

ORIGINAL LITERARY WORK DECLARATION

Name of Candidate: SITI KHADIJAH BT ZAIN

(I.C/Passport No: 891027025016)

Registration/Matric No: HGA120007

Name of Degree: MASTER OF PHILOSOPHY

Title of Project Paper/Research Report/Dissertation/Thesis ("this Work"):

CATALYTIC DEPOLYMERIZATION OF CELLULOSE TO NANOCELLULOSE USING HETEROPOLY ACID

Field of Study: CHEMISTRY

I do solemnly and sincerely declare that:

(1) I am the sole author/writer of this Work;
(2) This Work is original;
(3) Any use of any work in which copyright exists was done by way of fair dealing and for permitted purposes and any excerpt or extract from, or reference to or reproduction of any copyright work has been disclosed expressly and sufficiently and the title of the Work and its authorship have been acknowledged in this Work;
(4) I do not have any actual knowledge nor do I ought reasonably to know that the making of this work constitutes an infringement of any copyright work;
(5) I hereby assign all and every rights in the copyright to this Work to the University of Malaya ("UM"), who henceforth shall be owner of the copyright in this Work and that any reproduction or use in any form or by any means whatsoever is prohibited without the written consent of UM having been first had and obtained;
(6) I am fully aware that if in the course of making this Work I have infringed any copyright whether intentionally or otherwise, I may be subject to legal action or any other action as may be determined by UM.

Candidate's Signature Date: 3 th September 2015

Siti

Subscribed and solemnly declared before,

Witness's Signature Date: 3 th September 2015

Name: DR. SHARIFAH BEE ABD HAMID

Designation: PROFESSOR

ABSTRACT

Heteropoly acid (HPA) and its acidic salts have been widely applied as catalysts for various types of chemical reactions. The substitution process involving proton with larger monovalent alkaline cation (cesium) within the Keggin structure has tremendously affected the microstructure of heteropoly compounds. Generally, higher content of cesium (Cs), posses higher surface area and porosity. Nevertheless, low cesium content of heteropoly compound was selected for better hydrolysis environment in depolymerization of cellulose. This is because, none or low cesium content of Heteropoly compound can generate high concentration of hydronium ions when dissolved in water. That characteristic has increased the possibility of proton to hydrolyze the β- linkages of cellulose polymer chain. Heteropoly acid and its acidic salts were screened for their performance towards depolymerization of cellulose to nanocrystalline cellulose (NCC) with the assistance of powerful ultrasonication. Ultrasonication treatment introduced has enhanced the depolymerization of cellulose through defibrillation of cellulose polymer chain, which eases the function of HPA catalyst. Ionizable proton generates from HPA can easily penetrate the amorphous region of cellulose thus release the crystalline domain. The generated NCC were analyzed by Fourier Transform Infrared (FTIR), X-ray Diffraction (XRD) , Raman spectroscopy, Dynamic Light Scattering (DLS), Zeta potential, Surface Tension, Thermogravimetric analysis (TGA), Scanning Electron Microscope (SEM), Transmission Electron Microscope (TEM), and Atomic Force Microscopy (AFM). The results from the material characterization revealed that when HPA was applied as a catalyst, the treatment time was reduced by 5 minutes and the crystallinity index (CrI) calculated through XRD analysis was 88.0 %, similarly when the reaction was carried out at 15 minutes in the absence of HPA catalyst. Furthermore, the smallest particle

sizes obtained was 37.84 nm and 43.82 nm with the presence and absence of HPA respectively. However, TEM images of NCC showed some agglomeration and accumulation of cellulose particles thus indicating that the particles are highly attracted to each other due to surface hydrophilicity. From the TEM images, the diameter measured was at range of 10-30 nm. Therefore, this study shows that the choices of appropriate hydrolysis condition in producing NCC are very crucial and important. For that reason, the best reaction condition for obtaining NCC were discovered at 225 W (ultrasonication) for 10 minutes with the presence of 4 g of Tungstophosphoric acid (TPA) catalyst. Therefore, it shows that HPA is one of the best alternatives in replacing classical sulfuric acid in hydrolysis of cellulose to nanocrystalline cellulose (NCC).

ABSTRAK

Asid heteropoli (HPA) dan garam keasidannya telah banyak diaplikasikan sebagai pemangkin dalam pelbagai jenis tindak balas kimia. Proses penukargantian yang melibatkan ion proton dan ion alkali monovalent yang lebih besar di dalam struktur Keggin telah menyebabkan perubahan yang drastik terhadap struktur mikro sebatian heteropoli tersebut. Semakin tinggi kandungan sesium, semakin tinggi luas permukaan dan keliangannya. Walaubagaimanapun, kandungan sesium yang rendah di dalam kompoun heteropoli adalah yang terbaik untuk keadaan proses hidrolisis di dalam penyahpolimeran sellulosa. Ini kerana, tiada atau kandungan sesium yang rendah di dalam sebatian heteropoli boleh menghasilkan kepekatan ion hidrogen yang tinggi apabila larut di dalam air. Hal yang berikut adalah sangat penting dalam memastikan keberangkalian ikatan β di dalam rantai polimer selulosa dihidrolisiskan. Prestasi penggunanan asid heteropoli dan garam asidnya dalam memangkinkan penyahpolimeran sellulosa dengan menggunakan bantuan ultrasonikasi yang kuat telah dipantau. Tindakan ultrasonikasi digunakan adalah untuk membantu menigkatkan proses penyahpolimeran melalui proses penyahdefibrilasi rantai polymer sellulosa telah memudahkan lagi tindakan pemangkin asid heteropoli. Proton yang terhasil daripada asid heteropoli dapat menembusi kawasan amorpos selulosa dengan mudah lalu membebaskan kawasan kristal selulosa. Nanoselulosa (NCC) yang dihasilkan telah dianalisa dengan mengunakan pengubah fourier inframerah (FTIR), pembelaun X-ray (XRD), spektroskopi raman, penyerakan cahaya dinamik (DLS), Zeta potential, ketegangan permukaan, Termogravimetrik analysis (TGA), mikroskop electron pengimbas (SEM), mikroskop electron penghantar (TEM), dan Atomic Force Microscopy (AFM). Hasil dari pencirian bahan tersebut, ia telah menunjukkan bahawa asid heteropoli yang telah digunakan sebagai pemangkin telah berjaya memendekkan masa tindakbalas kepada 5 minit dan index kekristilan yang dikira ialah 88.0 % dengan

menggunakan XRD analisa, keputusan yang sama telah dikecapi apabila tindakbalas tersebut dijalankan dengan lebih lama iaitu 15 minit. Tambahan pula, saiz zarah yang terkecil yang didapati ialah 37.84 nm apabila menggunakan asid heteropoli dan 43.82 nm apabila tiada asid heteropoli digunakan. Oleh yang demikian, imej TEM NCC telah menampilkan berlakunya pengumpalan dan pengumpulan zarah–zarah selulosa yang menunjukkan berlakunya tarikan yang kuat antara zarah–zarah berikutan daripada pemukaan selulosa yang hidrofilik. Diameter yang diukur daripada imej TEM berada di dalam julat 10-30 nm. Oleh sebab itu, kajian ini telah menunjukkan bahawa dalam proses penghasilan NCC, pemilihan keadaan yang sesuai adalah amat penting. Oleh yang demikian, keadaan tindak balas yang terbaik untk menghasilkan NCC (SN16) ialah pada 225 W (ultrasonikasi) selama 10 minit dengan menggunakan 4 g pemangkin asid tungstophosphorik (TPA). Hal itu telah menunjukkan bahawa heteropoli asid adalah merupakan calon yang terbaik di dalam mengantikan asid sulfurik dalam proses hidrolisis selulosa ke nanokristal selulosa (NCC).

ACKNOWLEDGEMENT

First of all I would like to acknowledge gratefully to my supervisor, Prof. Dr. Sharifah Bee Abd Hamid for giving me an opportunity to continue my studies in Master Degree and also for her excellent guidance and invaluable suggestion throughout my research work. I have benefited myself with her high standard of accomplishments and her open-minded approach to new ideas. This has inspired me to strive for a high quality research.

Moreover, I would also like to express my heartfelt appreciation to the members of Nanotechnology and Catalysis Research Centre (NANOCAT) especially Durga Devi for giving me support and guidance in having a great value in this study.

Last but not least, I would like to express my deepest gratitude to my mother, Rasul Abd Hamid, my father, Zain Mahmud, my brothers, Yusran Zain, Yusrizal Zain and Muhammad Khairuddin Zain for sacrificing a lot and giving me mental and physical support to further and finish my studies. Not to forget my best friends Muhammad Hadi Afnan Abd Razak, Ainaa' Syahirah Abd Hamid, Nadia Husna, and Khairul Fithriyati Khalid that always be by my side when I faced difficulties along my research work.

SITI KHADIJAH ZAIN

TABLE OF CONTENTS **Page** **Page**

CHAPTER 3: METHODOLOGY

LIST OF FIGURES

LIST OF TABLES

LIST OF ABBREVIATIONS AND SYMBOLS

% (w/v)	Wight /Volume Percent
% (w/w)	Weight / Weight Percent
° C	Degree Celsius
θ	Theta
3D	3 - Dimensional
Å	Armstrong
AFM	Atomic Force Microscope
BET	Brunauer – Emmet - Teller
BJH	Barrett, Joyner and Halenda
C_3H_7OH	Propanol
CNs	Cellulose Nanocrystals
CPO	Crude Palm Oil
CrI	Crystallinity Index
Cs: H	Ratio of Cs: H atom in Keggin structure
CS01	$H_3PW_{12}O_{40}$
CS02	$Cs_1H_2PW_{12}O_{40}$
CS03	$Cs_2H_1PW_{12}O_{40}$
CS04	$Cs_{2.5}H_{0.5}PW_{12}O_{40}$
CS05	$Cs_{2.8}H_{0.2}PW_{12}O_{40}$
CS06	$Cs_3PW_{12}O_{40}$
Cs_2CO_3	Cesium Carbonate
Cs-TPA	Cesium Salt of Tungstophosphoric Acid
$Cs_xH_{3-x}PW_{12}O_{40}$	Acidic Cesium Salt of Tungstophosphoric Acid
D	Diameter
DFT	Density Functional Theory
DP	Degree of Polymerization

EDX	Energy Dispersive X-ray
EFB	Empty Fruit Bunches
FTIR	Fourier Transform Infrared
GNI	Gross National Income
H_2SO_4,	Sulfuric Acid
$H_3PMo_{12}O_{40}$	12 –Molybdophosphoric
$H_3PW_{12}O_{40}$	12-Tungstophosphoric Acid
$H_4SiW_{12}O_{40}$	12- Tungstosilisic acid
HCl	Hydrochloric Acid
HNO_3	Nitric Acid
HPA	Heteropoly Acid
hrs	Hours
Hz	Hertz
I_{002}	Intensity at plane 002
I_{am}	Intensity at amorphous region
IUPAC	International Union of Pure and Applied Chemistry
JCPDS	Joint Committee on Powder Diffraction Standards
K	Kelvin
KBr	Potassium Bromide
kHz	Kilo Hertz
kV	Kilovolt
L	Length
L/D	Aspect Ratio
M	Molarity
m	Meter
mA	miliampere
mbars	Milibars
MCC	Microcrystalline Cellulose

min	Minutes
mN	Milinewton
Mo	Molybdenum
MPOB	Malaysia Palm Oil Board
N_2	Nitrogen Gas
NCC	Nanocrystalline Cellulose
NFC	Nanofibrilated Cellulose
nm	Nanometer
O_2	Oxygen Gas
OPF	Oil Palm Fronds
OPT	Oil Palm Trunk
P	Phosphorus
p/p_o	Relative pressure
Pa	Pascal
POMs	Polyoxometalates
PTMG	Polyoxytetramethylene Glycol
rpm	Revolutions Per Minute
SEM	Scanning Electron Microscope
SN01	Nanocellulose at 50 W, 10 min, with absence of catalyst
SN02	Nanocellulose at 100 W, 10 min, with absence of catalyst
SN03	Nanocellulose at 113 W, 10 min, with absence of catalyst
SN04	Nanocellulose at 140 W, 10 min, with absence of catalyst
SN05	Nanocellulose at 225 W, 10 min, with absence of catalyst
SN06	Nanocellulose at 240 W, 10 min, with absence of catalyst
SN07	Nanocellulose at 300 W, 10 min, with absence of catalyst
SN08	Nanocellulose at 225W, 1 min, with absence of catalyst
SN09	Nanocellulose at 225 W, 1.5 min, with absence of catalyst
SN10	Nanocellulose at 225 W, 2.5 min, with absence of catalyst

SN11	Nanocellulose at 225 W, 3.5 min, with absence of catalyst
SN12	Nanocellulose at 225 W, 5 min, with absence of catalyst
SN13	Nanocellulose at 225 W, 10 min, with absence of catalyst
SN14	Nanocellulose at 225 W, 15 min, with absence of catalyst
SN15	Nanocellulose at 225 W, 10min, with 2g of $H_3PW_{12}O_{40}$
SN16	Nanocellulose at 225 W, 10min, with 4g of $H_3PW_{12}O_{40}$
SN17	Nanocellulose at 225 W, 10min, with 6g of $H_3PW_{12}O_{40}$
SN18	Nanocellulose at 225 W, 10min, with 4g of $Cs_1H_2PW_{12}O_{40}$
SN19	Nanocellulose at 225 W, 10min, with 4g of $Cs_{2.5}H_{0.5}PW_{12}O_{40}$
SN20	Nanocellulose at 225 W, 10min, with 4g of $Cs_3PW_{12}O_{40}$
TEM	Transmission Electron Microscope
TGA-MS	Thermogravimetric Analysis – Mass Spectrometer
THF	Tetrahydrofuran
TPA	12-Tungstophosphoric Acid
UTP	Universal Temperature Programme
V	Vanadium
W	Watts
wt %	Weight percent
XRD	X-ray Diffraction

INTRODUCTION

1.1 Malaysian Palm Oil Industry

High technology development across Malaysia has transformed this country into a well-planned and strategic place for an oil palm industry. Export demand and production of Crude Palm Oil (CPO) increase throughout the year, which displayed an uptrend on the average price of CPO from RM 2221.00 in January 2013 to RM 2574.50 in December 2013. Based on Table 1.1, oil palm planted area has expanded 3.0 % from the previous year and this is mainly due to the opening of new plantations in Sarawak which recorded an increase of 7.9 %. Nevertheless, Sabah is still the largest contribution state on oil palm planted area with 28 % among other states in Malaysia followed by Sarawak with 22 % while all the states in Peninsular Malaysia accounted for 50 %.

Table 1.1: Summary on Palm Oil plantation area in Malaysia for 2012 and 2013 [Malaysian Palm Oil Board 2013)]

Planted Area (Hectares)	2012	2013	Difference (%)
Malaysia	5,076,929	5,229,739	3.0
Peninsular Malaysia	2,558,103	2,593,733	1.4
Sabah	1,442,588	1,475,108	2.3
Sarawak	1,076,238	1,160,898	7.9

Consequently, the local palm oil industry has offered exciting opportunities in biomass production. Palm oil industry has contributed to RM 50 billion to Malaysia's Gross National Income (GNI) while biomass market was projected to throw in RM 30 billion to GNI. The exploitation of biomass is on the generation of renewable energy on bio-ethanol production and manufacturing of value –added eco- products (bio-fertilizer, bio-pellet, bio-plastic and bio-composites). Capitalization of these opportunities however

will not only benefit companies that investing in this sector, but also Malaysian economy.

1.2 Oil Palm Biomass

Oil palm tree (*Elaeis guineesis*) has been introduced to Malaysia in 1870 as an ornamental plant and grows well under our tropical climate. Since palm tree can produce oil from its mesocarp and kernel, the accomplishment of Malaysia as the second world's top producer of palm oil has grown tremendously over the last 25 years which transformed palm oil industry into the most important agriculture –based industry in our country. The success of the Malaysia's oil palm industry with 5.23 million hectares oil palm tree planted area in 2013 however, has created large amounts of waste generated from empty fruit bunches (from the mills), oil palm fronds (during harvesting) and oil palm trunks (during replanting). In addition, oil palm tree is a multipurpose plant that generates oil (main) and biomass as a feed for many value – added industries. The biomass produced are extensively been exploited in the production of chemical, energy, and functionalized material. The estimated availability of oil palm biomass in 2009 can be illustrated in Figure 1.1 (Astimar et al., 2011).

The chemical and physical properties of palm tree biomass are differed based on their origin and species. However, the major constituent of the biomass are relatively composed-of cellulose, hemicellulose, lignin and ash. The composition of the major constituent was tabulated in Table 1.2 according to the main component of the oil palm tree.

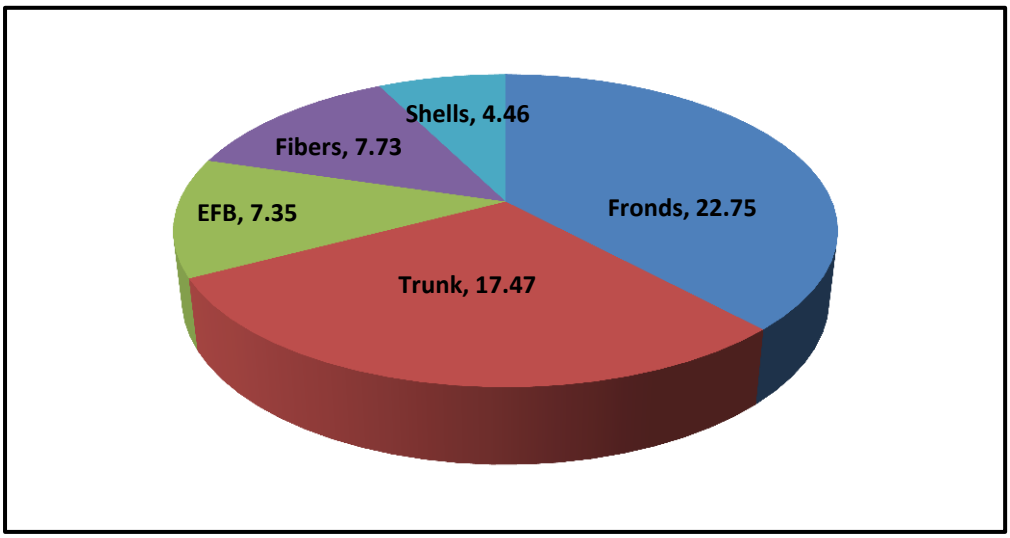

Figure 1.1: Types of oil palm biomass generated in 2009 in million tones.

Table 1.2: Proximate analysis of oil palm biomass (Astimar et al., 2011)

Components	Oil Palm Trunk (OPT)	Oil Palm Fronds (OPF)	Empty Fruit Bunches (EFB)
Lignin	18.1	18.3	21.2
Hemicellulose	25.3	33.9	24.0
α-celulose	45.9	46.6	41.0
Holocellulose	76.3	80.5	65.5
Ash	1.1	2.5	3.5
Alcohol benzene solubility	1.8	5.0	4.2

1.2.1 Cellulose

Cellulose is a natural occurring biopolymer which is biodegradable, renewable as well as non –toxic, plus it is the most ubiquitous and abundant organic compound that can be obtained from plants and microorganism. Cellulose carbohydrate polymer is a linear homopolymer of polysaccharides that consist of D- glucose united together through β-1,

4- glycosidic bond and commonly known as 1, 4, β- glucopyranoside (Klemm, Schmauder, & Heinze, 2005; Mohamad Haafiz, Eichhorn, Hassan, & Jawaid, 2013). Cellulose can be found in the lignocellulosic material that originated from agriculture waste, water plants, grasses and other plant – based substances. In lignocellulosic material, cellulose is interlinked together with hemicellulose and lignin through chemical, covalent, and hydrogen bonds (Harmsen, Huihgen, Bermudes Lopez & Bakker, 2009). Coalescences of several cellulose polymer chains lead to the formation of microfibrils which integrated to form macrofibril (fibers). Nevertheless, three free hydroxyl groups of the glucose monomer shown in Figure 1.2 create a great tendency in the formation of hydrogen bonds which is essential in giving the crystalline packing which also governs the physical properties of cellulose. The presence of intra and intermolecular hydrogen bonding within the cellulose polymer chain has structured cellulose molecule into supramolecular semi- crystalline structure with high degree of polymerization (DP) that makes cellulose molecule insoluble in water and dilute acid (Wertz, Bédué, & Mercier, 2010).

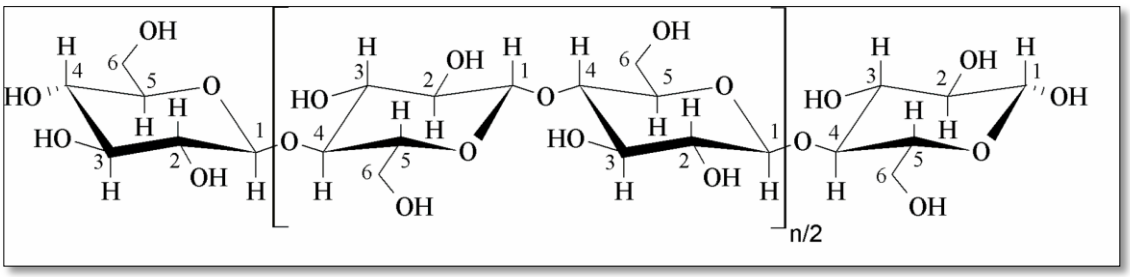

Figure 1.2: Chemical structure of cellulose unit.

1.2.2 Hemicellulose

Hemicellulose is a biopolymer-type polysaccharide that possesses 5 and 6 carbon rings. It can be classified by the classical backbones comprised of xylans, mannans, xyloglucans, and mixed linkages of β- glucans. Composition and structure of hemicellulose are widely affected based on their species. Xylan is the most ordinary

hemicellulose with homopolymer backbone of xylose linked together through β-1, 4-glycosidic bonds, Figure 1.3 shows the example structure of hemicellulose. It is insoluble in water and commonly found in hardwood (Habibi & Lucia, 2012). However, mannans- type of hemicellulose contains more branches which help its solubilization especially in alkaline solution (Fengel & Dietrich, 2011; Scheller & Ulvskov, 2010).

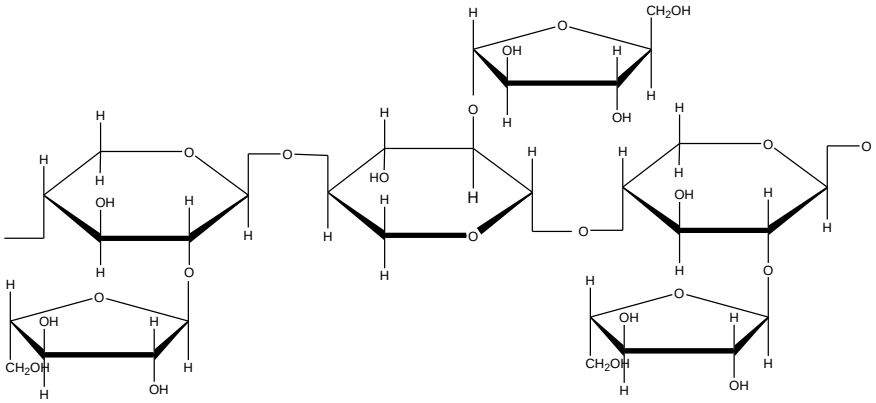

Figure 1.3: Chemical structure of hemicellulose (arbinoxylan).

1.2.3 Lignin

Lignin is an amorphous phenolic polymeric material that is highly abundant after cellulose. It acts as a natural binder within lignocellulosic material that provides rigidity to the plant. The percentage of lignin varies depending on different types of plant. Chemically, lignin comprised of phenyl propane units as the predominant building blocks. Based on Figure 1.4, through the process of oxidative coupling via free radical generation *p*-coumaryl alcohol, coniferyl alcohol and sinapyl alcohol are formed as the building block of lignin. Those structures play an important role in recalcitrant lignocellulose where it creates a remarkable resistance to compression, bending and impact (Ghaffar & Fan, 2014; Kubicek & Christian, 2012).

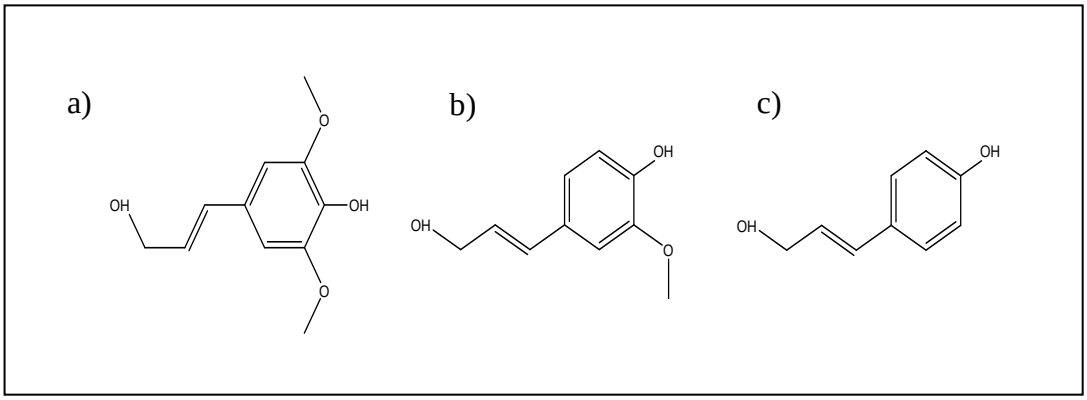

Figure 1.4: Dominant building block of lignin: a) sinapyl alcohol, b) coniferyl alcohol and c) *p-coumaryl* alcohol.

1.3 Application of Oil Palm Biomass

Palm tree biomass has contributed a lot to our country through its diverse usage in different industrial sectors. The common applications of biomass have been tabulated in Table 1.3. In this few decades, the attention of researcher has been directed to obtain nanocellulose through biomass utilization. The phenomenon is driven by the cheap raw material that can be easily obtained throughout the year especially in hot and wet climate country like Malaysia.

Table 1.3: Application of Palm Tree Biomass at different sectors of industry/product.

Industry/Product	**Application /Usage**
Wood based industries	1) Plywood and veneer 2) Particleboard 3) Pulp and paper
Agriculture	1) Compost and vermin-compost
Composite	1) Automotive plastic bio-composite 2) Automotive plastic sound dampering bio-composite 3) Medium density fiberboard
Green Chemicals	1) Cellulose /Microcrystalline cellulose 2) Lignin

1.4 Nanocellulose – A new class of nanomaterial

Nanocellulose is usually referred as cellulosic material having a dimension in nano-scale range, and precisely the range should be between 1 to 100 nm. Usually known as cellulose nanostructure, but other common name that is synonym to nanocellulose is Nanocrystalline Cellulose (NCC) and Nanofibrilated Cellulose (NFC). It can be produced from different sources of lignocellulosic material. Besides, different approaches applied to the cellulosic material will result in different structure of nanocellulose. For an example, NCC is being synthesized using acid hydrolysis (Eichhorn, 2011) while NFC can be prepared through mechanical treatment (Abdul Khalil et al., 2014).

Notably, cellulose is insoluble in water and most of the organic solvent, due to its hydrophobicity, the application of cellulose is limited compared to nano- scale cellulose. Thus, the hydrophobicity of cellulose can be encountered by transforming it into nanoscale dimension which broaden its physical properties spectrum. Scientifically, nanofibers cellulose shows greater hydrophilicity with excellent compatibility with different type of material (Siró & Plackett, 2010) which can be clearly illustrated through bio-composite application. Furthermore, its high aspect ratio, high mechanical performance and biodegradability create great possibilities in the application of smart and green material thus explained significantly why nano-size cellulose is favorable and expanding material of interest (Gardner, Oporto, Mills, & Samir, 2008). Isolation and application of nanocellulose has been rapidly expanding in different way for supporting scientific, industrial communities, economic and environmental motivations. Nanocellulose is very useful in making ultra- light material for an example film. Microfibrils are being applied to reinforce biopolymers like polylactic acid and starch type polymer for packaging materials that can be easily degraded.

Nano-scale cellulose serves a good toughness and strength to traditional paper products even in small quantities (Berglund, 2005; Nakagaito & Yano, 2004). Some of the other potential applications are (Koskinen 2011):

1) Paper and paperboard applications
2) Nano-biocomposites
3) Food applications
4) Cosmetics and creams
5) Medical and bio-medical applications
6) Absorbent application
7) Advance building product
8) Optical film.

1.5 Issues in nanocellulose production

A notable feature of nanocellulose has subsequently increased the demands of sustainable product in nanomaterial's industry. The demand continues to grow as the consumer, government and non –government organization are seeking for smart material that can balance the economic growth with the need to address environmental and social concerns. The driving force has led to several developments with (1) existence of pilot plant facilities in Northern European, Canada and Unites States; (2) nanocellulose precious physical properties and; (3) ease to functionalize which serving better and broader physical properties. Furthermore, the focused on the cellulosic material has broadened into agriculture wastes compared to only woody based and generally the production of that material is prepared by acid hydrolysis of microcrystalline cellulose.

Additionally, strong efforts have been exploited in order to introduce the standard method in developing test method for characterizing the nanocellulose. A lot of

researchers are using Transmission Electron Microscope (TEM) and Atomic Force Microscope (AFM) in order to characterize nanocellulose dimensions. However these techniques are expensive thus other alternatives that are more economical are highly recommended.

Classically, the acid hydrolysis process was being accompanied by concentrated sulfuric acid and other mineral acids. Non- environmental friendly, corrosiveness, and uncontrolled hydrolysis process displayed through sulfuric acid hydrolysis has increased the needs of replacing those acids with other suitable chemicals. Acid hydrolysis approaches produced NCC with low degree of amorphosity. Sometimes, due to excessive hydrolysis activity (over depolymerization), instead of having nano-scaled cellulose with high degree of crystallinity, glucose (monomer) will also be obtained as the final product. This has caused the yield of NCC to be affected. Application of mechanical treatment such as high pressure homogenization, grinder, cryocrushing, electrospining and high intensity ultrasonication produced NFC that is highly entangled with small size of diameter. It is understandable that those mechanical treatments are energy intensive treatment that required a lot of energy, thus make it less environmentally friendly. The combination treatment between chemical and mechanical treatment become less practical in improving the quantity of NCC, when the chemical used during the process is also too harsh thus led to lower yield.

The burden of those issues can be minimized by introducing a suitable acid catalyst that can help in producing good quality of NCC with higher yield. Solid acid catalyst that is widely used in petrochemical industries is chosen as a suitable candidate in replacing the conventional method. Keggin – type of heteropoly acid that is highly acidic is a suitable alternative in catalyzing cellulose depolymerization. In this work Keggin heteropoly acid was being chosen because of its acidity, ease of separation and reproducibility. The bulk structure of Keggin anion will also create the same effect as

sulphate group in sulfuric acid hydrolysis. High intensity ultrasonication will also be useful in that process together with the solid acid catalyst. The ultrasonication activity will not require an extremely high energy, as the power intended to use is low and not very long. The ultrasonication energy subjected to the cellulose fiber is useful, as it will act as a pre-treatment to the cellulose fiber prior to catalytic activity. The ultrasonication may help the cellulose fiber to expose more area or spaces for the catalytic reaction to take places. The synergy effect between the two main elements will be useful in producing high quality nanocellulose with higher yield.

1.6 Objectives

This research will be focusing more in producing NCC or cellulose nanocrystals (CNs) from microcrystalline cellulose (MCC) as a model compound. The strategy was constructed in order to study the correct or ideal reaction condition for producing NCC with the help of ultrasonication and HPA catalyst. Therefore, two main goals for these studies are:

1. To design and synthesis HPA catalyst with optimal acidity and phase.
2. To synergize interplant of sonication and catalyst for the synthesis of NCC, with different conditions and to evaluate the yield and the quality of NCC produced.

LITERATURE REVIEW

2.1 Catalyst and Catalysis: Overview

Catalysis is a multidisciplinary science that serves broader range of application especially in chemical industries. It is been defined as a chemical reaction that being catalyzed by a catalyst. The evolution of catalyst occurs on the earliest commercial processes through Haber process for the synthesis of ammonia. Catalyst is a compound that accelerates the rate of reaction without being itself being consumed or changed at the end of the reaction. It speeds up the reaction rate by lowering the activation energy. It provides an alternative pathway that reduces the free energy of activation. A catalyst can be anything including atom, compound or enzymes, but the fundamental is that it needs to possess electron dynamic otherwise it is just an ordinary material. Plus, an ideals catalyst has to meet a characteristic of active, selective, and stable to the reaction.

On top of that, industrial application defines an ideal catalyst as a material that is active, regenerable, reproducible, thermal and mechanically stable, and economical. A good catalyst allows the reactant to be absorbed temporarily on its surface and desorbed as the products formed. In addition, its high surface area also increases the reactant binding availability thus increase the productivity of the product. Moreover, catalyst support such as alumina and silica have been shown to increase the dispersion of the active components thus enhances the surface area of a catalyst (Chorkendorff & Niemantsverdriet, 2005).

2.2 Heteropoly compound

Polyoxometalates (POMs) are built up through incorporating of anion which having oxygen cluster as the basic structural units. Unique chemical and physical properties of POMs have attracted a lot of attention for variety of applications, predominantly in petrochemical (Tsukuda, Sato, Takahashi, & Sodesawa, 2007), medicine (Rafiee, Joshaghani, Tork, Fakhri, & Eavani, 2008), composite (Amirinejad,Madaeni,Rafiee, & Amirinejad, 2011), and catalysis (Morin et al., 2007). There are two common families of POMs:

i) Isopoly compounds (posses d^0 metal cation and oxide)

ii) Heteropoly compounds (contain one or more p-,d- or f- block and oxide)

Due to plenty choices of heteropolyanions, the structure and the chemical properties of heteropoly compound can be easily altered synthetically compared to isopoly compounds. Therefore, this compound is predicted to be the best preferences in acid catalysis (Kozhevnikov, 2002).

2.2.1 Structure of Heteropoly compound (Heteropolyacid)

Heteropolyacids (HPAs) are Bronsted acid with complex proton structure through assimilation of heteropoly anion that possess large group of complex oxygen (octahedral) as the basic units. General formula for heteropoly anion is $[X_xM_mO_y]^{a-}$, where:

i) M (addenda atom) - Tungsten (W), Molybdenum (Mo) or Vanadium (V)

ii) O - Oxygen

iii) X (heteroatom) - p–block element such as Silicon (Si), Phosphorus (P) or Arsenic (As)

Among many possibilities based on variety of elements that can be present in constructing the heteropoly anion, 4 different groups based on their molecular architectures can be created; a) Keggin b) Dawson c) Anderson d) Waugh and Silverton (Kozhevnikov, 2002; Timofeeva, 2003).

However, within the heteropoly anion structure, Keggin structure is the most preferable compound that has been intensively studied due to its relative superior activity. Other positive characteristics of Keggin structure include oxidation potential, thermal and hydrolytic. The acidity strength is higher than both mineral and Lewis acids. HPA are easy to handle, non - explosive and non - volatile. $H_3PW_{12}O_{40}$ is an example of Keggin Heteropolyacid that has been shown to be an effective catalyst for different kinds of acid catalyzed reaction. HPAs with Keggin structure are more thermally stable and capable of dehydration at 150 – 200 ° C compared to other HPAs structure.

Scientifically, HPA and its salts comprised of heteropolyanions and countercation, crystallized water and other molecules. Three dimensional (3D) of HPA is known as secondary structure. Six water molecules per Keggin unit is the most stable HPA. Those molecules are placed in body-centered cubic crystal structure through incorporation of water molecules through $H_5O_2^+$ bridges.

2.2.2 Properties of Keggin type –Heteropoly acid

HPAs are scientifically known as Bronsted acid, the acid strength can be measured using Hammett indicator. Through the Hammett indicator test, the value of Hammett acidity function, H_0 for $H_3PW_{12}O_{40}$ found to be less than -8.2 and it has been classified as superacid. Superacid is an acid with Hammett acidity value < -12. Acid strength for HPAs determined not only by the acid dissociation constant but also the salt effects (I. V. Kozhevnikov, 1995). Therefore, Keggin type HPAs that possess bulk structure of heteropoly anion help the stabilization of intermediate formed. The best technique to measure the acid strength of HPAs is by Microcalorimetry of ammonia sorption

(Bardin, Bordawekar, Neurock, & Davis, 1998) since the acidity of HPAs are not only accountable on the surface but also in the bulk structure.

The reaction catalyzed by HPA is through protonation mechanism. Due to low lattice energy, HPAs molecules are readily soluble in water and oxygen containing solvent. In aqueous medium, HPAs are fully dissociates and they are stronger than usual mineral acids such as H_2SO_4, HNO_3 and HCl with non-corrosive behavior. Homogeneous acid catalyzed reaction by HPAs follows the same mechansm like common mineral acid since it is soluble in aqueous media, but in contrast to mineral acid, HPAs have the ability in protonating the intermediate substrate thus enhances it to subsequent reaction. The softness of the heteropolyanions plays an important role in stabilizing the intermediate products (Kozhevnikov, 1998).

In addition, HPA can catalyze chemical reaction in biphasic system. This system is essential owing to the separation of product and catalyst that has become very effective thus eases the chemical processes. Biphasic system was applied through the fundamental of chemical polarity. HPA that act as a catalyst dissolve well in polar solvent, and the catalysis reaction proceed in that particular phase. During the reaction, the non –polar product formed through the reaction will predominantly move to a less – polar region thus form two distinct layers. That phenomenon can be clearly illustrated through polymerization of Tetrahydrofuran (THF). The process starts when the ratio between water and HPA is less than 10. The catalysis occurred in HPA phase, the polyoxytetramethylene glycol (PTMG) formed transferred into THF phase that is non – polar.

$$_{n}\mathbf{THF} + \mathbf{H_2O} \rightarrow \mathbf{HO[(CH_{2)4O}]_{\mathit{n}}H} \qquad \mathbf{(2.1)}$$

2.2.3 Catalysis Application of Heteropoly Compound

Heteropoly acid and its salts have created a new revolution in catalysis industrial processes. The first reaction catalyzed by HPA is for the production of propanol (C_3H_7OH) through hydration of propene. Heteropoly compound acts as acid or oxidation catalyst in homogeneous or heterogeneous system. The chemical properties employed by heteropoly compound have allowed it to be extensively applied in several large scale processes (Izumi, 1997; Misono & Nojiri, 1990). However, the polymerization of Tetrahydrofuran (THF) in liquid/liquid biphasic system was conducted in laboratory scale. This section will discuss several chemical reactions catalyzed by heteropoly compound.

2.2.3.1 Hydration of Olefins

Heteropoly acids play a vital role as an active catalyst for the production of alcohol via hydration of alkenes. The alcohol production followed a Markonikov's Rule that yield secondary or tertiary alcohol. Plus, common olefins used for the hydration process are propene and isobutene. With the assistance of 12- Tungstosilisic acid ($H_4SiW_{12}O_{40}$) as a catalyst, propene conversion achieves 60 -70 % with 99 % selectivity of isopropanol. In addition, the conversion of isobutene almost achieved 100 % with only 0.1 % n- butane conversion. The 12 –Molybdophosphoric acid ($H_3PMo_{12}O_{40}$) that was used for the reaction is very specific with long lifetime. Heteropoly acid used in catalysis possesses has more advantages over conventional mineral acids through low corrosion activity, high selectivity and high catalytic activity (I. Kozhevnikov, 2002; I. V. Kozhevnikov, 1995, 1998).

2.2.3.2 Selective Oxidation

Production of methacrylic acid from methacrolein was accomplished by introducing molybdenum (Mo), vanadium (V) and phosphorus (P) based heteropoly compound. Its application is for the manufacturing of crystal clear plastic Plexiglas®. Methacrylic acid from the process succeeds with 70 – 90 % methacrolein conversion with 80 – 85 % selectivity to methacrylic acid. Oxidation of methacrolein requires a bi-functional catalyst that can serve as both acid - base and redox catalysis properties (Bruckman, Haber, Lalik, & Serwicka, 1988; Serwicka, Bruckman, Haber, Paukshtis, & Yurchenko, 1991).

Acetic acid production is commonly manufactured through Monsanto process with methanol and carbon monoxide blending (Weissermel & Arpe, 2008). However, it can also be produced industrially through direct reaction from ethylene with two main reaction mechanisms using Pd–H_3PO_4/SiO_4 and Pd-Au-H_2SO_4/active carbon. In contrast, combination of palladium and $H_4SiW_{12}O_{40}$ shows better performance with single one – stage process by direct oxidation of ethylene with O_2 (Sano, Uchida, & Wakabayashi, 1999).

2.2.4 Heteropoly compound in cellulose depolymerization

It has already known that the hydrolysis of cellulose is less easy because of the poor contact of catalyst and cellulose. Therefore, the hydrolysis reactions required appropriate reaction condition to achieve maximum conversion.

The potential of heteropoly acid and its salts have been extensively applied to catalyze the hydrolysis of cellulose under certain condition. Since heteropoly acid is a Bronsted acid, the protonic sites serve as an excellent active site for depolymerization of cellulose. In (Juan Tian et al., 2010) , $H_3PW_{12}O_{40}$ was used to catalyze the hydrolysis of

cellulose to glucose. The study has achieved a remarkable high yield of glucose up to 50.5 %.

The substitution of acidic proton with larger alkaline Cs^+ has led to hydrophobicity of $Cs_xH_{3-x}PW_{12}O_{40}$ which displays easier catalyst separation. The catalyst was used to hydrolyze microcrystalline cellulose to reducing sugar and glucose. The highest yield was obtained with 27 % over $Cs_1H_2PW_{12}O_{40}$ catalyst compared to $Cs_{2.2}H_{0.8}PW_{12}O_{40}$ (J. Tian, Fang, Cheng, & Wang, 2011).

Cellulose depolymerization using heteropoly acid for the production of nanocellulose was rarely studied due its poor contact area. However, (Liu et al., 2014) managed to obtain the nanocellulose with the diameter of 15 – 40 nm by using a concentrated $H_3PW_{12}O_{40.}$ Plus, the catalyst was able to separate from the product by using diethyl ether solvent.

2.3 Nanocellulose and its polymorphism.

A great demand worldwide on nano- materials creates a rapid evolution in the formulation of producing nanocellulose. Therefore, this section will explain briefly on the preparation of nanocellulose polymorphism.

The texture displayed by NFC and NCC reflects the approaches applied during the preparation of that material. NFC can be prepared through mechanical treatment while NCC can be simply prepared with the help of mineral acids. Though it sounds simple but reliable recipe are required in order to obtain uniform size and aspect ratio. If the reaction is not well controlled, it will lead to the formation of reducing sugar (glucose) and other unwanted side products.

Production of NCC or cellulose single crystals (cellulose whisker) is accompanied through acid hydrolysis. Regular mineral acids that are being used for the process are hydrochloric acid, hydrobromic acid (Sadeghifar, Filpponen, Clarke, Brougham, & Argyropoulos, 2011), and sulfuric acid (Eichhorn, 2011). Sulfuric acid is the best

selection among others due to its ability in maintaining the cellulose colloidal suspension. This is because, bulk sulfate group of sulfuric acid can incorporate on the cellulose surface thus stabilize the suspension efficiently by creating a strong electrostatic repulsion which create more stable ultimate suspension (Gardner et al., 2008).

2.3.1 Nanofibrilated Cellulose (NFC)

Nanofibrilated cellulose (NFC) is described as a bundle of long, entangled, stretchable and interconnected cellulose polymer chains of approximately 10 to 40 nm diameter (Abdul Khalil, Bhat, & Ireana Yusra, 2012; Abdul Khalil et al., 2014). The presence of amorphous region within the cellulose polymer chain gives elasticity properties to the material. NFC can be obtained through defibrillation of cellulose using an intensive mechanical treatment revealing the underlying microfibrils that later provides irreversible changes to the product. Regardless of the starting material, mechanical treatment that has been subjected to obtain NFC are high pressure homogenization, cryocrushing, microfludization, grinding, and high intensity ultrasonification (Abdul Khalil et al., 2014; Gardner et al., 2008; Lavoine, Desloges, Dufresne, & Bras, 2012) . Powerful impact and shearing forces introduced are responsible in revealing the cellulose microfibrils by diminishing network of hydrogen bonds underlying the microfibrils.

2.3.2 Nanocrystalline Cellulose (NCC)

Nanocrystalline cellulose (NCC) obtained from acid hydrolysis has been identified as the new class of nanomaterial. NCC possesses many advantages, such as high surface area, high modulus and tensile strength, unique optical properties, etc. A recent review on NCC was published by (Habibi, Lucia, & Rojas, 2010) where a lot of chemical and physical properties of NCC were discussed. NCC derived from acid hydrolysis

employed different morphology and texture depending on the origin and hydrolysis time. NCCs are widely observed as cellulose whisker and rigid rod like crystals. It has a diameter range of 10 -20 nm with length of few hundred nanometers (Gardner et al., 2008). However, the NCCs dimensions are highly dependent on its origin. Table 2.1, shows the most common NCC dimension according to their source while Figure 2.1 shows images of different type of NCC.

Table 2.1: Variety of sources used for production nanocellulose and its dimensions

Source	**L (nm)**	**D(nm)**	**L/D**	**Crystallinity (%)**	**References**
Cotton Linter	177	12	19	91	(Morais et al., 2013)
Corncob	210.8	4.15	53.4	83.7	(Silvério, Flauzino Neto, Dantas, & Pasquini, 2013)
MCC	-	<100	-	-	
Rice Straw	117	11.2	-	91.2	(Bai, Holbery, & Li, 2009)
Sugarcane baggasses	170	35			(Lu & Hsieh, 2012)
Mengkuang leaves	50-400	5-25	10-20	>70	(Mandal & Chakrabarty, 2011)
					(Sheltami, Abdullah, Ahmad, Dufresne, & Kargarzadeh, 2012)

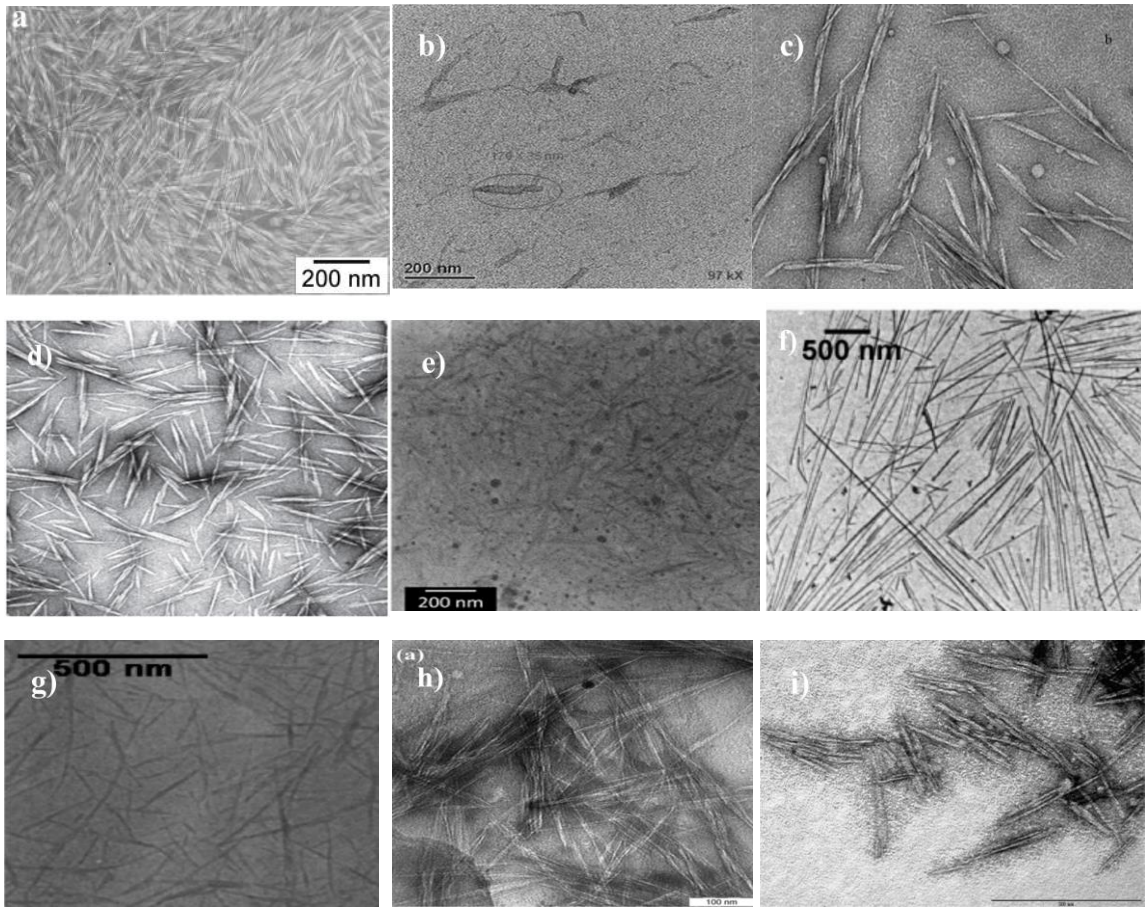

Figure 2.1: a) Rice straw (Lu et al., 2012), b) Sugarcane bagasse (Mandal et al., 2011), c) Mengkuang leaves (Sheltami et al., 2012) d) Ramie (Dufresne & Belgacem, 2013) , e) Jute fibers (Cao, Ding, Yu, & Al-Deyab, 2012) f) Tunicin (Angles & Dufresne, 2000) g) sugar- beet pulp (Azizi Samir, Alloin, & Dufresne, 2005) h) Kenaf bast (Zaini, Jonoobi, Tahir, & Karimi, 2013) , i) Eucalyptus wood pulp (Mesquita, Donnici, & Pereira, 2010)

2.3.3 Preparation method of Nanocrystalline Cellulose (NCC)

Preparation of NCC through acid hydrolysis is not relatively new, but most of the researcher used sulfuric acid as their choice in obtaining NCC. Reaction variables such as acid concentration, temperature, time, ratio between fibers: liquor and types of raw material are the most important variables that should be taken seriously in the preparation of NCC. Different reaction condition will result in different dimension of NCC. Typically, the most common reaction conditions proposed for the hydrolysis of cellulose are: concentration of sulfuric acid from 44 to 70 wt %, temperature from 25 to 70 °C and hydrolysis time from 30 min to overnight depending on the temperature (Ioelovich, 2012). Table 2.2 shows different types of reaction variables need in the preparation of various type of NCC.

Table 2.2: Reaction variables for the production of NCC

Reaction Details	Nanowhisker Dimensions	References
Raw material: Cotton Linter Chemical: 60 % (w/w) H_2SO_4 Fiber: Liquor: 1:20 (w/v) Temperature: 45 °C Time: 60 min Suspension obtained was centrifuged for 15 min at 13 000 rpm and was dialyzed with water until pH (6-7).	177 nm x 12 nm	(Morais et al., 2013)
Raw material: Cellulose Chemical: 64 % (w/v) H_2SO_4 Fiber: Liquor: 1:9 Temperature: 45 °C Time: 5 hrs Hydrolysis was stopped by adding 10 fold cold water. The suspension was centrifuged (5000 rpm, 15 min), the sediment collected was dialyzed and ultrasonicated in ice bath	4.7 nm x 143 nm	(Jiang & Hsieh, 2013)

'Table 2.2, continued' Reaction variables for the production of NCC

Reaction Details	Nanowhisker Dimensions	References
Raw material: Microcrystalline Cellulose Chemical: 64% (w/w) H_2SO_4 Fiber: Liquor: 1:15 Temperature: 44 °C Time: 3 hrs Establish under mechanical stirring and ultrasonic (50 Hz). The hydrolysis was stopped by adding 5 fold distilled water, centrifuged at 12 000 rpm. Lastly, dialyzed using a dialysis tube.	20 – 100 nm DP: 144	(Xiong, Zhang, Tian, Zhou, & Lu, 2012)
Raw material: Cellulose Chemical: 10 M H_2SO_4 Fiber: Liquor: - Temperature: 50 °C Time: 40 min The hydrolyzed material was washed by centrifugation at 10 000 rpm at 10 °C for 10 min. The step was repeated before neutralize it using a dialysis tube. The resulting suspension was then sonicated for 30 min.	10 – 15 nm	(Johar, Ahmad, & Dufresne, 2012)
Raw material: Bleached Cellulose Chemical: 5 % Oxalic acid Fiber: Liquor: - Pressure: 137 Pa Time: 1 hrs Undergo mild acid treatment and later was introduced to steam explosion. Lastly, the fibers were washed and subjected to mechanical stirring and sonication	5-50 nm	(Abraham et al., 2011)

'Table 2.2, continued' Reaction variables for the production of NCC

Reaction Details	Nanowhisker Dimensions	References
Source : Cellulose Chemical: 60 % (w/v) H_2SO_4 Fiber: Liquor: 1:20 Temperature: 50 °C Time: 5 hrs Hydrolysis was stopped by adding 5 fold cold water, centrifuged 5 times. The colloidal suspension was sonicated using Ultrasonic probe for 5 min.	170 nm x 35 nm	(Mandal et al., 2011)
Raw material: Cellulose Chemical: 64% (w/w) H_2SO_4 Fiber: Liquor: 2:21 Temperature: 45 °C Time: 1.5 hrs The hydrolysis was terminated by adding 400 ml cold water. The diluted suspension was centrifuges at 11 000 rpm for 10 min. The process was repeated to achieve neutrality and later was sonicated for 20 min using an ultrasonic homogenizer at 19.5 kHz and 300	1.96 ± 0.85 nm DP: 323	(Fahma, Iwamoto, Hori, Iwata, & Takemura, 2010)
Raw material: Microcrystalline Cellulose Chemical: 64% (w/v) H_2SO_4 Fiber: Liquor: 1:9 Temperature: 45 °C Time: 5 hrs The hydrolysis was stopped by adding 500 ml of water, centrifuged at 3500 rpm for 30 min. The suspension obtained was washed and filtered using ultra filtration membrane	< 100 nm	(Bai et al., 2009)

‘Table 2.2, continued’ Reaction variables for the production of NCC

Reaction Details	Nanowhisker Dimensions	References
Raw material: Bleached fiber Chemical: 64% (w/w) H_2SO_4 Fiber: Liquor: 1:10 Temperature: 60 °C Time: 30 min The hydrolysis was stopped by adding 100 ml cold water, the suspension obtained was centrifuged at 10 000 rpm for 10 min. The process was repeated until the supernatant became turbid. The collected material was dialyzed for 3 days and sonicated for 10 min.	25 – 30 nm x 400 – 500 nm	(R. Li et al., 2009)
Raw material: Cellulose Chemical: 60% (w/w) H_2SO_4 Fiber: Liquor: - Temperature: 45 °C Time: 30 min Produced under continuous agitation.	30.9 ±12.5 nm	(Morán, Alvarez, Cyras, & Vázquez, 2008)

2.3.4 Preparation method of Nanofibrilated Cellulose (NFC)

Preparation of NFC is usually associated with energy intensive equipments. The energy generated from the mechanical treatment is important in disintegrating the cellulose fiber into a nano-scale dimension. The most common mechanical treatment applied is homogenization, microfludization, cryocrushing, ultrasonication, grinding, electrospining etc. Table 2.3 shows the example of reaction variables for the production of NFC with different nanofibrils dimensions obtained

Table 2.3: Reaction variables for the production of NFC

Reaction Details	Nanofibrils Dimensions	References
Raw material: Cellulose Fiber : Solvent: 1 :400 Cellulose suspension was blended at 37 000 rpm for 1 h at 97 °C. The suspension was cooled and centrifuged (1500 rpm 15 min).	2.7 nm x 100 - 200 nm	(Jiang et al., 2013)
Raw material: Cellulose Fiber : Solvent: 1:100 Reagent: TEMPO + NaBr + NaClO + NaOH The suspension was centrifuged (1500 rpm, 15 min) and later concentrated using rotary evaporator, ultrasonicated (40 % amplitude) and then filtered	1.7 nm x 100 - 1000 nm	(Jiang et al., 2013)
Raw material: Cellulose Fiber :Solvent: 1: 100 Reagent: BmimCl Temperature: 130 °C Time: 2 h The mixture was dissolved by aid of microwave oven .The clear and viscous solution was then subjected to homogenizer at pressure level ranging 40 to 140 MPa for up to 50HPH cycles	10-20 nm	(Li et al., 2012)

‘Table 2.3, continued’ Reaction variables for the production of NFC

Reaction Details	Nanofibrils Dimensions	References
Raw material: Bleached pulps HNO_3:CH_3COOH: 1:10 Temperature: 120 °C Time: 15 min The mixture were cooled and washed with ethanol and water and dried in oven at 105 °C.	10 -50 μm	(Maheswari, Reddy, Muzenda, Guduri, & Rajulu, 2012)
Raw material: Cellulose pulps Solid content: 0.7% Pressure: 55MPa Cycles:20 The solid was homogenized with numbers of passes and cold at 45 °C.	Not determined	(Spence, Venditti, Habibi, Rojas, & Pawlak, 2010)
Raw material: Bleached cellulose Solid content: 1 % Pressure: 500 Bars Cycles:15 Temperature: < 95 °C The solid content was blended using a blender for 15 min, when the temperature reached 65 °C; the slurry was subjected into a homogenizer with 15 passes.	2-5 nm DP 850 -830	(Habibi, Mahrouz, & Vignon, 2009)

METHODOLOGY

3.1 Introduction

This chapter describes briefly on the chemical and gases used and experimental procedure in the synthesis of $Cs_xH_{3-x}PW_{12}O_{40}$ catalyst, and the production of NCC. The generated NCC and synthesized catalyst produced were further characterized using variety of chemical analytical techniques.

3.2 Chemical and Gases

All the chemical and gases used for catalysts preparation and their activation, followed by catalyst screening for the production of NCC are listed in Table 3.1

Table 3.1: List of chemicals and gases used

No	Chemical /Gases	Supplier	Description
1	Synthetic Oxygen	MOX	99.8 %
2	Nitrogen	MOX	99.9 %
3	Phosphotungstic acid ($H_3PW_{12}O_{40}$)	Friendemann Schmidt	Grade AR
4	Cesium Carbonate (Cs_2CO_3)	Acros Organics	99.5 %
5	Microcrystalline Cellulose (MCC)	Sigma -Aldrich	Cotton linter

3.3 Equipment

3.3.1 Universal Temperature Programmed (UTP) for catalyst activation.

Calcination of catalyst precursor was carried out using a tubular furnace referred to as Universal Temperature Programme (UTP) shown in Figure 3.1. The sample was placed inside a quartz tube and positioned inside the furnace. The tube was sealed with other quartz compartment, and was rotated at 270° in circular motion. The oxygen gas (oxidizing agent) was allowed to flow inside the tube through a connector. Flow rate of oxygen gas was controlled using a mass flow controller.

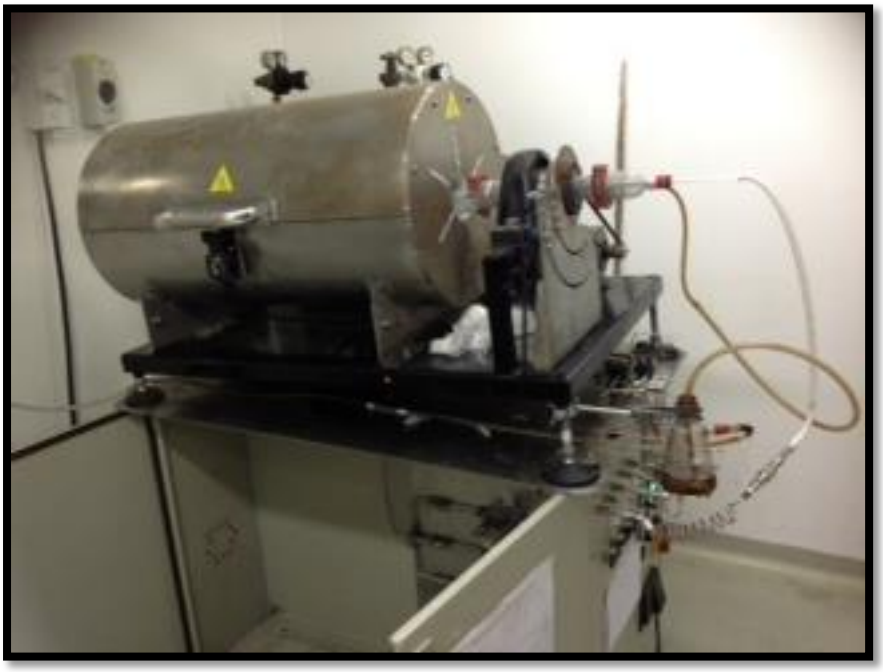

Figure 3.1: Universal temperature programme (UTP) equipment.

3.3.2 Ultrasonic Probe UIP1000hd for depolymerization of cellulose

Catalytic depolymerization of cellulose was carried out using ultrasonic probe UIP1000hd (1000 W, 20 kHz) shown in Figure 3.2. The Hielscher Ultrasonics consists of a transducer and generator, automatic frequency tuning, amplitude adjustable from 50 -100 %, and titanium horn. The power is transmitted at controlled amplitude, so that the magnitude of the mechanical ultrasonic vibrations at the sonotrode is constant under all load conditions. The titanium horn (sonotrode) has an excellent chemical compatibility with most of the chemical solvent.

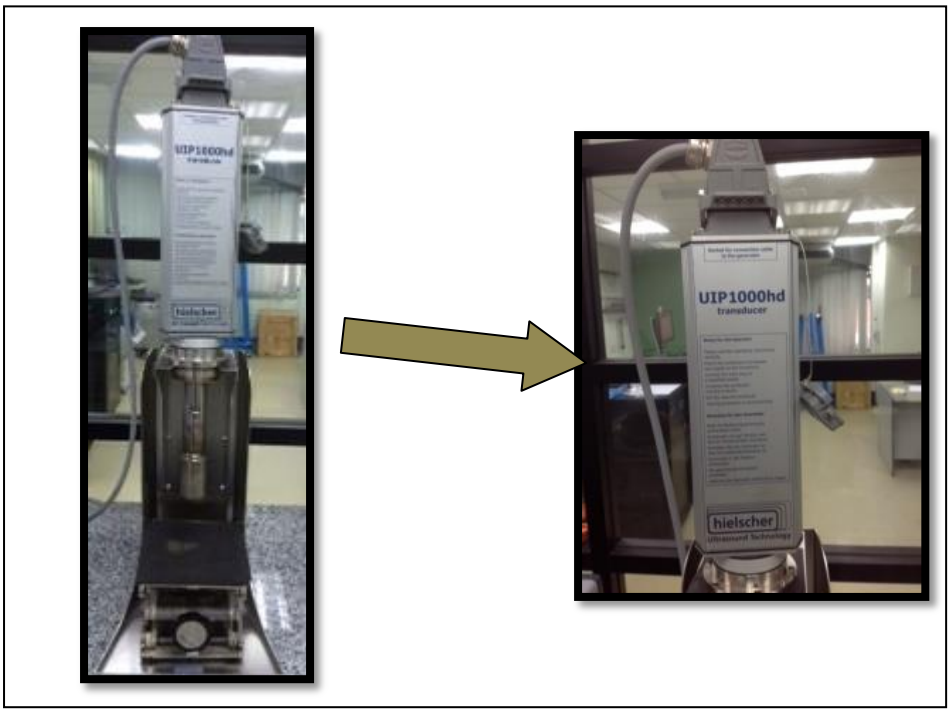

Figure 3.2: Ultrasonic probe UIP1000hd

3.4 Synthesis of Heteropoly Acid – based Catalyst

3.4.1 Synthesis of $Cs_xH_{3-x}PW_{12}O_{40}$ Catalyst Precursors

Synthesis of catalyst precursor was done using controlled precipitation method in order to obtain a suspension of catalyst precursor that will give a reproducible property. For acidic cesium salt of Tungstophosphoric Acid ($Cs_xH_{3-x}PW_{12}O_{40}$) precursor, the preparation procedure used, follows the controlled precipitation technique that has been extensively used by a lot of researchers worldwide (M. Amirinejad, S.S Madaeni, E Rafiee, & S Amirinejad, 2011; A. S. Dias, Lima, Pillinger, & Valente, 2006; Shiju, Williams, & Brown, 2009; Shobeiri, Pourayoubi, Heydari, Percino, & Ramírez, 2011). In this study, the method was further optimized by changing the variations of the controlled parameters. It was accomplished consecutively to establish a relationship between the varied parameters. The effect of each synthesis parameter on the acidic cesium salt of Tungstophosphoric Acid was examined thermally and structurally.

Tungstophosphoric acid hydrate was used as a source of Keggin framework with excellent acidity, while Cesium Carbonate (Cs_2CO_3) was used as a source of cesium atom. Cs_2CO_3 was used because it produces large monovalent cation; Cs^+ that is used for proton substitution thus modified the microstructure of Heteropoly acid. The precipitation process was done using an Autotitrator (Mettler Toledo T50). The overall reaction between Cs_2CO_3 and $H_3PW_{12}O_{40}$ was explained briefly in Figure 3.3.

Equation (3.1) shows the chemical reaction for the substitution process. Based on Table 3.2 an appropriate amount of Cs_2CO_3 solution was added to a fix volume of Tungstophosphoric acid solution (TPA) with a precision control on the rate of addition using Autotitrator. Both solutions were freshly prepared before starting the reaction and stirred until attaining homogeneity. The pH changes were monitored during the titration process. The addition of Cs_2CO_3 solution was stopped when the neutralization reaction reached completion. A milky suspension obtained were aged before drying in vacuum oven for 24 hours at 55 ± 5 °C (slowly evaporation).

$$\mathbf{H_3PW_{12}O_{40} + Cs_2CO_3 \rightarrow Cs_xH_{3-x}PW_{12}O_{40} + CO_2 + H_2O \ldots\ldots\ldots\ldots\ldots\ldots (3.1)}$$

Table 3.2: Details on metal salts solution preparation for respective samples.

Cs: H	Concentration of Cs_2CO_3 (M)	Concentration of $H_3PW_{12}O_{40}$ (M)	Volume of Cs_2CO_3 (ml)	Volume of $H_3PW_{12}O_{40}$ (ml)
1.0:2.0	0.25	0.08	21.4	41.50
2.0:1.0	0.25	0.08	32.6	40.16
2.5:0.5	0.25	0.08	36.0	38.94
2.8:0.2	0.25	0.08	39.4	38.47
3.0:0.0	0.25	0.08	43.2	38.18

`

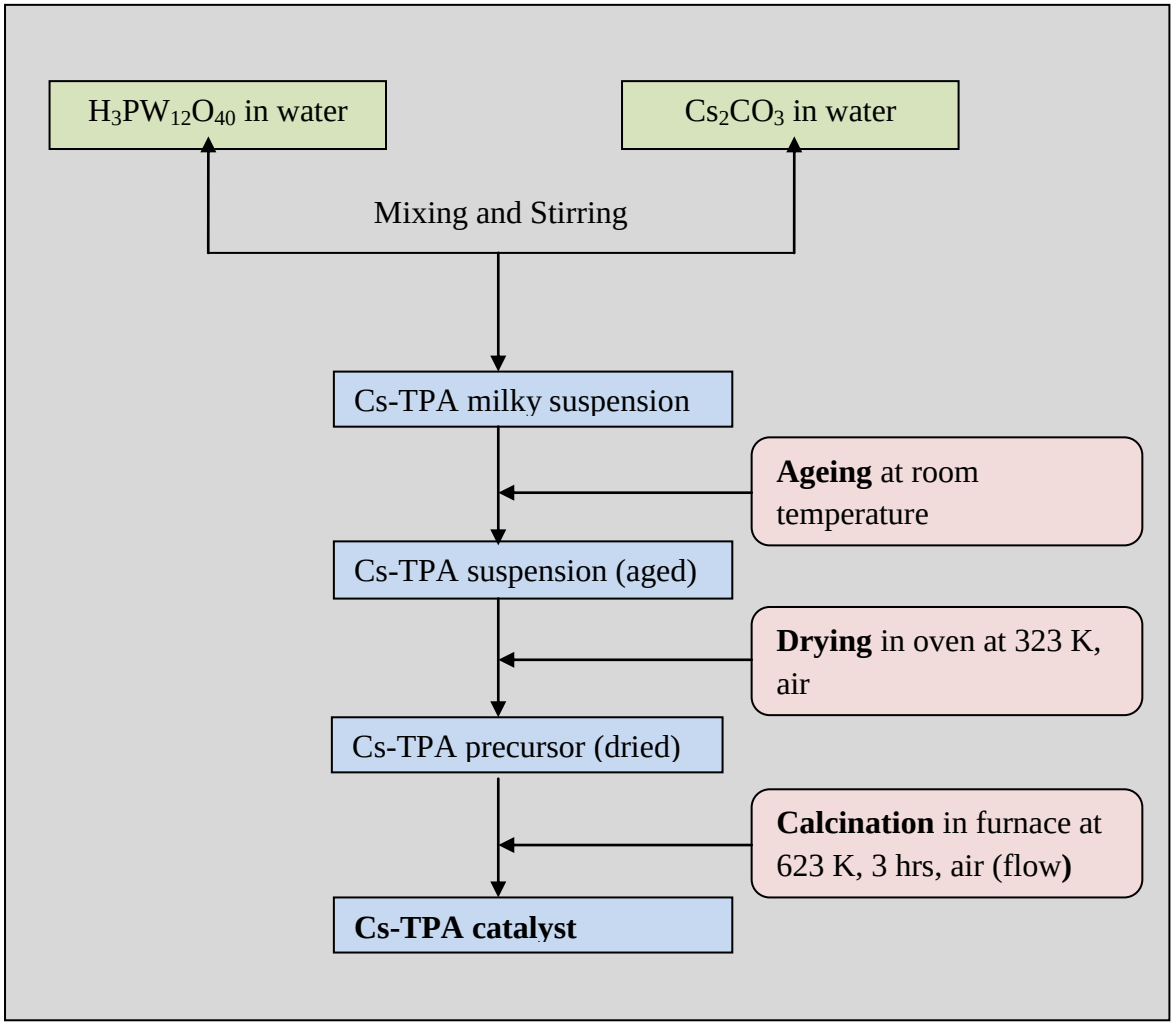

Figure 3.3: Flow chart for Cs-TPA catalyst preparation.

3.4.2 Activation of $Cs_xH_{3-x}PW_{12}O_{40}$ Catalyst Precursors

Activation is the last step for a substance to become a catalyst. This procedure helps in eliminating the remaining ligands, impurities and foreign things that are temporarily attached to the catalyst precursor. The ligands are being oxidized into stable forms by introducing a dynamic flow rate of oxidant gas. In addition, during activation the catalyst can undergo structural and crystallinity changes.

The catalyst precursor was placed into a tubular quartz tube, and the quartz tube it was subsequently positioned horizontally inside the UTP furnace. The sample was heated

from 30 °C to 350 °C, and the temperature holding time was 4 hours. The 4 hours holding time is sufficient in removing or eliminating water as well as the remaining ligands and impurities that may be present in the catalyst precursor. The explanation can be summarized by referring to Figure 3.4. Plus, the calcination procedure also helps to develop the catalyst porosity, hence increase the surface area of the catalyst. Finally, the sample was cooled down to room temperature and later collected and tested

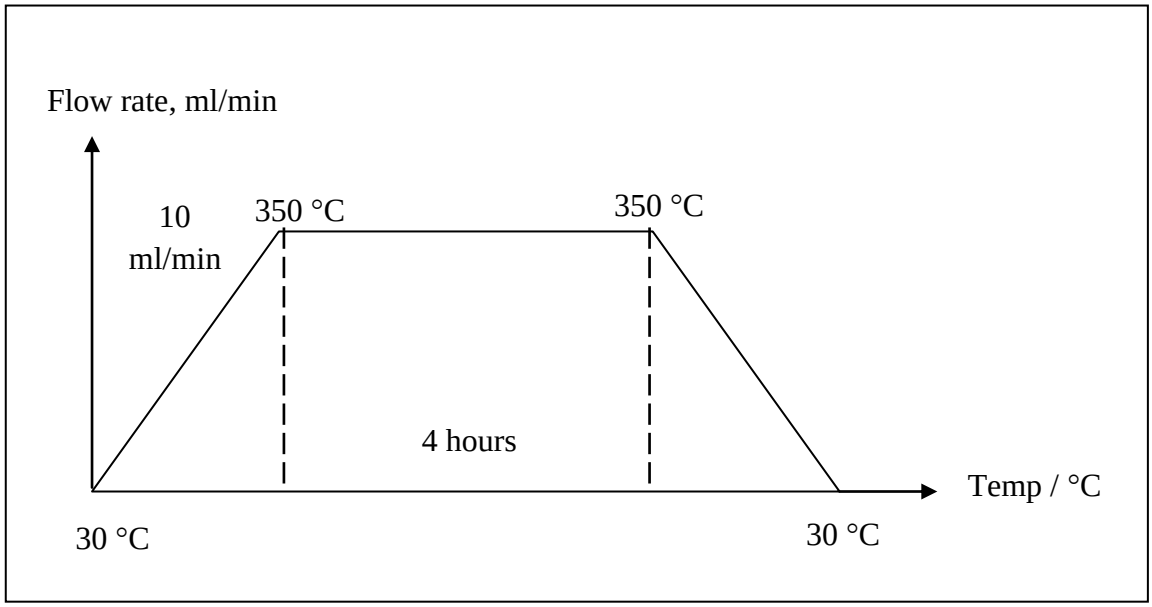

Figure 3.4: Temperature programmed set for Cs-TPA catalyst precursor.

3.5 Preparation of Nanocellulose from Microcrystalline Cellulose (MCC)

Depolymerization and separation of Nanocrystalline Cellulose (NCC) from MCC was accomplished through a catalytic approach with the assistance of Heteropoly acid (HPA) –based catalyst. The HPA catalyst is a Bronsted acid which plays an important role in replacing a conventional mineral acid liquid catalyst. In principle, HPA catalyst will donate protons during the reaction and subsequently can attack the easiest position with high electronegativity atom located within the cellulose polymer chains. Mechanical energy via ultrasonication treatments was applied during the reaction to enhance the defibrillation of cellulose polymer through breaking of hydrogen bonding which consequently, exposes more surface area and increase the accessibility for catalytic reaction to take place. The main reactions for nanocellulose production are

hydrolysis of cellulose polymer chain and delamination of cellulose polymer sheets are shown in Figure 3.5.

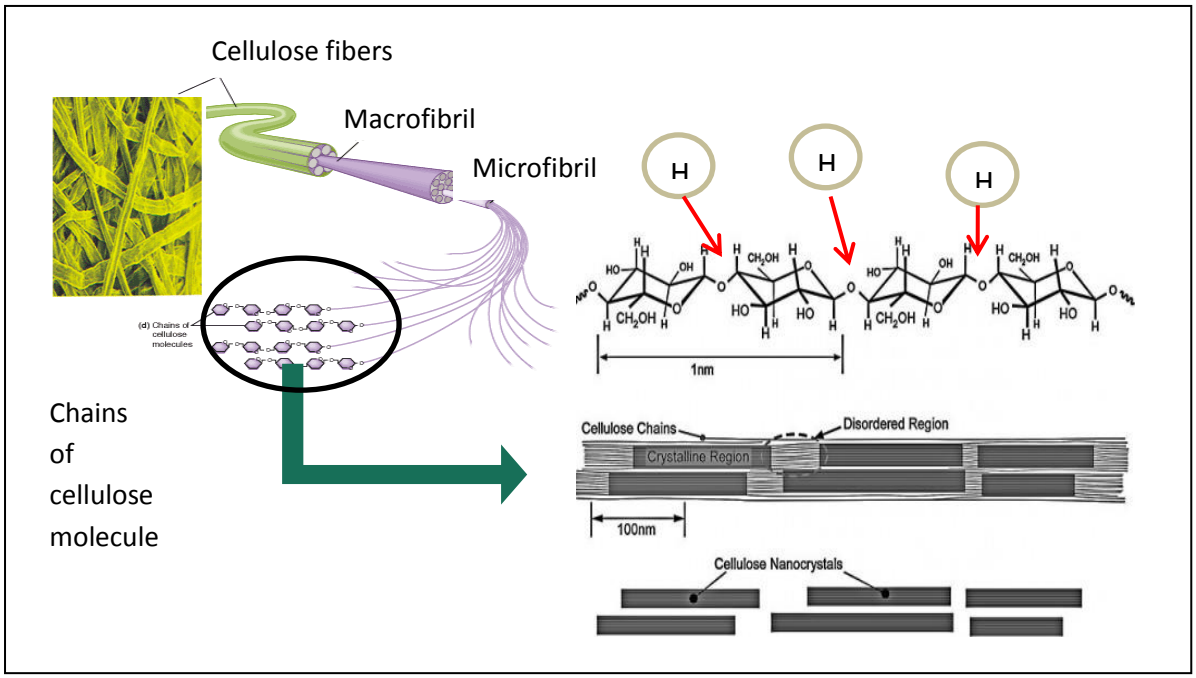

Figure 3.5: Reaction scheme that took place during the production of Nanocrystalline cellulose (NCC)

3.5.1 Flow Chart on Preparation of Nanocellulose

MCC was added to deionized water at ratio 1:10 in 250 ml borosilicate beaker. The mixture was stirred with glass rod, and it produced a temporary cloudy solution .The mixture was then introduced for ultrasonication treatment using Ultrasonic Probe UIP1000hd transducer at varying power output. After 10 minutes, a homogeneous milky color suspension was generated. The mixture produced has a stable suspension that does not separate nor settle down or sediment with time. The same procedure was adopted when HPA and Cs-HPA were used as a catalyst. Isolation of nanocellulose was studied by applying four different types of reaction variables which are 1) Sonication power, 2) Reaction time, 3) Type of catalyst and 4) Amount of catalyst used.

Upon completion, the resulting mixture was extracted using diethyl ether according to (Li et al., 2014) to separate and recover back the catalyst. A small amount of nanocellulose suspension was poured into a Petri dish, and was allowed to dry in a vacuum desiccator. The nanocellulose that is completely dry will stick out from the surface of Petri dish. The dried nanocellulose was further characterized thermally and structurally.

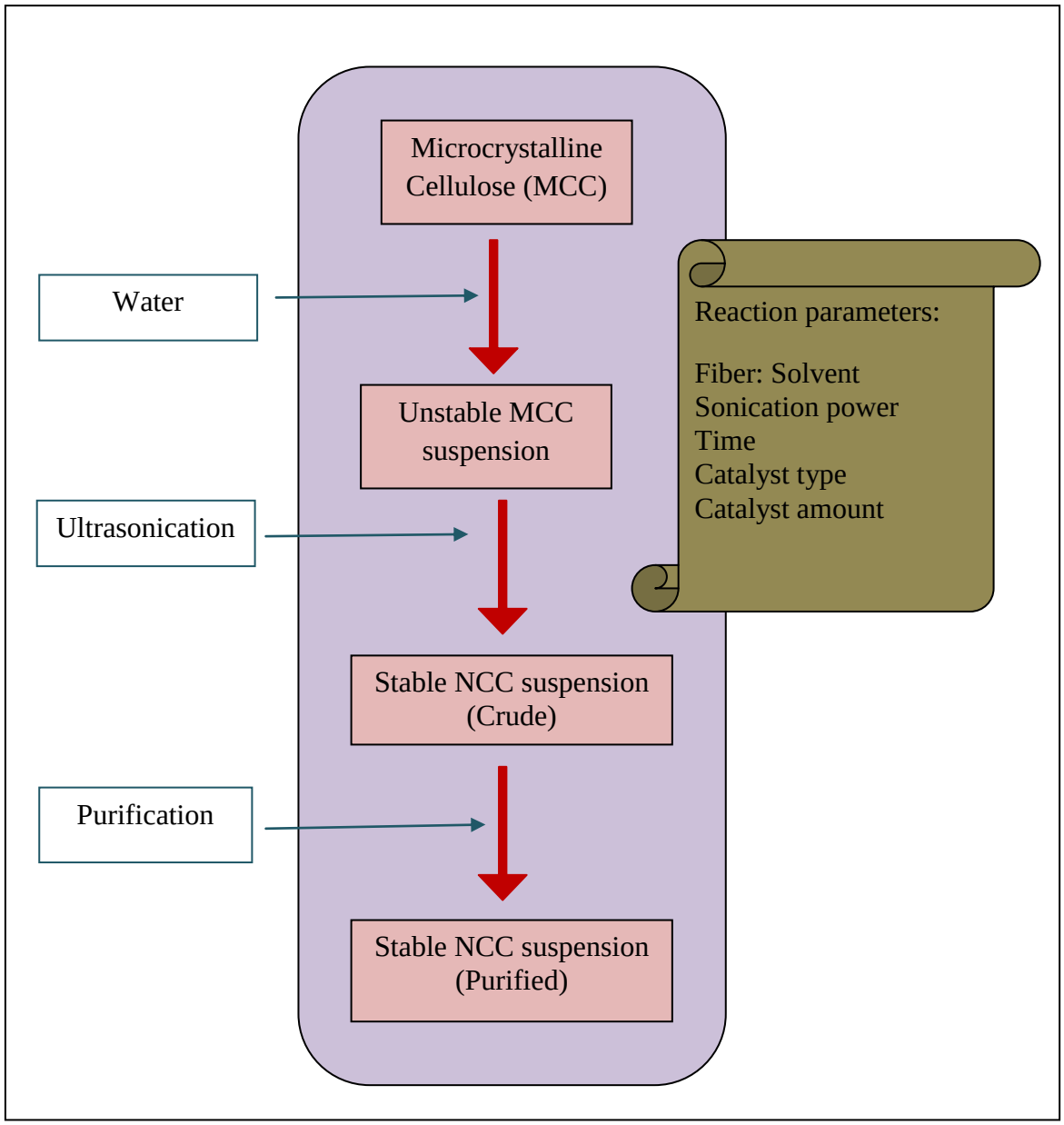

Figure 3.6: Flow chart of nanocellulose production from MCC raw material

The production of nanocellulose was being accomplished by using ultrasonication and catalytic route. The reaction variables for nanocellulose production were tabulated in Table 3.3. The generated nanocellulose was coded as SN starting from 01 until 20 depending on the reaction condition.

Table 3.3: Details on the reaction variables for nanocellulose production

Sample ID	Cellulose : Solvent	Sonication power (W)	Time (min)	Catalyst	Amount of catalyst (g)
SN01	1:10	50	10	-	-
SN02	1:10	100	10	-	-
SN03	1:10	113	10	-	-
SN04	1:10	140	10	-	-
SN05	1:10	225	10	-	-
SN06	1:10	240	10	-	-
SN07	1:10	300	10	-	-
SN08	1:10	225	1	-	-
SN09	1:10	225	1.5	-	-
SN10	1:10	225	2.5	-	-
SN11	1:10	225	3.5	-	-
SN12	1:10	225	5	-	-
SN13	1:10	225	10	-	-
SN14	1:10	225	15	-	-
SN15	1:10	225	10	$H_3PW_{12}O_{40}$	2
SN16	1:10	225	10	$H_3PW_{12}O_{40}$	4
SN17	1:10	225	10	$H_3PW_{12}O_{40}$	6
SN18	1:10	225	10	$Cs_1\ H_2PW_{12}O_{40}$	4
SN19	1:10	225	10	$Cs_{2.5}\ H_{0.5}PW_{12}O_{40}$	4
SN20	1:10	225	10	$Cs_3\ H_0PW_{12}O_{40}$	4

3.6 Characterization Techniques

This section discusses different types of characterization methods used in the quest to understand the properties of proprietary catalyst prepared in this project. Experimental procedures applied for sample characterization are explained here.

3.6.1 Structural Analysis

3.6.1.1 X-ray Powder Diffraction (XRD) analysis

XRD was performed using a Bruker X-ray Diffraction model D-8 equipped with EVA Diffract software for data acquisition and analysis. This instrument helps to identify and reveal the crystal lattice, structure, crystallinity index and composition of the material. This machine uses CuK_{α} monochromatized radiation source operated at 40 kV and 40 mA at ambient temperature.

The catalyst samples were finely grounded and placed in the sample holder, with the powder lightly pressed into place using a microscopic slide plus the surface of the sample was flattened and smoothens. The analysis parameter were accomplished at continuous 2θ scan mode from 5° to 80° with high degree scanning at step time of 2s and step size of 0.02° 2θ. A divergence slit was inserted to ensure that the x –ray focused only on the samples and not at the edges of specimen holder. The diffractograms obtained were matched against the Joint Committee on Powder Diffraction Standards (JCPDS) PDF 1 database version 2.6 to confirm the phases of catalyst the precursor and catalyst.

For cellulosic samples, the cellulosic film was placed onto the surface of sample holder. The analysis parameters were set at continuous 2θ scan mode from 5° to 60° with high degree scanning at step time of 2 s and step size of 0.02 ° 2θ. A divergence slit was inserted to ensure that the X –ray focused only on the samples and not at the edges of

specimen holder. The diffractograms obtained were matched against the Joint Committee on Powder Diffraction Standards (JCPDS) PDF 1 database version 2.6 to confirm the presence of cellulosic material and the crystallinity index was calculated based on the given value.

$$CrI = \frac{I_{002} - I_{am}}{I_{002}} \times 100 \qquad \textbf{(3.2)}$$

The crystallinity measurement was calculated from the ratio of the height 002 peak (I_{002}) and the height of the minimum (I_{am}). Noteworthy, I_{002} represents both amorphous and crystalline regions, while I_{am} signifies for amorphous domain at peak 18°.

3.6.1.2 Scanning Electron Microscope-Energy Dispersive X-ray (SEM-EDX)

SEM is an instrument that reveals the information about topography and the morphology of a solid material through three- dimensional (3D) images. EDX is a technique that used to analyze near surface elements and estimate their proportions at different position, thus giving an overall mapping of the sample.

The calcined samples were stacked to the aluminum stub with carbon conductive tape. The stub was then mounted on the stub holder and loaded into the chamber and later was evacuated prior to analysis. All samples were sputter –coated with gold before microscopic images were viewed and obtained. SEM images were taken at an accelerating voltage of 10 kV at various magnifications. Images were collected using Quanta 200 FEI microscope instrument.

3.6.1.3 Nitrogen Physisorption Measurements (BET)

Specific surface areas, pore sizes and pore size distribution for catalyst were determined using BET procedure by nitrogen adsorption and desorption. The N_2 adsorption and desorption carried out using Sorptometric 1990 Instrument.

Approximately 20 mg of catalyst were used for analysis. The sample was placed in a tube of known volume and heated to 250 °C for degassing under vacuum for 5 hours. After outgassing, the catalyst was reweighted and later was placed at the analysis station. The catalyst was cooled in liquid nitrogen. After equilibration, the pressure was measured and the sequence repeated with successive pulses of N_2.

3.6.1.4 Fourier Transform Infrared Spectroscopy (FTIR)

FTIR spectrums are capable in revealing information about the functional group present within a molecule. FTIR spectroscopy were performed in order to observe any significant changes occurred during the hydrolysis of cellulose and the chemical structures of Keggin anion of the catalyst.

FTIR spectra for a catalyst sample were recorded using Bruker spectrometer model IFS 66v/s using a KBr technique and working with resolution of 4 cm^{-1} in the Middle range. Before analysis was preceded, air evacuation was applied under vacuum (14 mbars) for 15 minutes.

FTIR spectra for cellulosic samples were also recorded using Bruker spectrometer model IFS 66v/s using a KBr technique and working with resolution of 4 cm^{-1} in the Middle range. Before analysis was preceded, air evacuation was applied under vacuum (14 mBars) for 15 minutes.

3.6.1.5 Raman Spectroscopy

The Raman spectra were obtained using Renishaw inVia Raman microscope. The analysis was conducted using 50 x objective lens while the laser (785 nm) was set at 10 % of 150 MW (100 %) with instrument grating 1200 1/mm grating. The sample was exposed for 30 s to the laser power before obtaining the Raman shift.

3.6.1.6 Dynamic Light Scattering

Measurement of all nanocellulose suspensions at 0.1 wt % were accomplished with Zetasizer Nano ZS Instrument (Malvern) using detection angle of 173 ° at temperature of 25 ° C. The dispersant used is water with material refractive index 1.67 and dispersion refractive index is 1.33.Three measurements of 120 s of each were taken and the averaging was done.

3.6.1.7 Zeta Potential

Zeta potential or surface charge analysis was conducted using Zetasizer Nano Zs Instrument Malvern Model ZEN3600 using Zetasizer Software. The analysis was performed using a conductive cuvette consisting 0.01 wt % of nanocellulose suspension.

3.6.1.8 Transmission electron microscopy (TEM)

The morphology and the nanoscale measurements of NCC were carried out using HR-TEM. The samples were observed after five days using HR-TEM in order to make sure that the samples are completely dry. Few drops of 0.01 wt % nanocellulose suspension were deposited on copper grids and were dried in vacuum desiccator before observed with JEOL, JEM -2100F field emission electron microscope operated at an acceleration voltage of 200keV.

3.6.1.9 Atomic Force Microscopy (AFM)

1 % (w/w) of NCC suspension was dropped on the glass slide and was dried in oven for several minutes. The sample was viewed using AFM model NT-MDT at scan rate of 1.01 Hz. The cantilever used has a length of 125 ± 5μ, width 30 ± 5μ and thickness of

1.5- 2.5μ.The resonance frequency applied was 87- 230 KHz with force constant of 1.45-15.1 N/m.

3.6.1.10 Surface tension

The surface hydrophilicity was measured by using Tensiometer model DCAT $_{11}$EC with 12 V DC using SCAT software. The Wilhelmy plate technique was employed for measuring the surface tension of the NCC suspension. A Platinum (Pt) plate was suspended from a torsion balance. As the plat touches the solution, the instruments begin to measure until stable values are obtained. The strength of the samples' surface was measured as the plate was pulled from the mixture.

3.6.2 Thermal Analysis

3.6.2.1 Thermogravimetric Analysis (TGA)

TGA is a quantitative analysis that measures the weight loss as a function of temperatures change. The mechanism can be confirmed through the analysis of solid and gases of the decomposed product.

The measurement was accomplished using Mettler Toledo TGA/SDTA 851° unit, equipped with a microbalance and furnace that is capable of heating up to 1873 K. This Mettler Toledo balance technology on this unit allows the horizontal flow of gases that minimize the chimney effect and more stable weight signal. Since, nitrogen gas is an inert gas, it is necessary to allow it to flow continuously at 50 cm^3 min^{-1} in order to avoid any harmful gases from flowing backwards towards the microbalance.

For catalyst sample, about 50 mg of catalyst were measured in an open alumina crucible (70 μl), the sample was heated at an elevated temperature from ambient to 1373 K at 10 ° C min^{-1}. Nitrogen gas was applied as an inert medium for the sample and flow at the

constant flow rate of 40 cm^3 min^{-1}.The result obtained was evaluated with the V7.01 STAR^e software packages. The DTG curve was calculated as derivatives of the TG curve. For cellulosic sample, about 50 mg of cellulosic material were measured in an open alumina crucible (70 μl), the sample was heated at an elevated temperature from ambient to 1073 K at 10 ° C min^{-1}. Nitrogen gas was applied as an inert medium for the sample and flow at the constant flow rate of 40 cm^3 min^{-1}.The result obtained was evaluated with the V7.01 STAR^e software packages. The DTG curve was calculated as derivatives of the TG curve.

RESULTS AND DISCUSSION

This chapter is organized into 2 major sections, i.e. Section 4.1 to Section 4.4: Presentation of results and discussion of catalyst synthesized and characterization, Section 4.5 to 4.7: Presentation of results and discussion of cellulose depolymerization to yield nanocellulose together with products assay.

PART A: CATALYST

4.1 Introduction

This section discusses the results obtained from various catalysts prepared and their characterization techniques where their syntheses have been briefly described in Chapter Three. It is divided into two categories i.e structural and thermal properties. The study of structural property comprises of chemical fingerprint, crystal structure, surface area and porosity, topography and morphology. Thermal properties in various environmental atmospheres are also evaluated to explain the compositional and structural change with temperature.

Catalysts prepared and characterized in this study are listed and coded in Table 4.1. The catalyst selection criteria are based on the corresponding acid properties of the catalyst. Effect of sonication power, sonication time, catalyst amount and Cs:H ratio in Tungstophosphoric (TPA) catalyst was examined in order to identify the effectiveness of cellulose depolymerization. The nanocellulose produced was examined and analyzed for the structural and thermal properties.

Table 4.1: List of catalysts prepared and their corresponding acidity.

Catalyst Code	Composition	Cs:H ratio	Acidity (pH)
CS01	$H_3PW_{12}O_{40}$	0:3	0.4
CS02	$Cs_1H_2PW_{12}O_{40}$	1:3	2.6
CS03	$Cs_2H_1PW_{12}O_{40}$	2:3	4.1
CS04	$Cs_{2.5}H_{0.5}PW_{12}O_{40}$	2.5:0.5	4.3
CS05	$Cs_{2.8}H_{0.3}PW_{12}O_{40}$	2.8:0.2	5.7
CS06	$Cs_3PW_{12}O_{40}$	3:0	6.6

4.2 Structural Analysis

4.2.1 X-ray Diffraction (XRD)

X-ray powder diffraction (XRD) is an important analysis for revealing information about bulk crystalline phases, and to estimate the crystallite sizes. Therefore, the structural properties and phase integrity of catalyst's samples CS01, CS02, CS03 and CS04, CS05 and CS06 were evaluated using XRD. Table 4.2 shows the main diffraction peaks for all the Heteropoly compound types of catalysts.

The diffraction patterns of CS01, CS02, CS03, CS04, CS05 and CS06 are displayed in Figure 4.1. The diffractograms displayed for the catalyst's samples were in the range of $2\theta = 8 - 50°$. The displayed patterns show HPA characteristic peaks at 10.5°, 18.3°, 23.6°, 26.0°, 30.2°, 35.5°, 38.8°, 41.8°, 43.0° and 54.8° (which matches PDF-file: 00-050-1857/041).

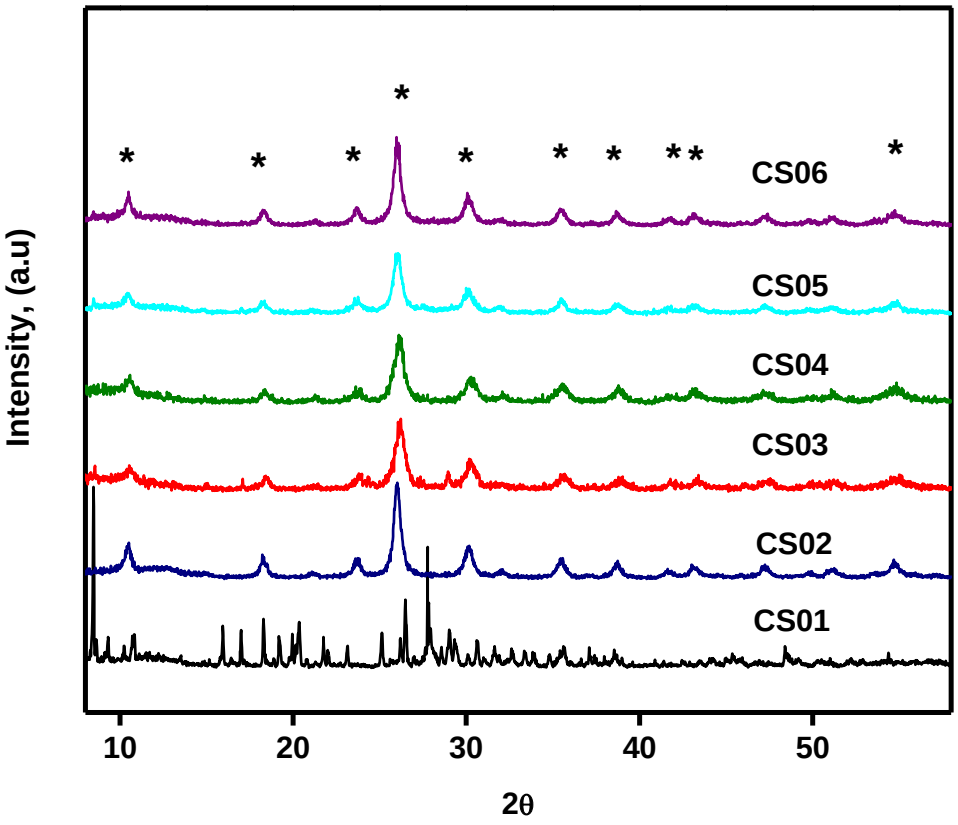

Figure 4.1: Main XRD diffraction peaks related to CS01, CS02, CS03, CS04, CS05 and CS06.

Table 4.2: Main diffraction peaks related to cesium salts of tungstophosphoric (PDF-file: 00-050-1857/041).

No	2θ (°)	d-spacing (Å)	Intensity (%)
1	10.5	8.41	36
2	18.3	4.84	36
3	23.8	4.19	34
4	26.0	3.42	100
5	30.2	2.98	17
6	35.5	2.53	15
7	38.8	2.32	13
8	41.8	2.16	7
9	43.2	2.09	28
10	54.8	1.67	23

Substitution of cation with a larger atomic radius (Cs) within the Keggin network modifies the originality microstructure of HPA through the rearrangement of the secondary structure which increases the surface area of the compound. Secondary structure of HPA are consisted of Keggin anion and positively ion (Santos et al., 2011). The highest intensity peak at $2\theta = 26\ °$ has been marked as the signature peak of tungstophosphoric acid with Keggin structure .All the cesium salts of tungstophosphoric acid curves displayed the same diffractogram patterns. However each of the catalyst possesses different lattice strain (%). Lattice strain and crystallite size, D were calculated using Scherrer equation in Equation 4.1, and the values calculated are listed in Table 4.3.

$$D = k\lambda / \beta \cos\theta \quad \text{……} \quad \textbf{(Equation 4.1)}$$

$$\beta = (B^2 - b^2)^{1/2}$$

With k constant 0.9,

$\lambda = 0.1542$

(Cu Kα) radiation,

β = is true line width

B = measured line width, and

b = instrumental broadening of Diffractometer

Table 4.3: Crystallite size and lattice strain for CS01, CS02, CS03, CS04, CS05 and CS06.

Catalyst ID	Composition	Bragg Angle 2θ	Crystallite size (Å)	Lattice Strain (%)
CS01	$H_3PW_{12}O_{40}$	27.00	1007	0.587
CS02	$Cs_1H_2PW_{12}O_{40}$	26.03	296	0.520
CS03	$Cs_2H_1PW_{12}O_{40}$	26.09	290	0.511
CS04	$Cs_{2.5}H_{0.5}PW_{12}O_{40}$	26.18	230	0.500
CS05	$Cs_{2.8}H_{0.2}PW_{12}O_{40}$	26.18	230	0.493
CS06	$Cs_3H_0PW_{12}O_{40}$	26.20	229	0.480

When the Cs:H ratio number increased from 0 to 3, the lattice strain (%) decrease. This is due to the small lattice parameters created by the diverse effect generated by exchanging cation diameter (Pizzio & Blanco, 2003) . Furthermore, the substitution of bigger (Cs) and smaller (H) diameter cation within the Keggin anion has decreased the crystallite size up to 71 % from CS01 to CS02 and the value continue to decrease in smaller range when the ratio increase from 1 to 3 (Cs:H).

The XRD patterns displayed for CS03 and CS04 correspond to cubic phase, while CS02 is a mixture between cubic and triclinic phase. That information was gained from HighScore database (PDF-file: 00-050-1857/041). This is due to the significant difference in ionic radius of protons and Cs^+, which altered the crystal structure of the catalyst produced. It has been mentioned by Srilatha et al., (2012) that the existence of triclinic phase decrease when the ratio of Cs:H increase, leaving a homogeneous cubic phase inside. Exchanging more cesium atom within the Keggin anion has restructured its crystal structure through rearrangement of the secondary structure.

4.2.2 Fourier Transform Infrared (FTIR)

Infrared spectroscopy is a study of the interaction of electromagnetic radiation with chemical substances. The main purpose of this FTIR analysis is to reconfirm the structure of the Keggin network after the substitution process. This method helps to reveal a lot of information about the stretching and bending vibrations of functional group presence. The frequency bands generated will be the fingerprint band for the Keggin structure of each catalyst.

Based on FTIR spectra obtained in Figure 4.2 and the description in Table 4.4, there is no disruption of Keggin network occurred upon the substitution of hydrogen ion with cesium ion. This has been successfully illustrated through the presence of all the main characteristic peaks of Keggin anion. Nevertheless, there is no specific information revealed through these FTIR spectra which can explain briefly about the cesium content present in each catalyst analyzed.

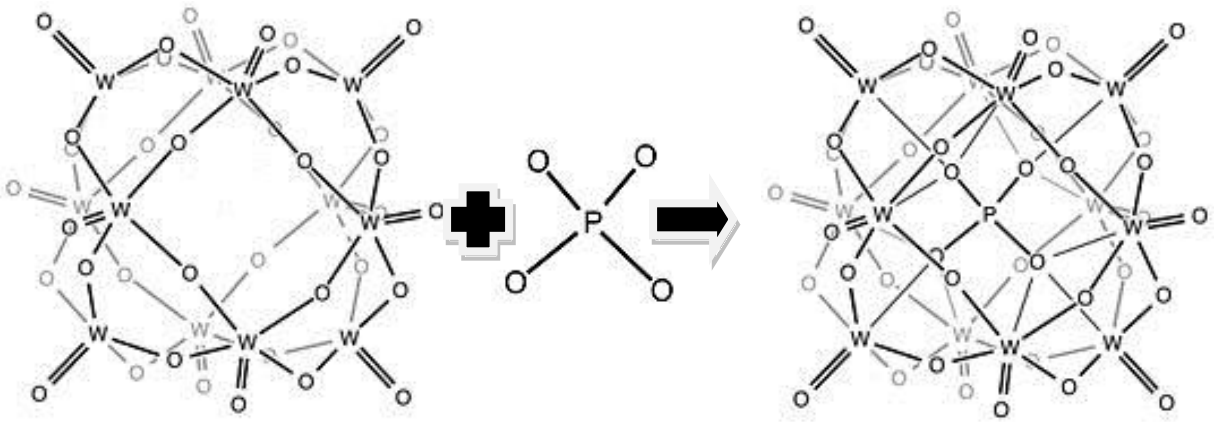

Figure 4.2: (a) Three - dimensional (3D) of Keggin network.

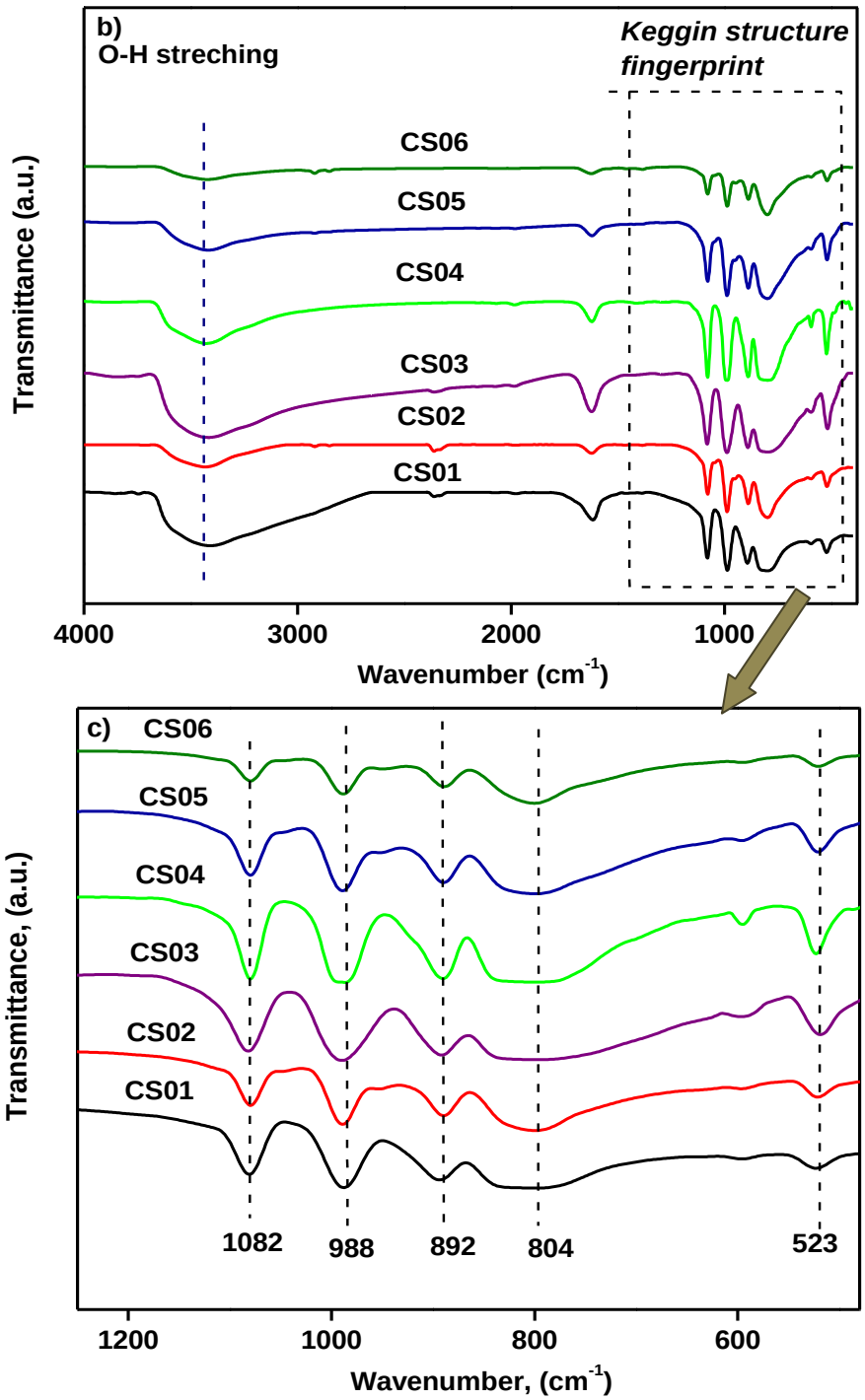

Figure 4.2: (b) Chemical fingerprint displayed from FTIR spectra for the Keggin structure of CS01, CS02, CS03, CS04, CS05 and CS06,

(c) Chemical fingerprint for Keggin anion focused at wavenumber of 1250 -500 cm^{-1} for CS01, CS02, CS03, CS04, CS05 and CS06.

Table 4.4: Assignment characteristic peaks for Keggin structure.

Code	Wavenumber (cm^{-1})	Band assignment	Remarks
i	1082	P-Oa	Oa: oxygen atom bonded to 3 tungsten (W) atoms and to phosphorus (P)
ii	988	W=Ot	Ot: terminal oxygen atom
iii	892	W-Ob-W	Ob: corner sharing bridging oxygen atom
iv	804	W-Oc-W	Oc: edge sharing bridging oxygen atom
v	523	O-P-O	Phosphorus atom is bonded in tetrahedral configuration with oxygen atom.

Keggin anion were constructed through the primary structure (anion structure) that consist of central atom of Phosphorus (P) in a tetrahedral arrangement with Oxygen (O) atoms, and linked together with twelve octahedral oxygen containing Tungsten (W) as addenda atom. Twelve WO_6 formed four group of W_3O_{13} where each of WO_6 shared edges and corner with W_3O_{13} group and central PO_4 respectively through oxygen-bridging. Therefore, FTIR spectra of Keggin anion are consisted of four types of oxygen atoms (1) central oxygen, (2) bridging oxygen- corner, (3) bridging oxygen – edge and (4) terminal oxygen which displayed different vibration frequency.

Cesium salt of tungstophosphoric acid possesses a discrete unit of Keggin network, which is comparatively stable upon substitution mechanism. Consequently, FTIR result shown in Figure 4.2(a) has strongly confirmed that there is no abruption on Keggin domain structure. Based on Table 4.4, the spectra before and after substitution displayed a great similarity with absorption at 1082 cm^{-1}, 988 cm^{-1}, 892 cm^{-1}, 804 cm^{-1} and 523 cm^{-1}. All those absorption are related to asymmetric vibration of P-Oa (Oa is oxygen atoms bonded to three tungsten (W) atoms and to phosphorus (P), W=Ot (Ot is terminal oxygen atom), W-Ob-W (corner sharing bridging oxygen atom), W-Oc-W (edge sharing bridging oxygen atom) and O-P-O vibration respectively. Broad range of asymmetric vibration between 3000 cm^{-1} to 3700 cm^{-1} is assigned to hydroxyl group presence from protonated water cluster, ($H_5O_2^+$) in the catalyst, and later confirmed with the presence of bending vibration at 1620 cm^{-1} due to water molecules (Essayem, Holmqvist, Gayraud, Vedrine, & Ben Taarit, 2001). Based on Figure 4.2(b), O-H asymmetric vibration curve for CS01 at 3000 cm^{-1} to 3700 cm^{-1} is broader compared to CS02, CS03, CS04, CS05 and CS06. This can be further explained in terms of their hydrophobicity, CS03, CS04, CS05 and CS06 are insoluble in water, and CS02 are sparingly soluble in water while CS01 is highly soluble in water. Therefore, CS01 displayed great interaction with water molecules compared to others with the presents

of 6 molecules of crystallization water. Water that mainly refers to water that is found in the crystalline framework of Keggin network.

4.2.3 Nitrogen Physisorption Measurement

Adsorption is the accumulation of liquefied adsorbate molecules onto the surface of an adsorbent. This process creates a liquid film of the adsorbate on the adsorbent's surface, while desorption is a reverse process of adsorption at given temperature and pressure. Adsorption is usually described through adsorption isotherms that are the amount of adsorbate adsorbed/desorbed on/from the adsorbent as a function of its pressure at constant temperature of liquid adsorbate. Brunauer, Emmet and Teller (BET) theory states that the physical adsorptions of gas molecules on the solid surface it serves as the basis for an important analysis technique for the measurement of the specific surface area of a material. The gas molecules are physically adsorbed on the solid layer infinitely with no interaction between the adsorption layers (Fagerlund, 1973).

Fundamentally, when the samples are subjected to BET analysis, the isolated sites on the sample surface begin to adsorb the gas molecules at low pressure. As the gas pressure increases, the coverage of adsorbed molecules increases to form a monolayer. Further increase in the gas pressure will lead to multi-layer coverage where smaller pores in the sample will be filled first. Lastly, a further increase in gas pressure will cause complete coverage of the sample and fill all the pores (Lombardo & Bell, 1991).

The physical absorption- desorption process of nitrogen on external and internal surface areas of a catalyst, and the filling of pores is called physisorption. Nitrogen physisorption technique is carried out at 77 K and widely applied to help reveal the textural properties of the catalyst. It also provides information about surface area and porosity of the catalyst. Generally, large surface area has a positive relationship to

catalyst ability, correspond to higher catalytic activity. The first stage in the interpretation of nitrogen isotherms is the identification of the physisorption mechanism. Surface area and pore size distribution were quantified using Density Functional Theory (DFT) method. All catalyst samples were calcined prior to analysis.

The specific surface area and average pore diameter of all the calcined catalysts are tabulated in Table 4.5, and the isotherms are depicted in Figure 4.3 to Figure 4.6.

Table 4.5: Textural properties of all the catalysts after calcinations.

Catalyst	Cs : H ratio	Particle Size (nm)	S_{BET} (m^2g^{-1})	Average pore diameter (nm)	Total pore volume (cm^3g^{-1})
CS01	0.0:3.0	n.a	1	n.a	0.00
CS02	1.0:2.0	105.7	14	7.5	0.03
CS03	2.0:1.0	91.2	25	5.0	0.05
CS04	2.5:0.5	78.8	115	3.9	0.11
CS05	2.8:0.2	43.8	137	4.1	0.12
CS06	3.0:0.0	37.8	138	4.7	0.14

Typical N_2 adsorption –desorption isotherms measured on the cesium salt of tungstophosphoric acid held at 77 K is characterized by sharp increase in the quantity of N_2 adsorbed at low relative pressure (Figures 4.5 to 4.8), which can be attributed to the filling of micropores (d < 2 nm). The existence of mesopores (2 -50 nm) in cesium salt of tungstophosphoric acid can be inferred from the presence of hysteresis loop in their respective isotherms. Large disparity in the specific surface areas area between CS01, CS02 and CS03 (1-25 m^2g^{-1}) with CS04, CS05 and CS06 (115-138 m^2g^{-1}) were observed.

Ascending value of surface area ranging from non-substituted Cs^+ to fully substituted Cs^+ are illustrated in Table 4.5. The CS04 – CS06 exhibits much higher surface area by an average of 5 fold, which is dramatically higher than 1 m^2g^{-1} determined for CS01. The values listed in Table 4.5 show similarities with other authors (Dias, Caliman, &

Loureiro, 2004). The drastic changes occurred on the surface area of the catalyst is due to the formation of the micropores and losses of mesopores. The total of pore volume also increases with the increase of cesium content (Bond, Frodsham, Jubb, Kozhevnikova, & Kozhevnikov, 2012; Koyano, Ueno, & Misono, 1999; Pizzio & Blanco, 2003). Figure 4.5(a) and Figure 4.6(a) show the difference in micropores and mesopores volume. As the cesium content increase, the volume of mesopores was being suppressed by the development of micropores.

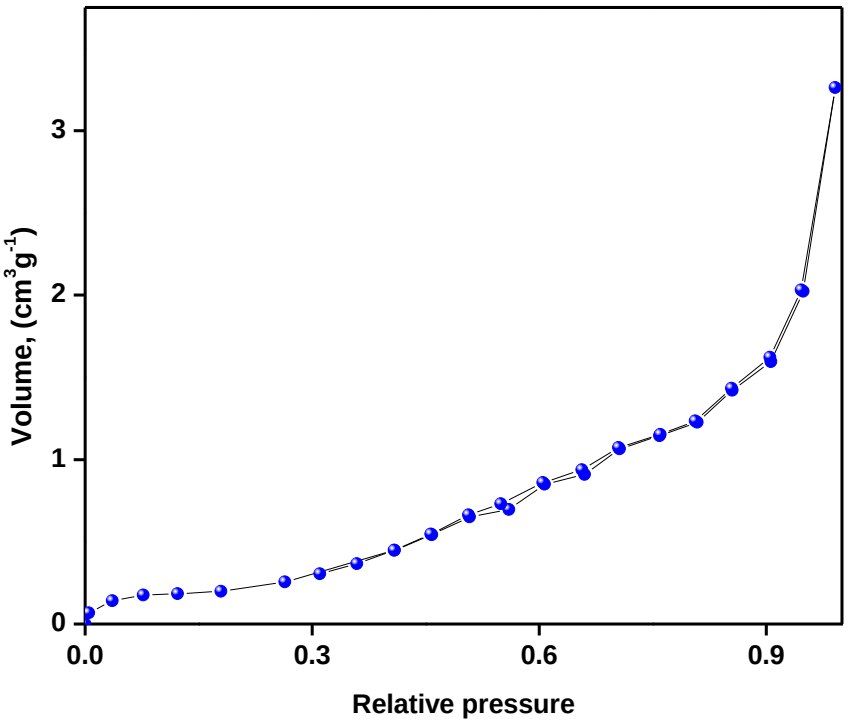

Figure 4.3(a): Nitrogen adsorption-desorption isotherms for CS01

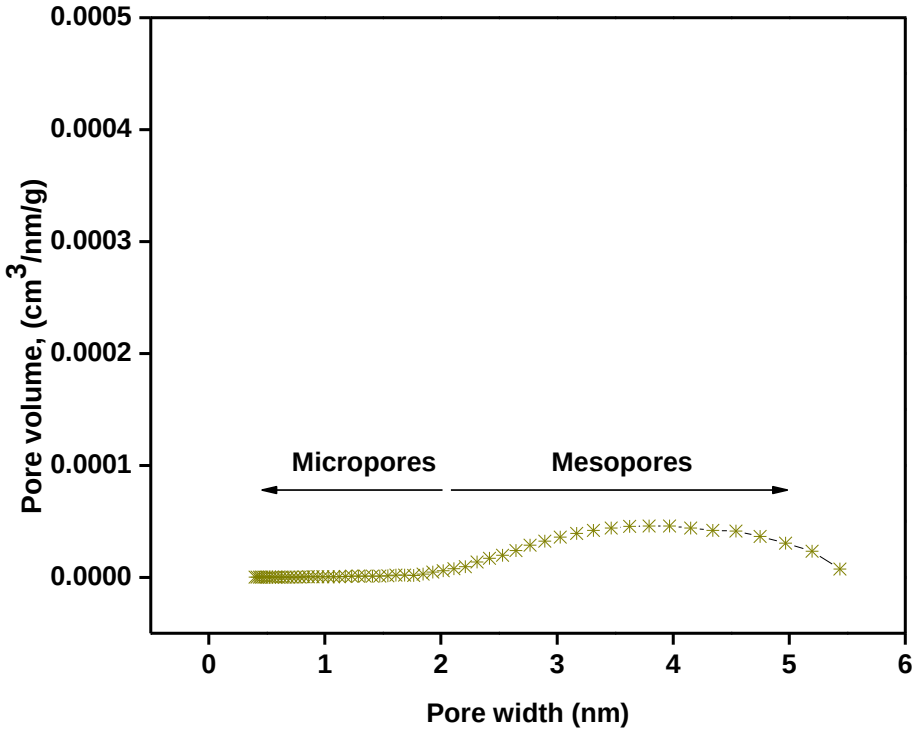

Figure 4.3(b): DFT method for pore size distribution for CS01

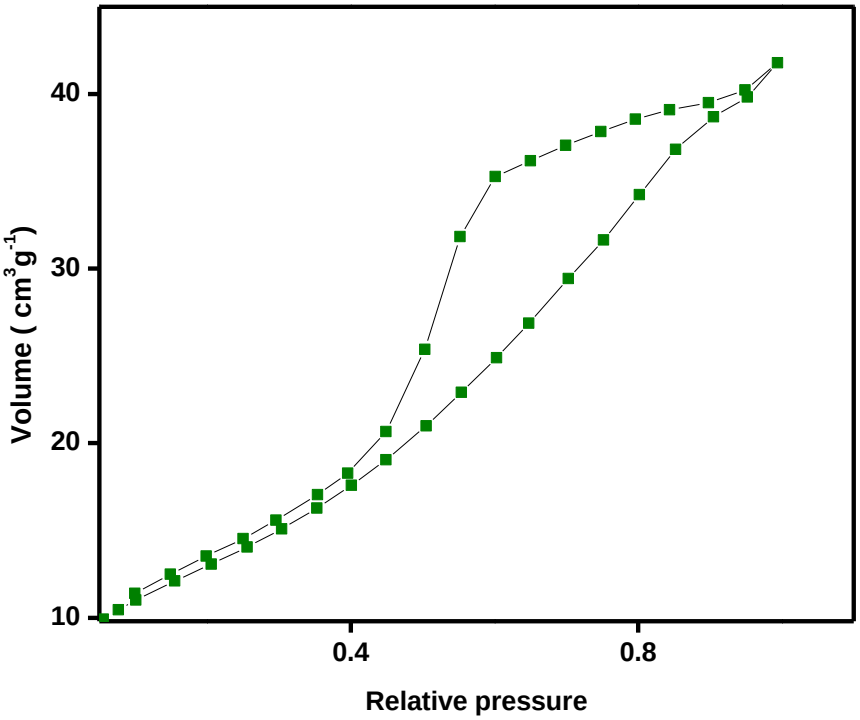

Figure 4.4(a): Nitrogen adsorption-desorption isotherms for CS02

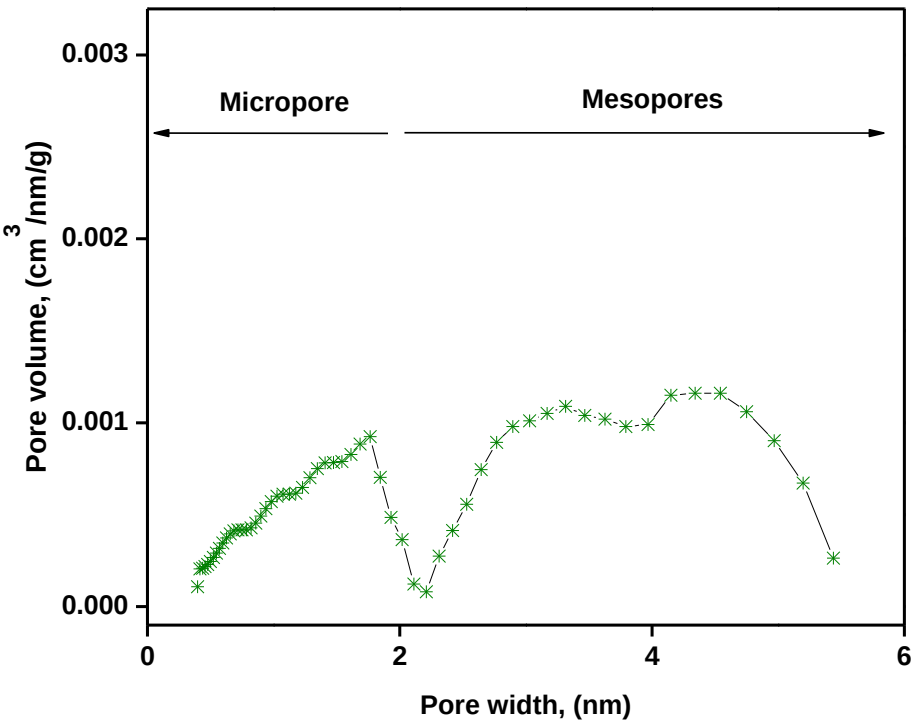

Figure 4.4(b): DFT method for pore size distribution for CS02

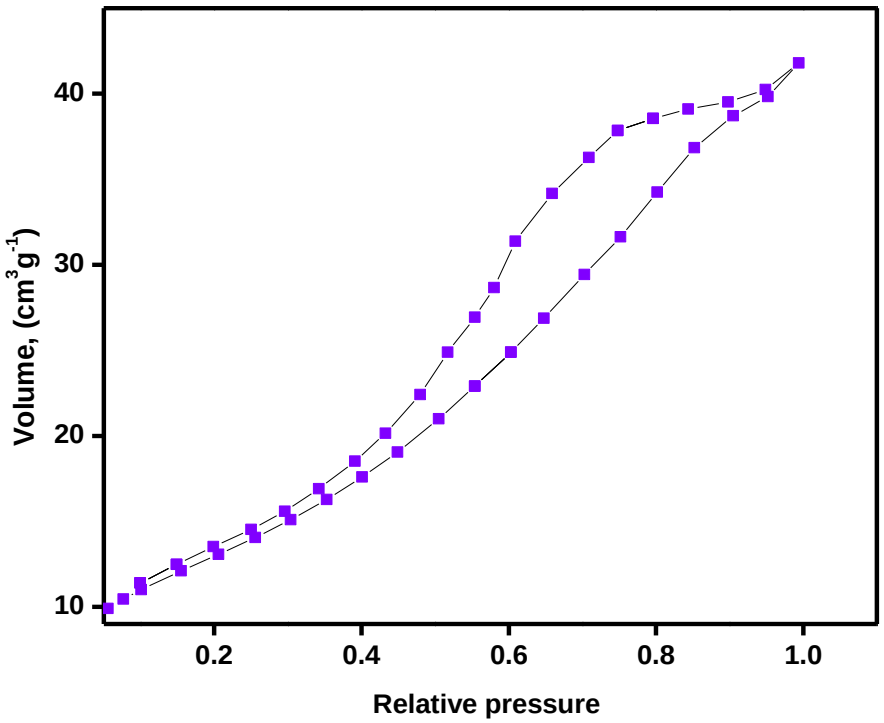

Figure 4.5(a): Nitrogen adsorption-desorption isotherms for CS03

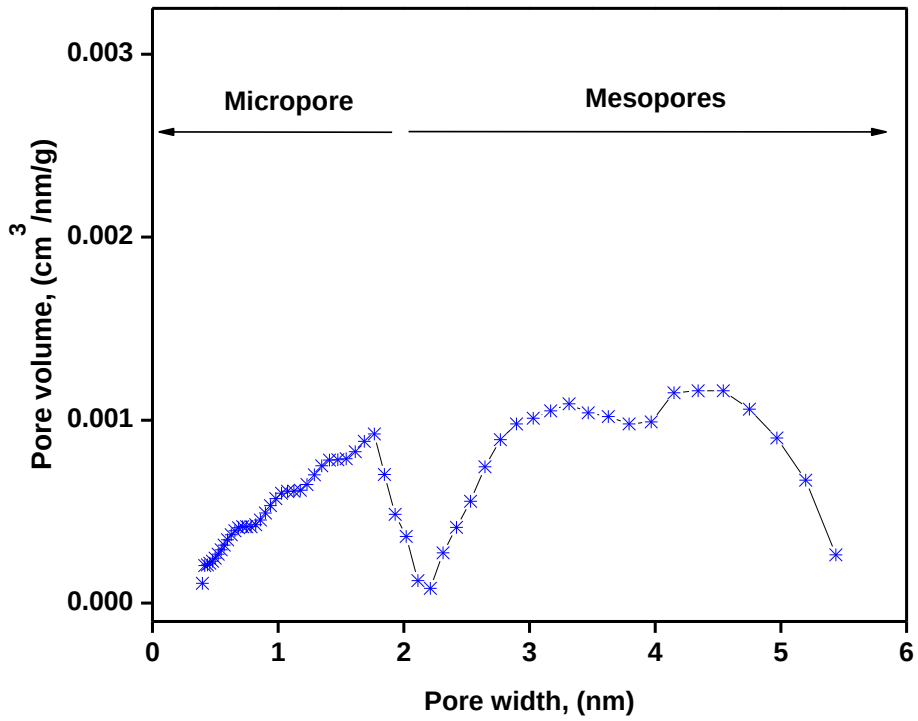

Figure 4.5(b): DFT method for pore size distribution for CS03

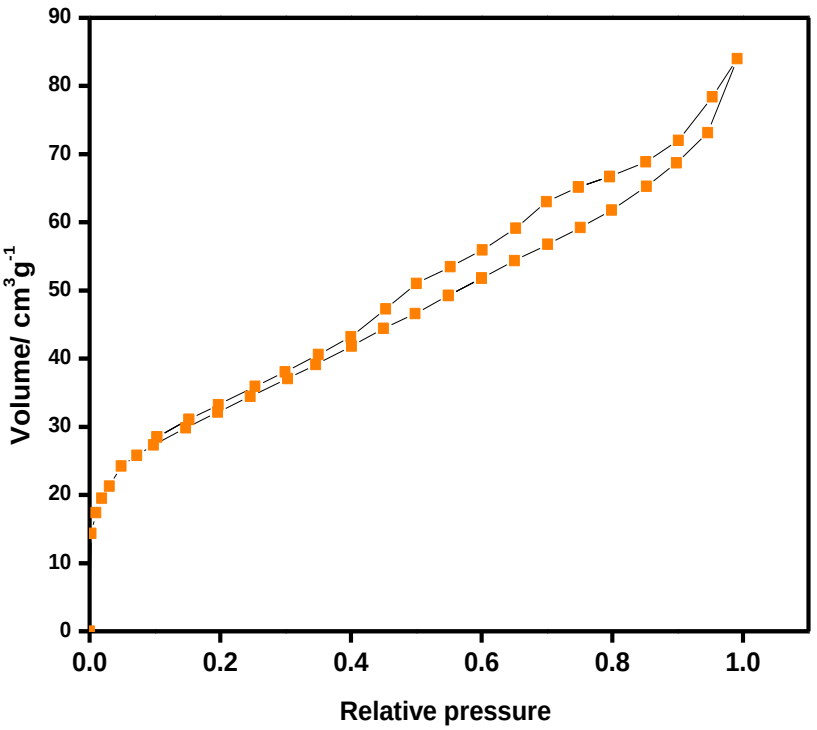

Figure 4.6(a): Nitrogen adsorption-desorption isotherms for CS04

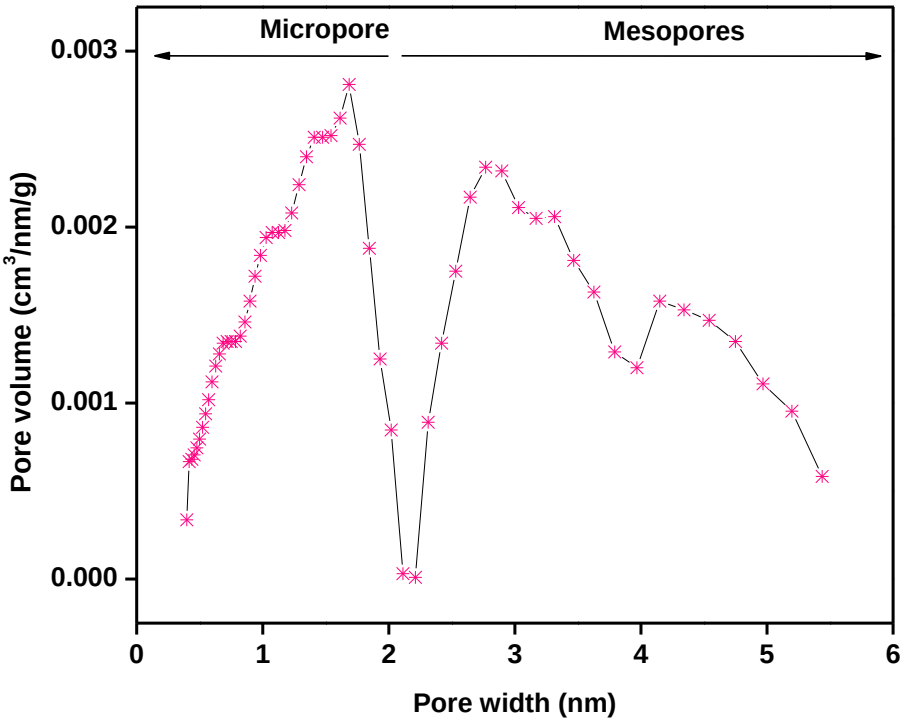

Figure 4.6(b): DFT method for pore size distribution for CS04.

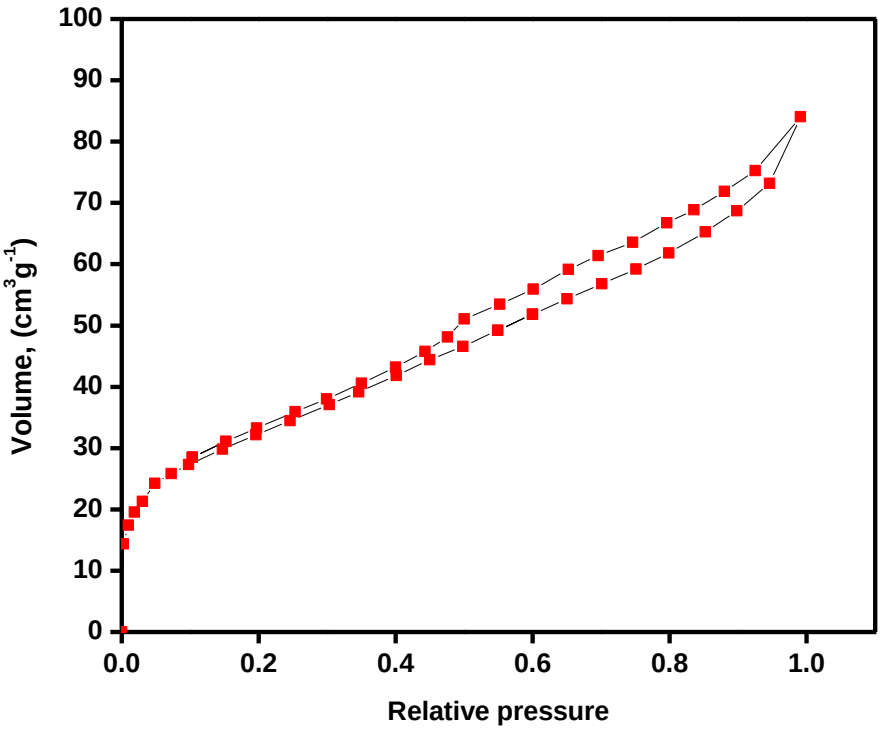

Figure 4.7(a): Nitrogen adsorption-desorption isotherms for CS05

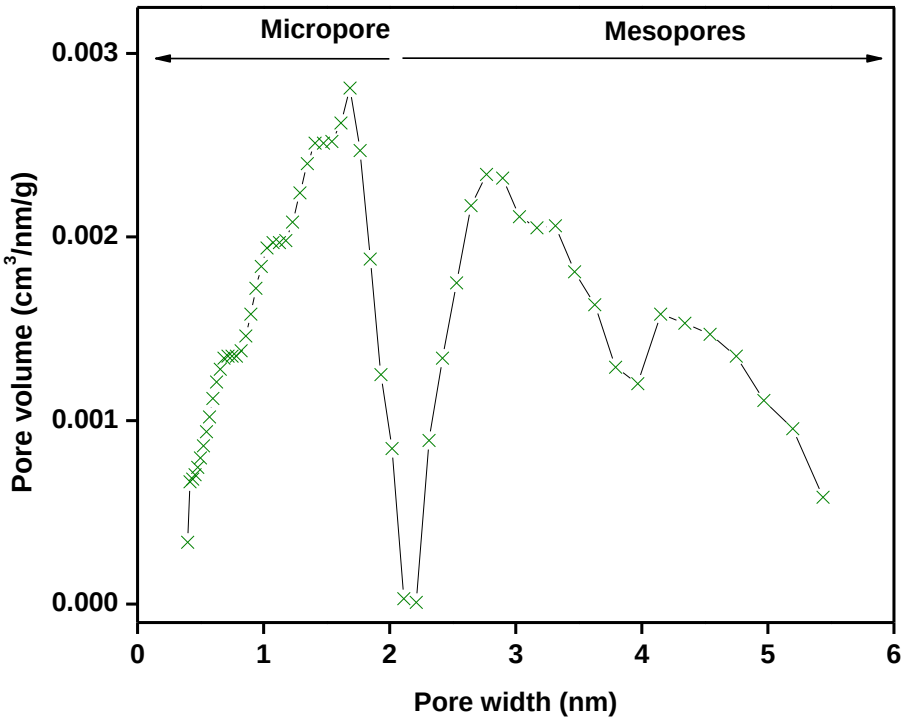

Figure 4.7(b): DFT method for pore size distribution for CS05.

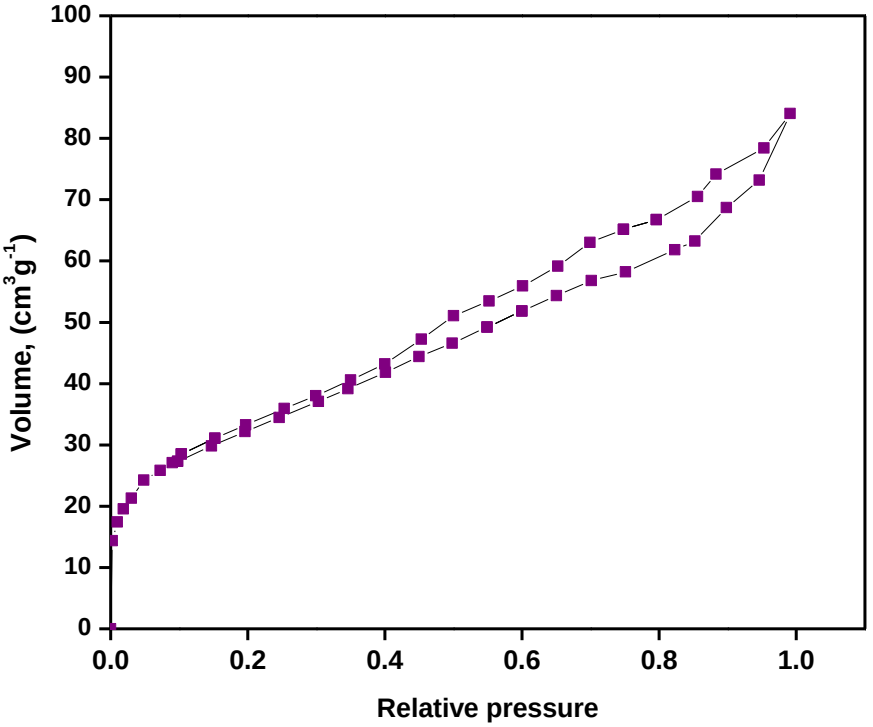

Figure 4.8(a): Nitrogen adsorption-desorption isotherms for CS06

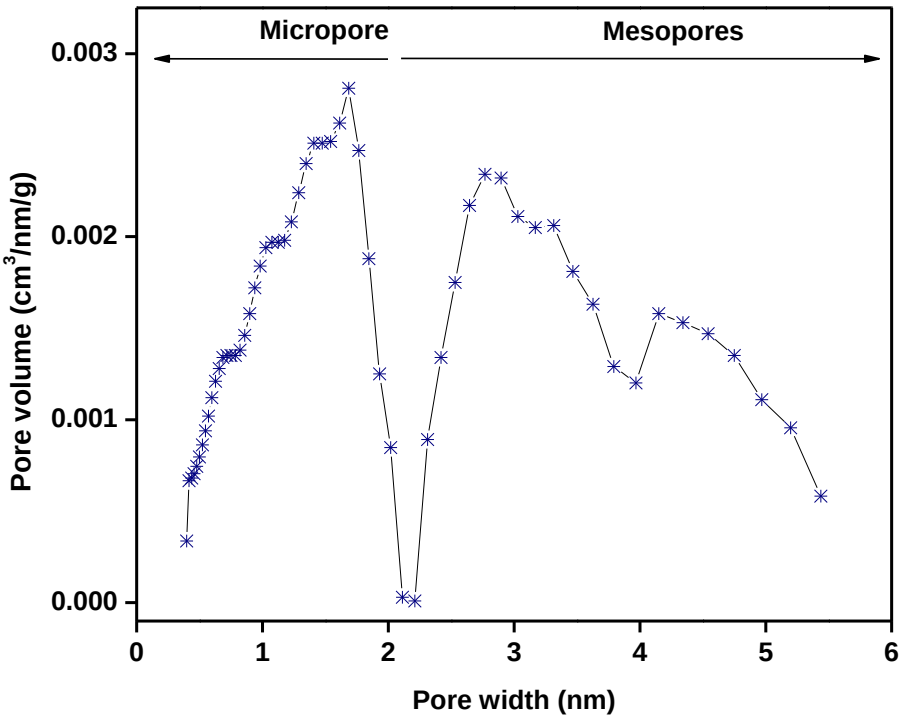

Figure 4.8(b): DFT method for pore size distribution for CS06.

CS01 is non- porous, and it has low surface area and narrow pore distribution. The absent of foreign cation within the Keggin network caused the CS01 to lack of porosity. The high surface area and porosity on the parent acid can be modified by substitution process by controlling the cation contents exchanged within the Keggin anion. This happen due to the difference in cation diameter occupied the substituted place. The non – substituted heteropoly acid shows adsorption isotherms Types II based on IUPAC classification. The non-porous structure of CS01 shows that it possess unrestricted monolayer multilayer adsorption, where the monolayer coverage is completed at low relative pressure.

CS02 has lower cesium: hydrogen content, therefore CS02 displayed isotherms Types IV with H2 hysteresis loop. The volume adsorbed has rapidly increased at low relative pressure due to first energetic region. As the relative pressure reaches unity, a wide hysteresis loop is formed. Capillary condensation occurred at 0.9 partial pressure. Types H2 hysteresis loop are generally found in disordered porous material. In such systems, the distribution of pore sizes and the pore shapes is not well defined or irregular. This statement can be further supported based on SEM images of CS02 in Figure 4.10. A sharp step on the desorption isotherms is usually understood as a sign of interconnection of the pores (percolation). Same explanation can be adopted to CS03.

CS03 and CS04 catalyst have mesopores as well as micropores, which are inter-particle voids of the crystallites. The high catalytic activity of CS04 reported in a lot of solid-liquid petrochemical reaction system is attributed to the strength and number of accessible acid sites and the mesoporous structures that allows rapid transport of reactants and product within the heteropoly acid. Regardless of non- porous Keggin unit, secondary structure of CS04, CS05 and CS06 are consisted of fine particles in

microcrystallite. The aggregation of the microcrystallite has directed to the formation of tertiary structures that possess interstices between particles.

The size of the primary particles (crystallite) has been measured by line width of XRD peaks in Table 4.3. As synthesized, the surface area (m^2g^{-1}) and crystallites size (nm) within the agglomerated powders of CS01 and CS04 are 1 and 115, and 100.7 and 23.0, respectively. Thus, the Cs salts are comprised of aggregates of extremely small crystallites linked together, which in turn build the mesoporosity and microporosity which account of the high surface area. Similar approaches can be adopted for CS05 and CS06.

When the ratio of cesium: hydrogen reached 2, the shape of the adsorbed isotherms shows some similarity with a defined hysteresis loop. CS03, CS04, CS05 and CS06 are referred as Types IV isotherms. Rounded knee indicates approximate location of monolayer formation, the closure at approximately relative pressure ~ 0.2 indicates the presence of small mesopores. The low slope region in the middle of isotherms indicates the first few multilayers. Figure 4.6(a) to Figure 4.8(a) show the presence of higher volume of micropores as compared to mesopores.

Typically, the formations of mesopores are based on the collapse of micropores wall structures. The pore volume sintering can decrease the porosity of the structure. However, in this case, the observed figure has an opposite situation, where the development of micropores increases at the expense of mesopores with Cs substitution. The shrinkage of mesopores porosity happens with the evidence of hysteresis loop at high value of relative pressure. This is because solid heteropoly acid and its salts have a discrete structure which mainly consist of bulk heteropoly anions and counter cation. Substituting smaller size H^+ with a larger size Cs^+ created large effects on its microstructures. Due to the lattice expansion effect, Cs ion that is relatively bigger than

proton occupies bigger interstitial spaces, thus creating more micropores structure and reduces mesopores structure.

4.2.4 Scanning Electron Microscope – Energy Dispersive Electron (SEM-EDX)

SEM technique is an important analysis for developing understanding on the texture and morphology of the catalysts. The electron generated from SEM gun tip interact with the lattice of catalyst subsurface, producing different signal which is detectable and contain information of the catalyst‘s surface topography and composition.

All the images captured were further analyzed using EDX analysis in order to determine the amount of elements in the catalyst. This technique is used in conjunction with SEM. The analysis depth is commonly about 1000 to 2000 nm. Due to the subsurface scattering of the electron beam, the analyzed volume is shaped like a Florence flask with the narrow neck shortened and reaching subsurface volume form which most of the elemental composition data comes. The lateral dimensions tend to be about 1000 nm. One can be caster the electron beam and obtain the average composition over larger too much larger areas, which can relieve the problem of getting accurate average results when all the signal with a point analysis might come from a single particle.

The morphology and elemental analysis in the heteropoly acid and its substituted cesium ion were studied using SEM–EDX. The elemental mapping was being accomplished on the sub- surface of the material. The action was applied to confirm the presence of all elements in the particular synthesized catalyst quantitatively. Figure 4.9 is the parent acid of all the substituted cesium types of catalyst. It has been mentioned previously that pore size of cesium salt of tungstophosphoric acid can be specifically controlled by substituting different cation content within the Keggin unit. As a result, the original microstructure of the catalyst has been altered and was further confirmed through SEM micrograph.

Based on Figure 4.9, the surface of CS01 is smooth and flat. Obviously, no porosity was observed in CS01 images. The micrograph confirmed the low surface area/porosity from BET adsorption isotherm. The low surface area and low porosity obtained are in agreement with the SEM images captured. Upon cesium substitution process, the morphology and the surface texture of each catalyst changes drastically. When the Cs: H ratio started to increase, for example Cs:H = 1:2, the surface morphology of the catalyst has transformed into a rougher surface. However, further increase of cesium content in the Keggin network from 2 to 3 somehow transforms the catalyst into crystalline spherical particles. In CS04- CS09, at 40 000x magnification, the presence of small and spherical shape with size about 90 nm was observed. The formation of the spherical shapes has created an irregular texture on the surface which resulting excellent porosity compared to its parent acid. The replacement of small cation (H) with big cation (Cs) give a crystalline HPA with defined geometry of bigger cation into a smaller interstitial space serves by the proton change has increased the roughness of the catalyst surface. The big different in cation diameter has significantly modified the roughness of that surface.

EDX analyses were also performed to observe elemental composition of the samples. The EDX spectrum of $H_3PW_{12}O_{40}$ and its salt showed the presence of P, W, O and Cs. Based on Table 4.6, the commercial parent acid of $H_3PW_{12}O_{40,}$ showed the elemental ratio of $PW_{12}O_{39.3}$. The results obtained are in good agreement with the theoretical value. This indicates that the synthesis procedure and catalyst activations did not lead to leaching. The Keggin anion remains the same without any changes of chemical formula as well as chemical structure. The only exchangeable unit involved during the process is Cs and H. Cs experimental values are crucial in defining the overall chemical formula.

Therefore, based on Table 4.6 to Table 4.11, the given atomic percent of Cs element represent almost 96 % accuracy of the real value. This can be confirmed though the

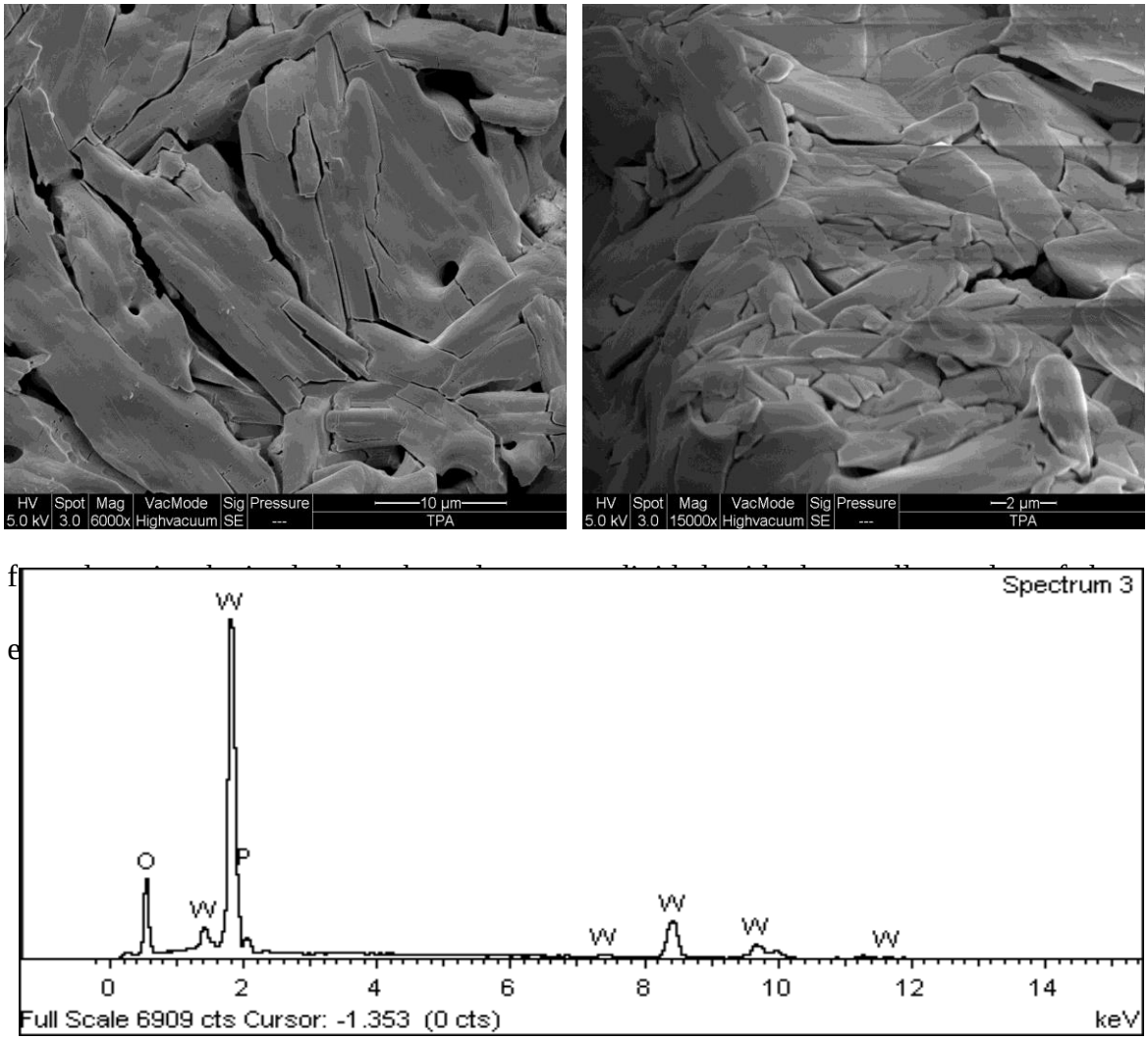

Figure 4.9: SEM –EDX images of CS01

Table 4.6: Atomic % of $H_3PW_{12}O_{40}$

Element	Symbol	Average atomic weight (%)	Element ratio	Theoritical ratio
Phosphorus	P	1.91	1.0	1
Tungsten	W	22.96	12.0	12.0
Oxygen	O	75.13	39.3	40.0

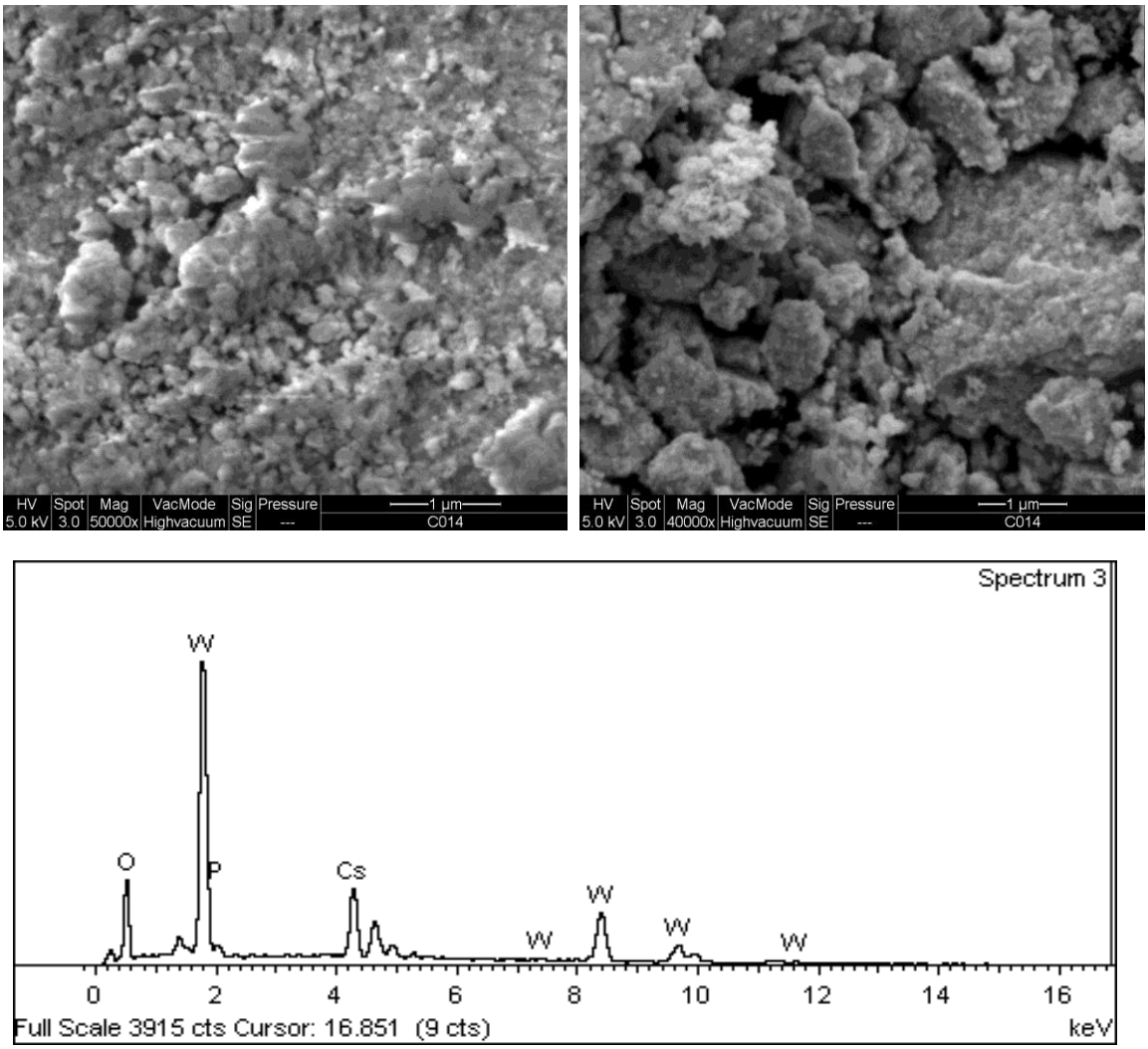

Figure 4.10: SEM-EDX images for CS02

Table 4.7: Atomic % of $Cs_1H_2PW_{12}O_{40}$

Element	Symbol	Average atomic weight (%)	Element ratio	Theoritical ratio
Cesium	Cs	1.94	1.0	1.0
Phosphorus	P	2.01	1.0	1.0
Tungsten	W	22.11	11.4	12.0
Oxygen	O	73.94	38.1	40.0

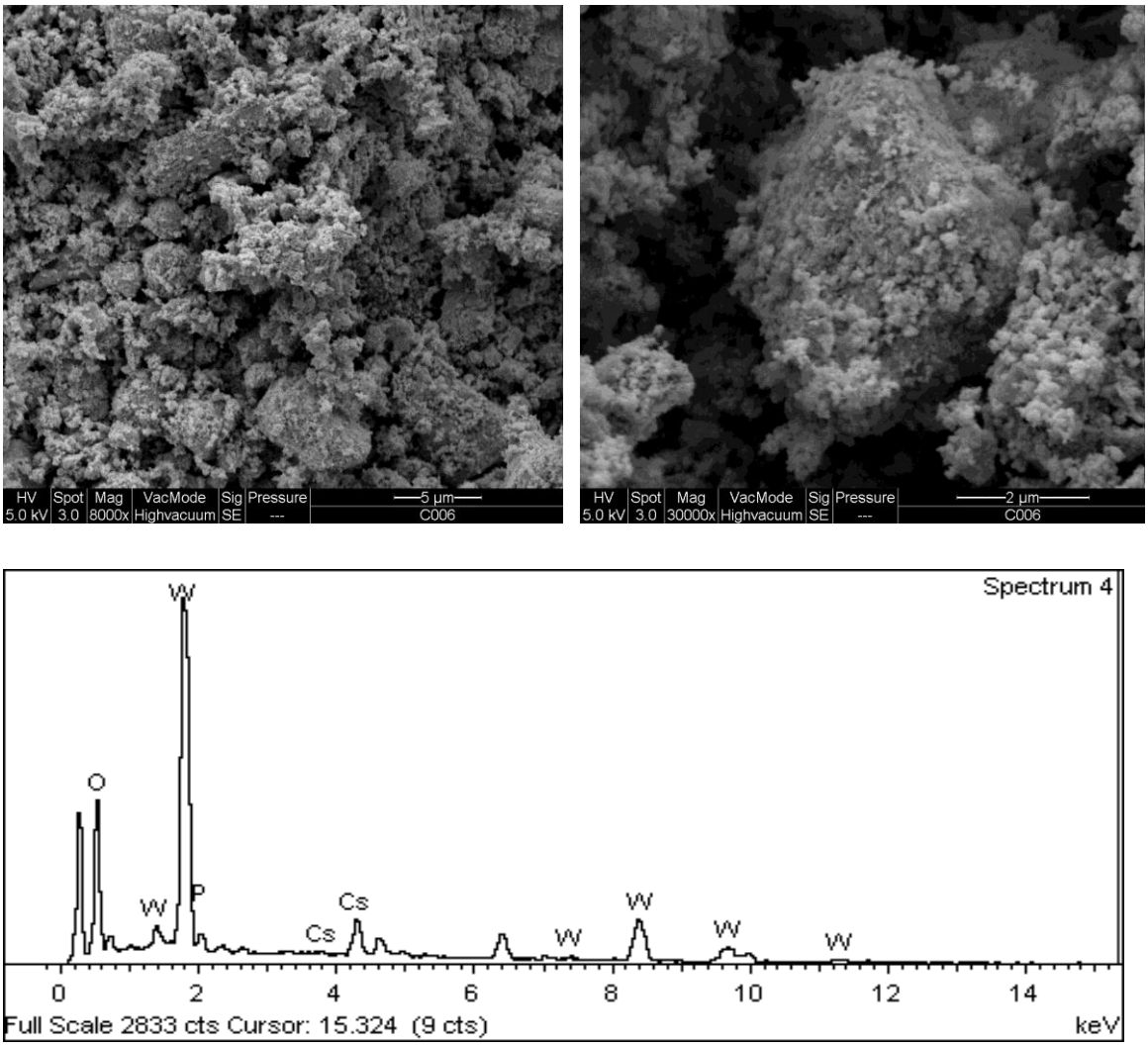

Figure 4.11: SEM-EDX images for CS03

Table 4.8: Atomic % of $Cs_2H_1\ PW_{12}O_{40}$

Element	Symbol	Average atomic weight (%)	Element ratio	Theoritical ratio
Cesium	Cs	3.98	2.0	2.0
Phosphorus	P	1.99	1.0	1.0
Tungsten	W	23.88	12.0	12.0
Oxygen	O	70.15	35.3	40.0

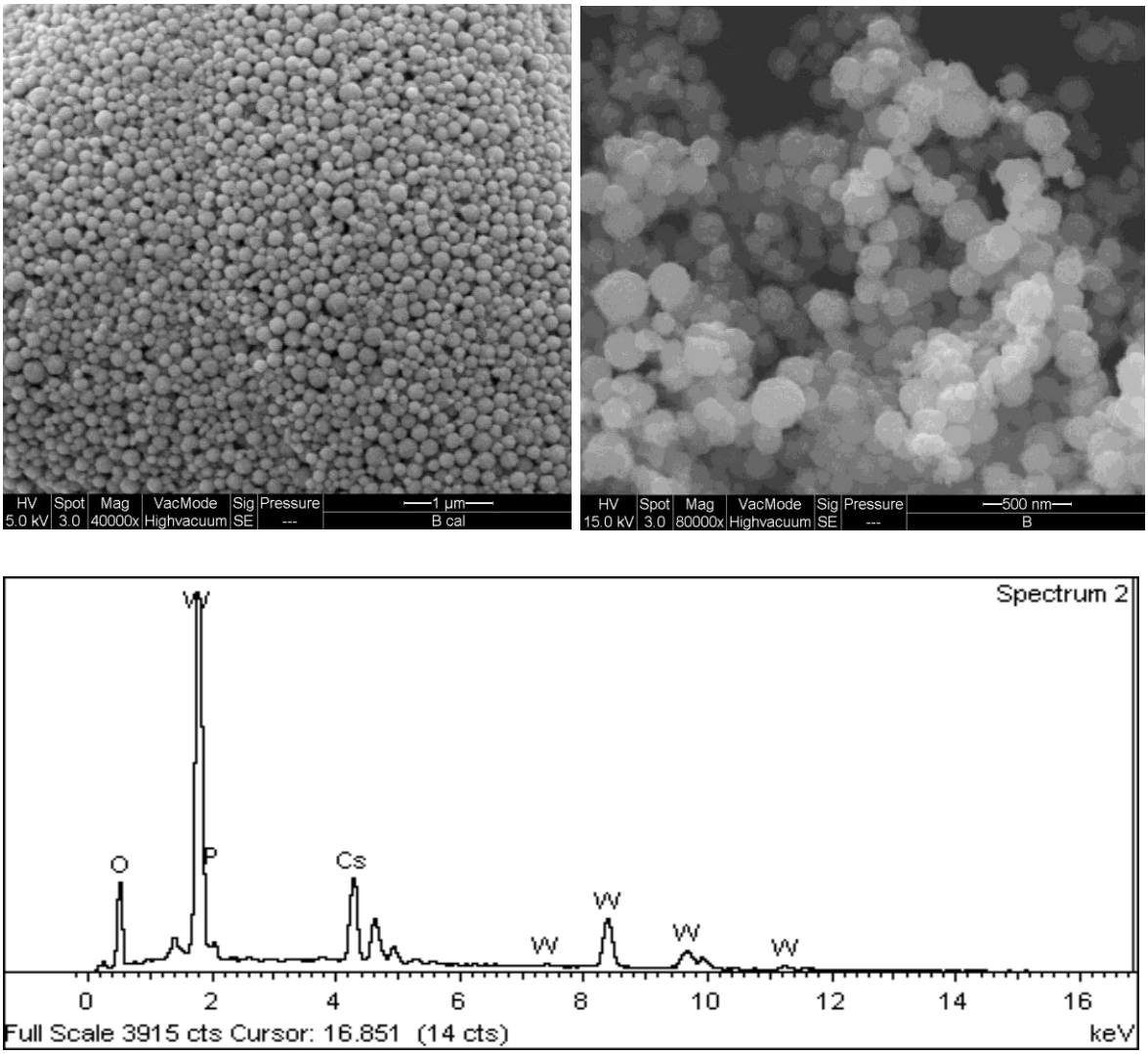

Figure 4.12: SEM-EDX images for CS04

Table 4.9: Atomic % of $Cs_{2.5}H_{0.5}PW_{12}O_{40}$

Element	Symbol	Average atomic weight (%)	Element ratio	Theoritical ratio
Cesium	Cs	4.78	2.4	2.5
Phosphorus	P	1.99	1.0	1.0
Tungsten	W	23.51	11.8	12.0
Oxygen	O	69.72	35.0	40.0

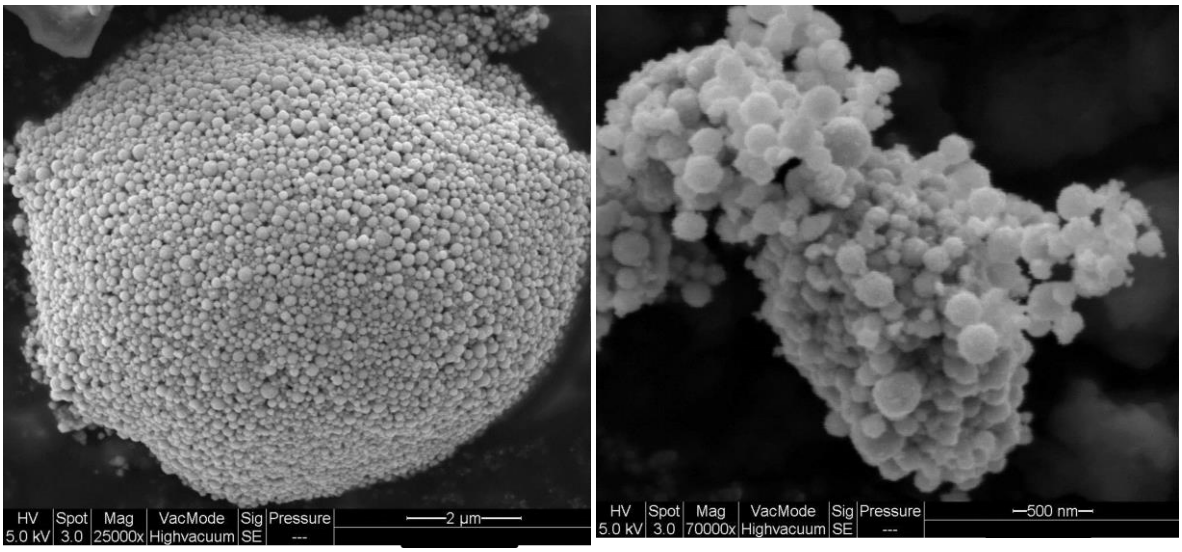

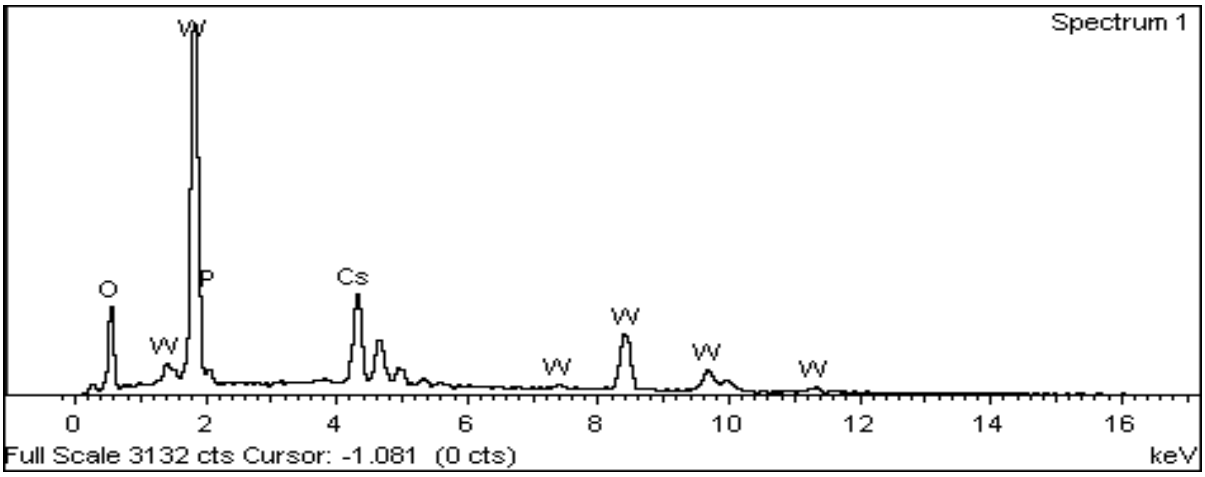

Figure 4.13: SEM-EDX images for CS05

Table 4.10: Atomic % of $Cs_{2.8}H_{0.2}PW_{12}O_{40}$

Element	Symbol	Average atomic weight (%)	Element ratio	Theoritical ratio
Cesium	Cs	5.46	2.8	2.8
Phosphorus	P	1.95	1.0	1.0
Tungsten	W	23.4	11.8	12.0
Oxygen	O	69.19	35.5	40.0

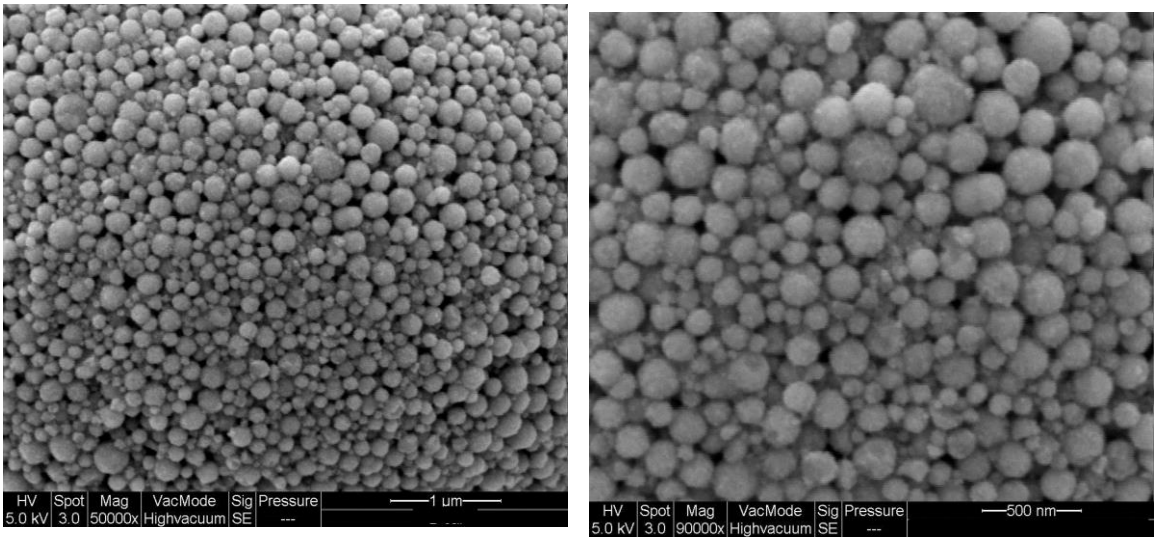

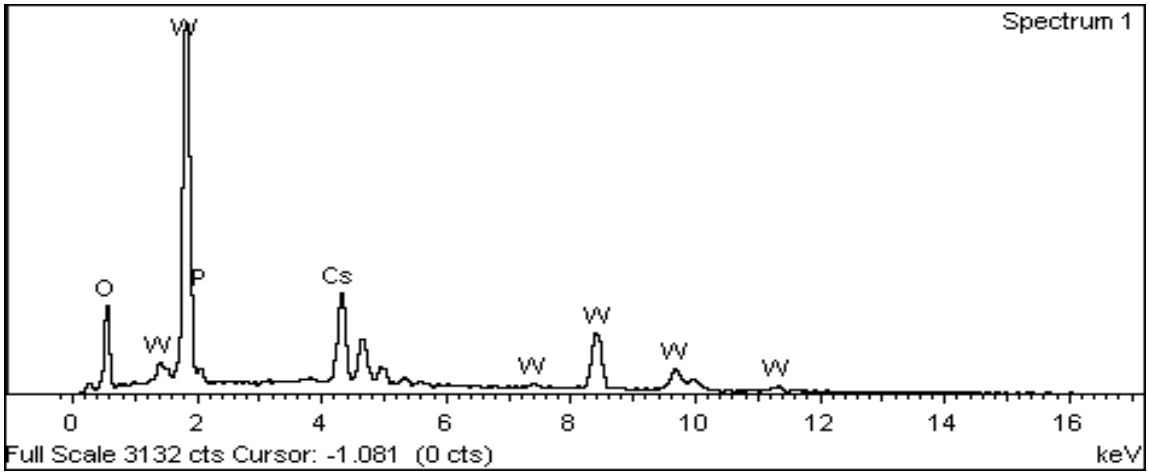

Figure 4.14: SEM-EDX images for CS06

Table 4.11: Atomic % of $Cs_3H_0PW_{12}O_{40}$

Element	Symbol	Average atomic weight (%)	Element ratio	Theoritical ratio
Cesium	Cs	5.89	3.0	3.0
Phosphorus	P	1.99	1.0	1.0
Tungsten	W	18.11	9.5	12.0
Oxygen	O	74.01	37.2	40.0

4.3 Thermal Analysis

4.3.1 Thermogravimetric Analysis – Mass spectroscopy (TGA-MS)

TGA coupled with mass spectrometer (TG-MS) helps to identify the number of chemical reaction taken place under a specific temperature programme. It will allow us to discover the decomposition process involving evaporation of water molecules and ligands or drying process. Equation 4.2 shows the possible product gained when the catalyst is subjected to heat under oxidizing environment. Therefore, the existence of mass spectrometer is important and crucial in order to confirm the particular gaseous compound evolved during the heating process.

It is very useful to record the first derivatives of TGA curve (DTG) for tracking any changes in weight loss during the process. It can clearly revealed changes to the samples when subjected to heat treatment under specific environment. Plus, DTG curve also illustrated the inflection point where the highest weight loss has occurred during heating process.

The analysis was carried out in air in order to allow direct comparison with the real calcination condition. The analysis was accomplished to all the precursor samples. The observed weight losses accompanied for all the catalyst is tabulated in Table 4.12 while thermogram of TGA-DTG are shown in Figures 4.15 and 4.16. Mass spectrometer data were selected based on the major peaks which indicate the present of any gaseous product released within the temperature range during the weight loss.

$$PW_{12}O_{40}^{3-} \rightarrow WO_3 + P_2O_5 \quad \text{..... (Equation 4.2)}$$

Table 4.12: Weight losses at various steps and temperature as obtained from thermal analysis data.

Precursor	TGA						
	1st weight loss		2nd weight loss		3rd weight loss		Residue (%)
	Ts (°C)	Wt loss (%)	Ts (°C)	Wt loss (%)	Ts (°C)	Wt loss (%)	
CS01	25-113	0.40	113-298	3.44	313-544	1.09	95.07
CS02	25-168	1.33	-	-	305-632	0.32	98.35
CS04	25-177	2.02	-	-	305-632	0.71	97.27
CS06	25-82	2.15	-	-	305-632	1.70	96.15

TGA analysis is crucial in understanding the behavior of certain material under specific temperature programme. The correct calcination temperature on weight loss was revealed through TGA thermogram (Figure 4.15).

Early mass losses at temperature below 100 °C corresponds to evaporation of loose and physisorbed water on the catalyst surface (Xian-e et al., 1997). The observation is supported by the mass spectrometer (MS) result at mass number (m/e) of 18 that correspond to water molecule released. Quantity of water released at the early stage varies since it is not easy to control the amount of water during synthesis of cesium salt of tungstophosphoric acid.

Second weight loss, at 113 - 298 °C, is attributed to weight from coordinated or crystalline water. It accounted for the loss of 6 moles of H_2O molecules per Keggin unit equivalent to dehydration of a stable hexahydrate $H_3PW_{12}O_{40}.6H_2O$. The amount of crystal water identified through a thermal analysis method shows similarities with the broad curve of hydroxyl group fingerprint detected at ~ 3400 cm^{-1} (Misono, 2013). This behavior is only observed in CS01, and not in other substituted cesium salt samples, CS02- CS06. The weight losses were not observed in that catalyst's sample

because the substituted cesium salt catalyst did not contain any coordinated or crystalline water.

Water molecules and acidic proton are linked together through hydrogen bonding. Temperature range of 313 – 544 °C centered at about 450 °C corresponds to the loss of acidic proton through expatriation of constitutional water (water that formed from H^+ and the terminal oxygen of $[PW_{12}O_{40}]^{3-}$) and prior to collapse of the Keggin structure through the formation of WO_3 and P_2O_5. Both WO_3 and P_2O_5 are not detectable in the mass spectrometer due to the limitation of the instrument atomic mass capability (Sasca et al., 2013).

That 3rd weight loss (temperature range of 313 – 544 °C) for CS02, CS04 and CS06 are ascribed to the thermal stability of HPA catalysts. It shows that all the catalysts exhibit similar degradation temperature range. Thermal degradation of Keggin anion is accompanied by the collapse of its Keggin structure. The beginning of the decomposition of the intermediate PW_{12} anion, to what is possible as final mixtures of oxides, occurs at temperature near 305 °C and its complete degradation is observed at higher temperatures (Gamelas et al., 1999).

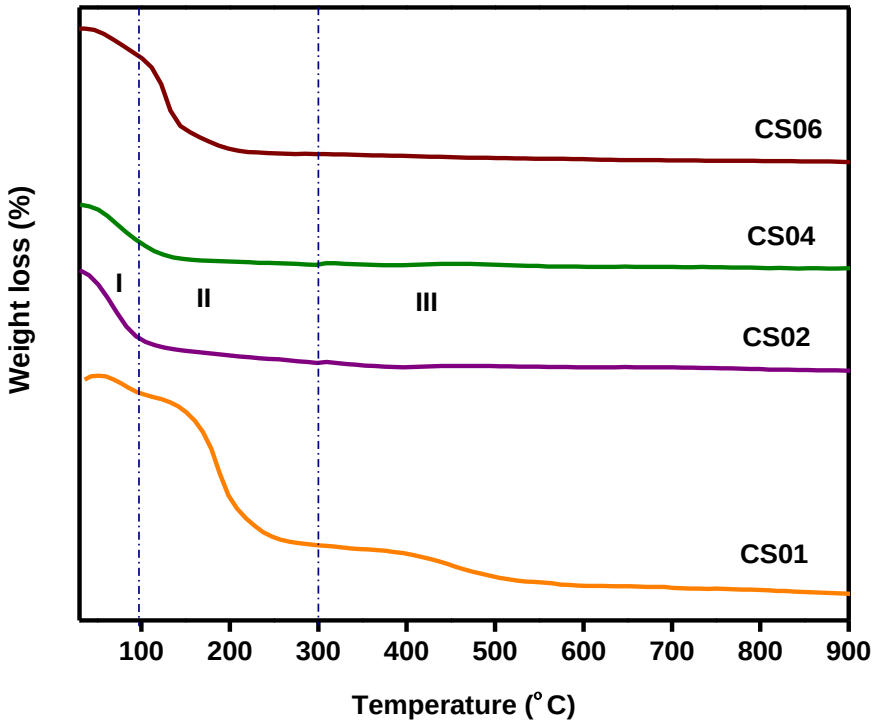

Figure 4.15: TGA thermogram for precursor CS01, CS02, CS04 and CS06.

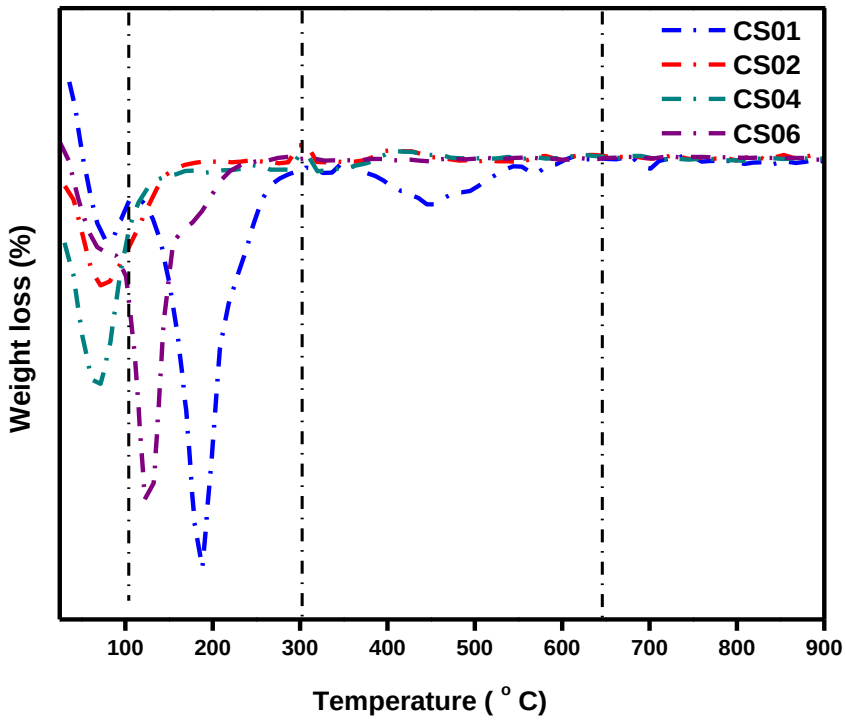

Figure 4.16: DTG thermogram for precursor CS01, CS02, CS04 and CS06.

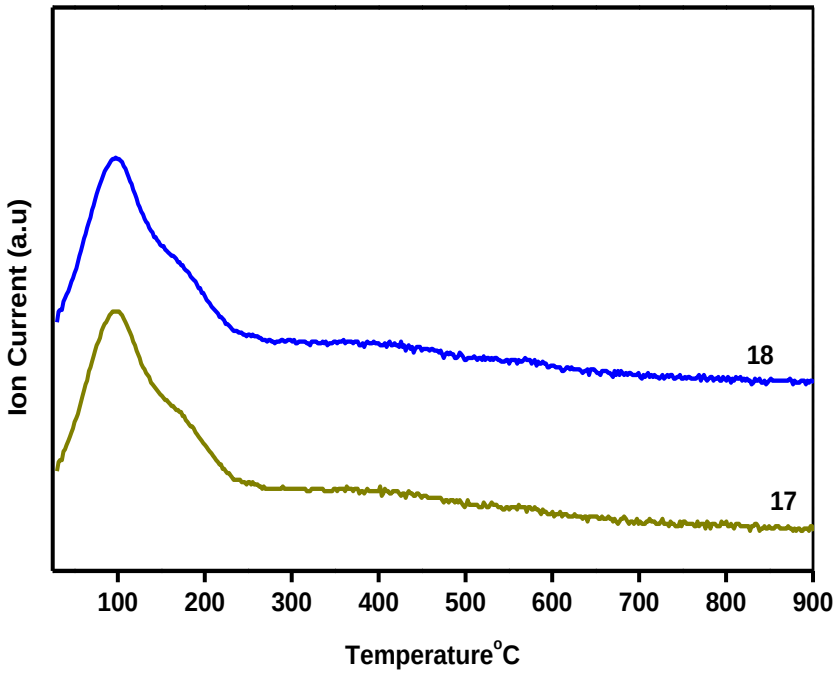

Figure 4.17: Mass spectroscopic analysis of gaseous products generated during TGA analysis for all precursors (CS02 – CS06).

4.4 Discussion and summary

Catalysis by heteropoly acids (HPAs) and their compounds is a field of increasing interest and attention worldwide. It is known that, HPAs are generally applied as catalysts in commercially important process such as hydro cracking, hydrogenation and isomerization. HPA, 12- tungstophosphoric acid, $H_3PW_{12}O_{40}$, (TPA) is known as a strong Bronsted acid. The substitution of proton with other cation such as Cs^+ reduces the number of acid sites but increase acid strength. The substitution of small cation (H^+) with a bigger cation (Cs^+) changes the morphology and porosity of HPA catalysts drastically. It increases microporosity at the expense of mesoporosity due to the big differences in cation diameter during the substitution process. It has significantly leaded to high surface area as well as increasing surface hydrophobicity. In this study, the effect of cesium content was evaluated by preparing the catalyst with different cesium

content, $Cs_xH_{3-x}PW_{12}O_{40}$ (x = 1, 2, 2.5, 2.8 and 3) and characterization was performed using FTIR, XRD, BET, SEM- EDX and TGA.

The entire synthesized compounds (CS03-CS06) have a cubic crystal structure. The XRD patterns are in full agreement with other published reports. The width of the diffraction maxima increase with the increase of Cs: H ratio. This could be an effect of the crystallite size changes with the chemical composition. The crystallites size decrease from 100 nm to 23 nm as the Cs loading increases. As expected, substitution of acidic proton with larger monovalent cation has changed the physical properties of TPA as well as its acidity. Higher cesium content has decreased the acid properties of $Cs_xH_{3-x}PW_{12}O_{40}$ in terms of pH value (Table 4.1). The biggest difference that has taken place over the substitution process is the surface area. Higher cesium content has caused the surface area to increase from 1 m^2g^{-1} to 138 m^2g^{-1} with excellent porosity. The chemical structure of Keggin network remains unchanged after the exchanging process occurred. The FTIR spectrum of Cs-TPA salts exhibits similar characteristic bands compared with the pure TPA. This can be concluded that the substitution process has not caused any disruption on the integrity of Keggin structure. The morphological analysis of substituted cesium atom was studied, and the images generated has revealed that when the ratio of Cs to H is bigger than 2, the roughness of the surface increases. Generally, the substitution process has drastically changed the smoothness and the flatness of TPA surface into uneven and high porosity material. It can be clearly seen in Figure 4.9 to Figure 4.11, $Cs_{2.5}$ to Cs_3 are having irregular shape with well-defined spherical shape. BET measurements showed an abrupt increase in the specific surface area with the increase in Cs content. The images shown in SEM also showed a great correlation with the surface area values obtained by BET analysis. A laser diffraction technique afforded the size of all the synthesized $Cs_xH_{3-x}PW_{12}O_{40.}$ The particle size distribution of all the substituted Cs in tungstophosphoric acid varies between 70 – 100 nm. The particles size

obtained does not represent the real crystallites size of the catalyst this is due to the formation of secondary and the tertiary structure of $Cs_xH_{3-x}PW_{12}O_{40}$. It was found that the average crystallite size of all synthesized $Cs_xH_{3-x}PW_{12}O_{40}$ is approximately the same with the value of 30 nm.

The most important factor that needs to be accounted during cellulose depolymerization is catalyst acidity. TPA will be the best candidate in the process due to its acidity and high interaction with water molecules. The hydrophilicity characteristic of TPA makes it highly soluble in water and generates concentrated hydronium ion. Among a lot of synthesized $Cs_xH_{3-x}PW_{12}O_{40,}$ the acceptable cesium: hydrogen ratio is 1: 2 for cellulose depolymerization, and other ratio selected for catalytic screening of cellulose depolymerization is $Cs_{2.5}$ and Cs_3.

The rationale of choosing $Cs_{2.5}$ and Cs_3 are to demonstrate the Bronsted acid properties from both catalysts in catalyzing the cellulose depolymerization. It was shown in the chemical formula that Cs^+ ions are completely settled in $Cs_3PW_{12}O_{40}$ salt and not showing any bronsted acidity. Thus, explained the absence of acidic proton which employed to a lower acidity behavior reflected to $Cs_3PW_{12}O_{40.}$ Excellent interaction of $H_3PW_{12}O_{40}$ with the water molecules has increased the concentrations of ionizable proton in the reaction medium. Hence make it a preferable choice for the depolymerization of cellulose.

PART B- Catalytic Reaction of Cellulose to Nanocellulose

4.5 Catalytic depolymerization of cellulose to nanocellulose

The reasonable way to avoid the aforementioned issues such as depletion of non-renewable resources is to fully utilize the renewable resources produces from oil palm tree. Large amount of biomass was produced from oil palm tree industry every year. The utilization of oil palm tree biomass is one of the best methods to reduce the amount of waste generated from that industry. Biomass mainly consists of cellulose, hemicellulose, and lignin. One of the easiest ways to upgrade biomass into high value material is to depolymerize the cellulose into nano-scale dimension. Nano-structured cellulose or nanocellulose is the target material rather than glucose or others value-added chemicals derived from cellulose.

Cellulose is a linear polymer with a chemical formula of $(C_6H_{10}O_5)n$, where n is the repeating units. Cellulose is distinguished from other polymer of glucose by 1, 4-β-glycosidic bonds which also leads it to a straight chain structure. The 1, 4-β- glycosidic bonds enables an intense intramolecular H-bonding among the groups around the glycosidic bond. As a result, the cellulose polymer sheets are stacked on one another connected together by Van der Waals forces which lead it to a supramolecular structure that form a crystalline domain of cellulose microfibrils (Rinaldi & Schüth, 2009). Along the same microfibril, the amorphous regions are also present and are highly exposed to chemical changes with ease compared to crystalline domain. In any chemical reaction, only exposed cellulosic chains of the microfibrils are easily accessible to chemical, enzyme and catalyst. For that reason, the hydrolysis degree of cellulose is relatively low compared to other natural polymer.

The main strategy for the production of nanocellulose is based on the synergy effect of mechanical enhancement and catalysis. The contribution of both aspects is expected to

create a good quality of nanocellulose with higher yield. A mechanical treatment applied during the reaction will help in defibrillation of cellulose polymer chain into a less complex structure. The effect of sonication power and time are crucial in determining the best reaction condition in obtaining nanocellulose. However, introduction of heteropoly acid as a catalyst during the mechanical treatment will also help the process of fiber fragmentation which helps to increase the quality of the nanocellulose produced.

4.5.1 Catalyst screening

The process of cellulose depolymerization through aid of ultrasonication was investigated during the catalytic reaction. The standard reaction conditions were at 10 minutes with 225 watt output power. Based on Table 4.13, the appearances of the products were observed as white in color.

Based on the physical appearance of the product produced after the process, it is clearly observed that the initial two distinct layers of water and cellulose were converted into homogeneous gel-like solution. The appearance of non-settling turbidity in the colloidal suspension was a definite indication on formation of nano-scale cellulose. The viscosity of the homogeneous solution was also being observed through its physical appearance. It shows that the homogenous solution is highly viscous compared to the previous solution (Figure 4.18(a)). The inference was strengthened through the illustration captured in Figure 4.18. High intensity ultrasonication applied to the cellulose colloidal has converted it into highly dispersed colloidal suspension. This is because, the energy generated has significantly loosened and weakens the hydrogen bond underlying between the cellulose polymer chains.

Different ultrasonication power and time introduced to the reaction were studied as there are very crucial in determining the efficiency of the process. The early

determining steps in confirming the product formed from the process are through surface tension and surface charge analysis. The surface charge analysis was examined using zeta potential where the movements of negatively charged hydroxyl groups were tracked. Based on the results obtained, all the nanocellulose surface charge shows a negative sign.

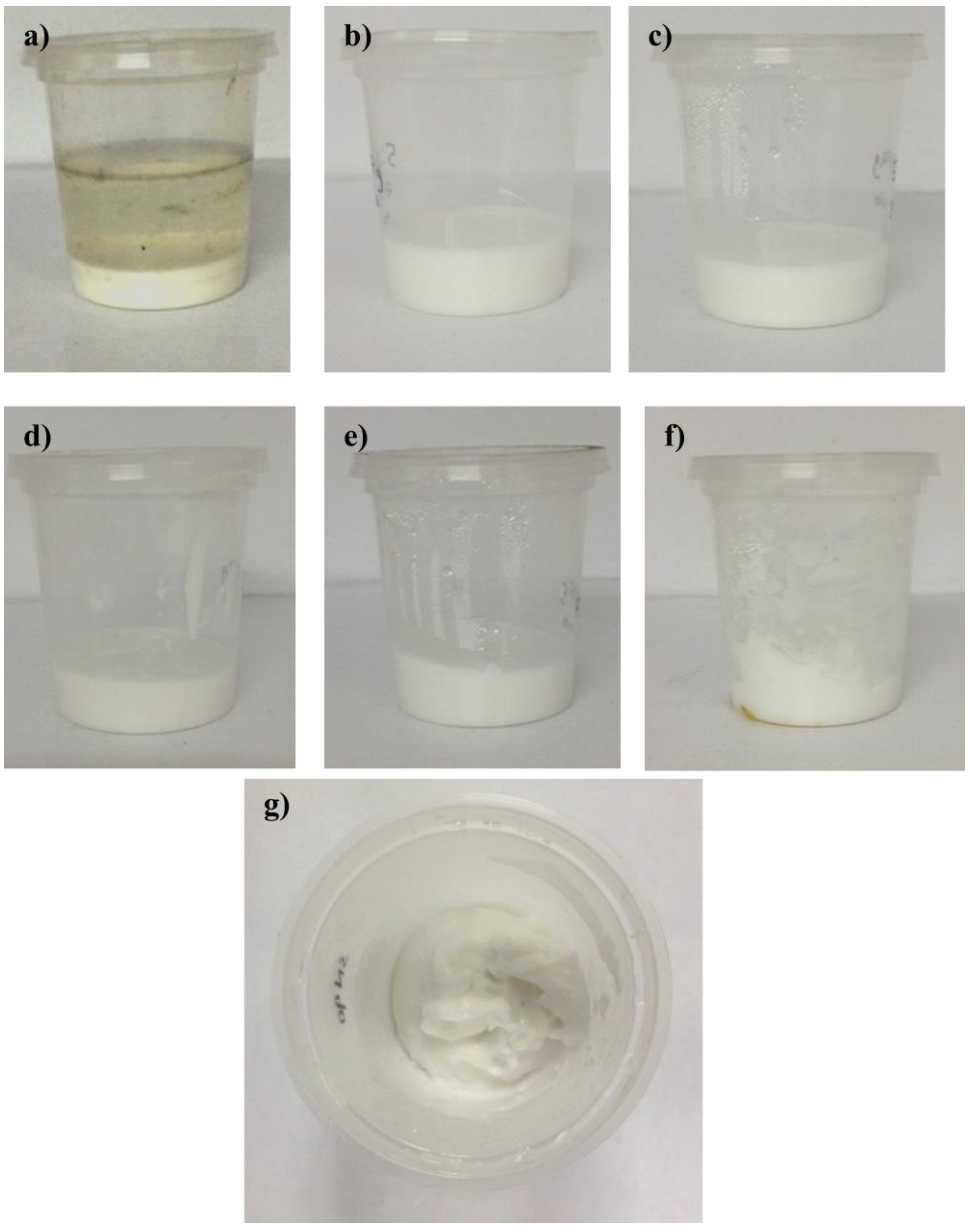

Figure 4.18: Physical appearance of nanocellulose with ultrasonic output power of a) before treatment b) 50 W, c) 100 W, d) 113 W and e) 140 W f) 225 W from side view and g) 225 W from top view.

4.5.2 Effect of sonication power.

When high intensity ultrasound is applied, cavitation bubbles develop and grow. A huge amount of energy is released from the collapse of these bubbles, producing a mechanical shock wave effect and leading to the disruption of hydrogen bonding network. When low sonication power was applied, only the weak bonds such as Van der Walls will break. However, when higher power was applied, strong bonds such as hydrogen bond could be broken up by sonication. The suspension stability of all samples can be illustrated in Figure 4.19.

Table 4.13: Uncatalyzed depolymerization of cellulose by varying the power (W), at constant time.

Sample ID	Power (W)	Physical appearance	Zeta potential (mv)	Surface tension (mN/m)	Yield (%)
Water	-	Clear liquid	n/a	72.00	n/a
Cellulose	-	White powder solid	-14.8	53.50	n/a
SN01	50	Watery milky solution	-21.1	61.22	30
SN02	100	Watery milky solution	-24.1	76.87	44
SN03	113	Watery milky solution	-30.6	79.80	57
SN04	140	Whitish gel and viscous	-34.1	86.90	70
SN05	225	Whitish gel and viscous	-36.6	88.77	85
SN06	240	Whitish gel and viscous	-36.9	89.02	86
SN07	300	Whitish gel and viscous	-37.5	90.55	87

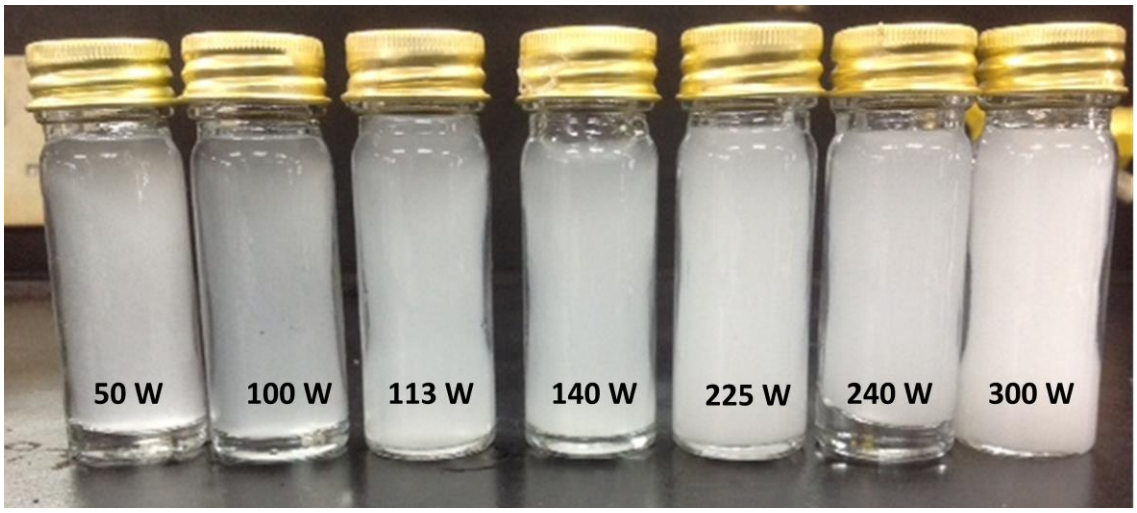

Figure 4.19: Dispersion state of nanocellulose at different sonication power.

Based on Figure 4.20, the highest yield of nanocellulose isolated when ultrasonication mechanical enhancement was subjected to the process is 85 %. It can be clearly seen that the yield increase when the output power increase, and remain almost constant at 240 W and reduced when the power was further increased to 300 W. That is the basis on selection of power chosen for the isolation of nanocellulose to be at 225 W when other effects of other nanocellulose synthesis variables were studied

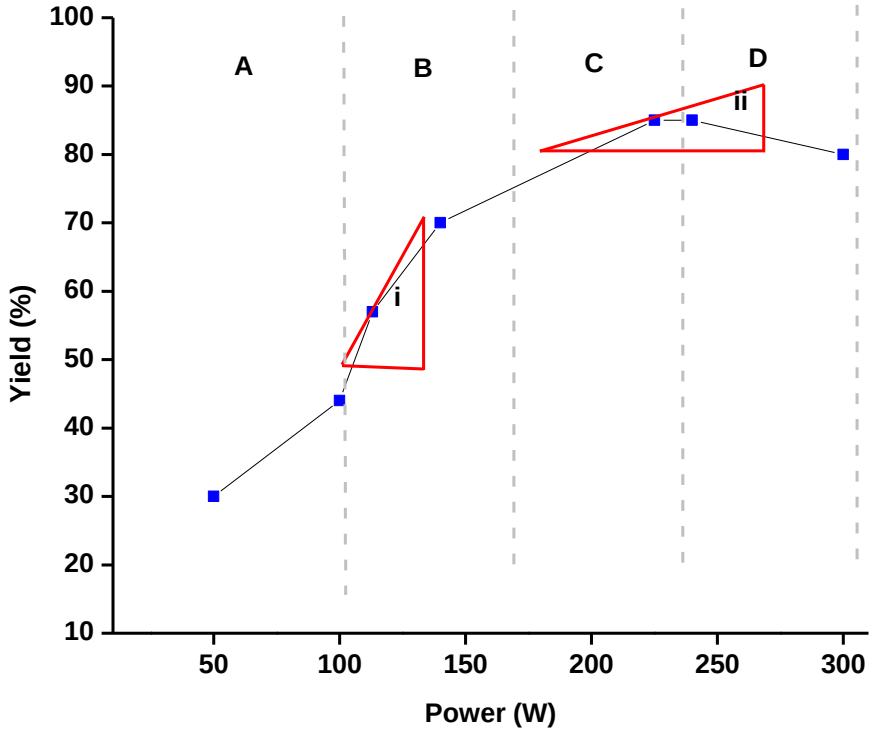

Figure 4.20: Yield of nanocellulose produced at different sonication power.

The production of nanocellulose through ultrasonication mechanical enhancement can be divided into 4 main regions. Region A which is the 1st region shows an increment of 32 % in yield when the output power was doubled from 50 W to 100 W. In region B, the increment was higher, and the calculated slope was 0.66 % / W. In Region B, it was suspected that defibrillation process takes place, where the energy generated was applied to release cellulose fibrils through breaking of interconnected network of

hydrogen bonds. Region C shows a less steep slope with the value of 0.11 % / W. This region was assigned to fibril fragmentation process. Rather than fiber defibrillation, the energy subjected to the reaction has also lead to fibril fragmentation. It was predicted that, the exposed defibrillated fibrils were fragmented into a shorter dimension. Region D is a region when the power was increased from 225 W to 240 W. The yield remains almost the same before it drops to 80 % when 300 W of output power were subjected. From the abovementioned, it can be concluded that defibrillation process occurred at higher rate compared to fibrils fragmentation based on the calculated slope.

Based on Table 4.13, higher power output, generates bigger absolute values of zeta potential. Moderate stability of nanocellulose colloidal suspension was reached when the output power applied was 113 W. Output powers less than 113 W produces nanocellulose colloidal suspension that are easily agglomerated while at 225 W the zeta potential obtained was -36.6 mV. Increasing the sonication output power increase the cloudiness of the nanocellulose suspension. Higher power of sonication has created adequate energy for defibrillation of cellulose fibers. As a result, the fibers are able to detach themselves from the van der Waals forces and inter- and intramolecular hydrogen bonding that primarily creates the compactness of the cellulose fibers. The detachment of cellulose fiber with other cellulose fibers has increased the density of hydroxyl group on the fiber surface. The phenomenon has created good dispersion of nanocellulose colloidal suspensions thus prevent it from settling down.

Other than that, surface tension is also measured in order to understand the interfacial tension between water and (nano) cellulose, thus changes to its surface hydrophilicity. These appear due to the cohesive forces present within the fluid molecules on the surface. Strong attractive forces between the fluid molecules on the surface allow it to resist external forces subjected. The action is taken by the exterior molecules since it

tries to maintain a minimum surface area. Therefore, Wilhelmy plate technique was adopted in examining the equilibrium surface tension of cellulose colloidal suspension. Water is use as a medium during the ultrasonication of cellulose and the surface tension of water at 25 °C is 72 mN/m. The surface tension analysis was done immediately when the temperature of the water-NCC mixtures reached 25 °C. The reading was given automatically by the Tensiometer instrument after the values reaches equilibrium. Highly polar O-H group present has caused ultimate interaction between cellulose surfaces and aqueous solution thus increases its surface tension.

Based on Table 4.13, the values of surface tension increase when the sonication power subjected increase from 50 W to 225 W. The values given were significantly due to the mechanism introduced during ultrasonication process. It was known that ultrasonication process helps to defibrillate the cellulose fiber into less entangle fibrils. The action has notably increase the density of exposed hydroxyl group present within the cellulose polymer chain. Higher sonication power indicates higher exposed free hydroxyl group due to effective defibrillation and fragmentation due to breaking of hydrogen bond underlying the polymer sheet. Concentrated polar hydroxyl group present in the exterior surface of colloidal suspension create a stronger attractive forces among the others hydroxyl group. The action is taken for maintaining the smallest surface area. As a result, the surface shows an elastic behavior which increases the surface tension value.

4.5.3 Effect of sonication time.

Effect of sonication time during the delamination process is also a crucial parameter that should not be taken for granted. Time dictates the quantity and quality of nanocellulose product, this is because longer time gives good dispersion. If the sonication time is longer, more cellulose fibrils will be broken and change its morphology into shorter nanocellulose with smaller diameter (Frone et al., 2011).

Table 4.14: Uncatalyzed depolymerization of cellulose by varying the time, at constant power.

Sample ID	Time (Min)	Physical appearance	Zeta potential (mv)	Surface tension (mN/m)	Yield (%)
Water	-	Clear liquid	n/a	72.00	n/a
Cellulose	-	White powder solid	-14.8	53.50	n/a
SN08	1	Watery milky solution	-17.0	42.86	20
SN09	1.5	Watery milky solution	-19.1	55.33	36
SN10	2.5	Watery milky solution	-24.1	59.33	43
SN11	3.5	Watery milky solution	-30.1	72.42	55
SN12	5	Whitish gel and viscous	-35.6	80.97	76
SN13	10	Whitish gel and viscous	-36.6	88.77	85
SN14	15	Whitish gel and viscous	-39.1	94.26	88

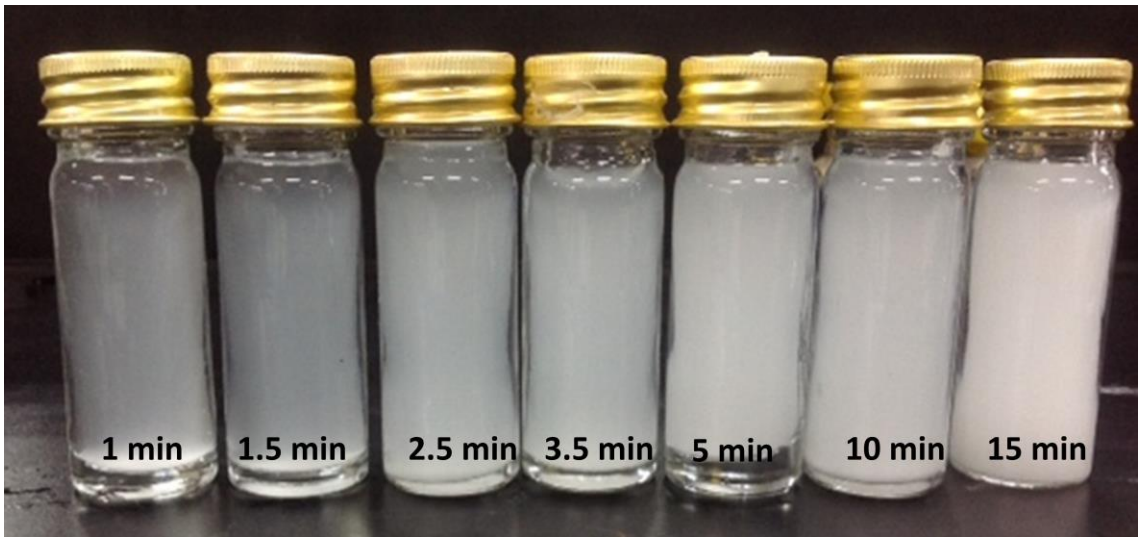

Figure 4.21: Dispersion state of nanocellulose at different sonication time.

Based on Figure 4.22, the highest nanocellulose obtained was at 15 min with 88 %. Since the increment of yield between 10 to 15 min is only 3.4 %, reaction time chosen for all the depolymerization reaction using ultrasonication is 10 min. Graph on Figure 4.22 shows almost the same pattern of graph obtained when effect of duration time was examined in the preparation of nanocellulose. This graph can be divided into 3 main regions, A, B, and C.

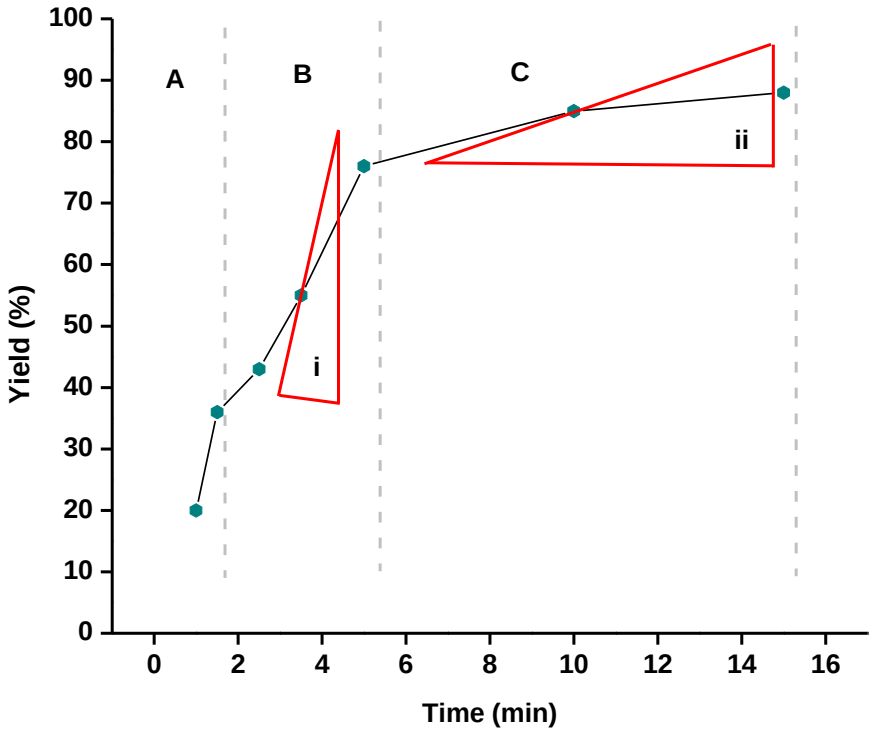

Figure 4.22: Yield of nanocellulose produced at different sonication time.

Region A and B shows a steep slope compared to region C. The calculated slope of region B is 31.15 % / min. The design of the graph in region B is expected to be the mechanism of fiber defibrillation. It explains that, when ultrasonication was applied to the process, the phenomena occurred at higher rate. In region C, the calculated slope is 2.37 % / min. The process that expected to occur at that region is fibrils fragmentation. The calculated slope obtained at that region explained that the process occurred at a lower rate compared to fiber defibrillation.

A viscous and whitish gel like nanocellulose was obtained when the duration time is higher than 5 min. This shows that the nanocellulose obtained has undergone both fiber defibrillation and fragmentation. As a result, conclusion made in effect of sonication power can also be adopted when effect of sonication duration was studied.

Fiber defibrillation process occurred at higher rate compared to fragmentation process, but both mechanisms are important in obtaining high quality nanocellulose.

Zeta potential is an important tool for understanding the start of the nanoparticle surface and predicting the long term stability of the nanoparticle. From Table 4.14 the shortest time introduced is 1 min while the longest is 15 min. Duration time of 10 min and 15 min displayed zeta potential value greater than 35 mV, which consequently represent the stability in colloidal suspension. By looking at sample SN02 (Table 4.13 and Figure 4.21) and SN10, the same value of zeta potential is achieved. That value is achieved at shorter period of time when high sonication power is introduced. Short time introduced has given a low zeta potential value, where the particles will eventually aggregates due to the Van der Walls interparticles attractions. Appropriate duration time applied is essential to make sure that time allocated for the defibrillation is enough. Duration of 15 min posses zeta potential -39.1 mV, the value has significantly informed that the higher surface charge value has created electrostatic repulsive forces to the system. The electrostatic repulsive forces help the nanoparticle from reunited or rebinding thus formed a stable colloidal suspension.

For surface tension analysis, similar approaches of sonication power were applied when effect of treatment time was issued to the nanocellulose. The surface tension increases to 54 % when the reaction duration time was prolonged from 1 min to 15 min. Longer treatment time gives better opportunities for the defibrillation process to happen efficiently as well as fiber fragmentation. Less ordered cellulose fragments that have high susceptibility towards sono – energy was first disturbed, and consequently, exposed the hydroxyl groups through fiber fragmentation. The longer the sonication duration time, the higher the viscosity of the nanocellulose mixture. Eventhough both viscosity and surface tension are independent variables, the viscosity of the mixture can still be useful in explaining the concentration of hydroxyl group on the fiber's surface. Highly exposed hydroxyl group has created high hydrophilicity on the nanocellulose surface which increases its surface tension. The saturated exposed hydroxyl group on

the molecule surface has increased the viscosity of the mixture due the interaction of OH^- with the water molecules.

4.5.3 Effect of Tungstophosphoric acid, $H_3PW_{12}O_{40}$ (TPA) catalyst loading.

The production of nanocellulose was obtained from exposing few cellulose microfibrils to high intensity ultrasonication. A few hundred micrometer of cellulose microfibril was directly introduced to heteropoly acid. In this case, sonication was the dominant role in making nanocellulose facilitated by the existence of heteropoly compound as a proton donor. The loosen spaces generated has increased the opportunity of heteropoly compound's proton in hydrolyzing the ether linkages, producing more nano-structured cellulose.

Table 4.15: Catalyzed depolymerization of cellulose by different loading of $H_3PW_{12}O_{40}$ at 225 W for 10 min.

Sample ID	Catalyst loading (g)	Physical Appearance	Zeta potential (mv)	Surface tension (mN/m)	Yield (%)
Water	-	Clear liquid	n/a	72.00	n/a
Cellulose	-	White powder solid	-14.8	53.50	n/a
SN05	-	Whitish gel and viscous	-36.6	88.77	85
SN15	2	Whitish gel and viscous	-36.8	67.02	86
SN16	4	Whitish gel and viscous	-38.9	65.21	90
SN17	6	Whitish gel and viscous	-39.3	64.33	77

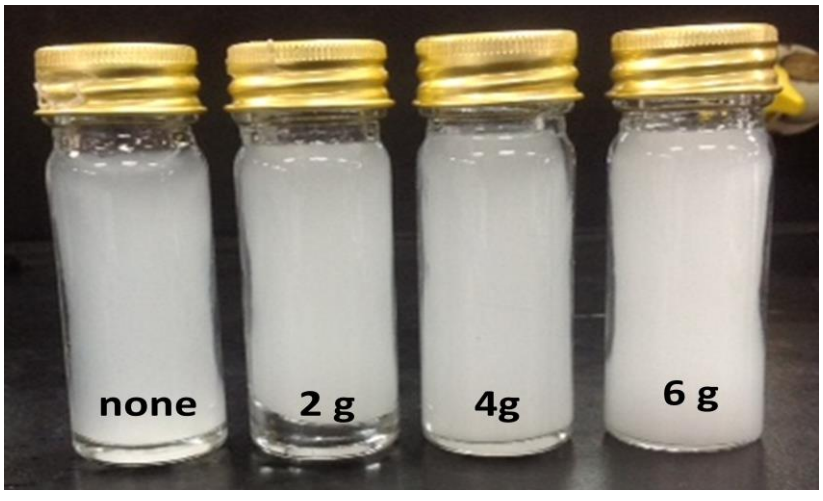

Figure 4.23: Dispersion state of nanocellulose at different loadings of TPA

The commercial production of nanocellulose was being dominated by sulfuric acid hydrolysis. Eventhough the production route is widely applied in many industries, the yield obtained is not satisfying. Synergy effect of high intensity ultrasonication and heteropoly acid hydrolysis has led to a better reaction performance in terms of product yield. As shown in Figure 4.24, under the same reaction condition, 1.16 % of nanocellulose yield increased when 2 g of TPA was added to facilitate the reaction. The calculated slope at region A is 4.45 % / g while at region B is 15.94 % / g. The values has given a rough indication about the fibril fragmentation that has taken place during the process.

Once the heteropoly acid was added to the process, the production of nanocellulose was further enhanced through fibril fragmentation. The higher slope reported above, has explained that when 4 g of TPA was applied , the yield is increased. It shows that fibrils fragementation work efficiently in acidic condition. However, the value dropped when 6 g of TPA was introduced to the process. 6 g of TPA represent a highly acidic environment for cellulose depolymerization which reduced the yield of nanocellulose through uncontrolled cleavage of glycosidic linkages. The yields of nanocellulose obtained in SN17 (6 g) possess zeta potential of -39.3 mV, this shows that higher content of TPA create good quality of nanocellulose but at a lower yield.

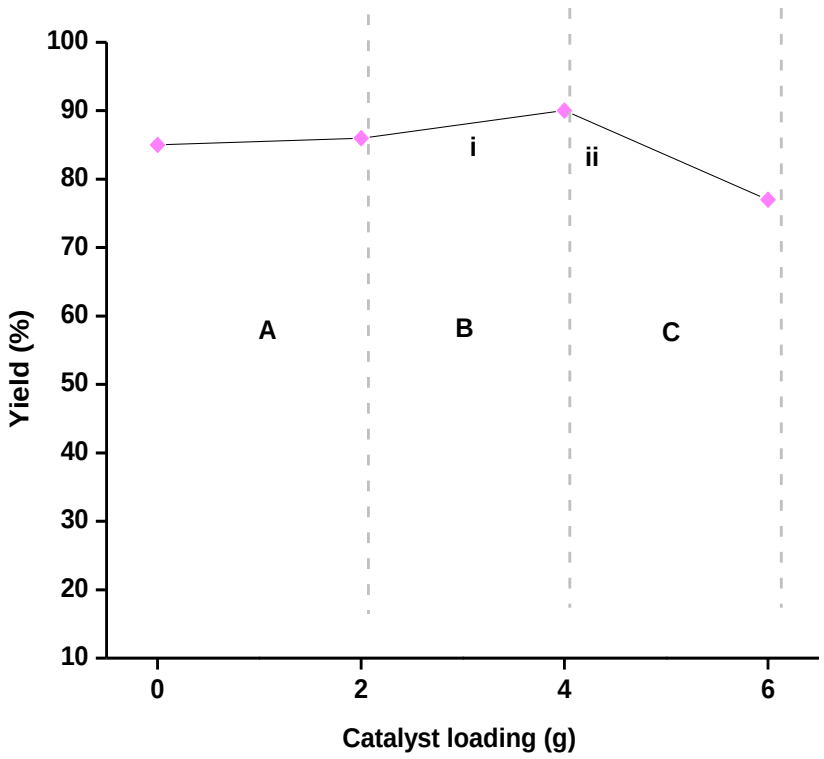

Figure 4.24: Yield of nanocellulose produced at different loading of TPA.

As a result, 4 g of TPA was chosen to be the optimal value of catalyst loading for catalytic depolymerization of cellulose. Commercial production of nanocellulose employs sulfuric acid liquid catalyst. This catalyst, although highly active, can lead to corrosion and environmental issues. Use of solid acid catalysis for the reaction could potentially overcome those drawbacks. Therefore, the reaction will be more likely to occur effectively with liquid phase Bronsted acid compared to the solid phase Bronsted acid. This is because the intrinsic catalytic activity of liquid phase heteropoly compound is higher in this reaction (Huang & Fu, 2013).

Miniaturization of cellulose to nanofibers size cellulose not only requires high sonication power and appropriate treatment time but also proton donor capability to facilitate the depolymerization process. The presence of TPA in the reaction medium is crucial for determining the effectiveness of the hydrolysis. TPA is a Bronsted acid type where the reaction goes through protonation reaction step. The Bronsted acid action at this stage has become more predominant, where the proton generated will be oriented to

highly accessible amorphous region of cellulose microfibril. The amorphous region that is less susceptible towards the acid attack was hydrolyzed, leaving the crystalline region intact. The relationship between amounts of TPA subjected with the zeta potential of the nanocellulose suspension was investigated. In Table 4.15, it shows that addition of 2 g, 4 g, and 6 g TPA catalyst generates zeta potential of -36.8mV, -38.9mV and -39.3mV respectively.

Zeta potential (ZP) values increase when the amount of TPA catalyst used increase. The ZP values indicate that the generated cellulose nanocrystals (NCC) have a good dispersibility in water dispersant, i.e have nanoparticle colloidal suspension stability. Introduction of acidic medium to the reaction has increase the breaking of intramolecular hydrogen bonding [O (2) ---O (6) bonding and O (3) ---O (5)] between the glucose molecules thus exposing more hydroxyl group of NCC. The presence of negatively charged hydroxyl groups on the NCC's surface encourages the formation of electrostatic layer covering the NCC and supports their spreading in water thus prevent it from flocculation and sedimentation.

However, adding of TPA catalyst in catalyzing the reaction has resulted in lower surface tension of NCC colloidal suspension. Amount of TPA added is inversely proportional to the surface tension values. The higher the amount added, the lower the value. This phenomenon is mainly due to the bulkiness of Keggin anion. TPA dissolves in water to produce proton and Keggin anion. Incorporation of anionic Keggin ions with freely hydroxyl group on the surface of NCC has reduced the self- association tendency among the hydroxyl group. This is because Keggin anion act as a cluster- surfactant (Texter, 2011) thus reduces the surface tension. High value of surface area gives good indication on the quality of nanocellulose. It shows that the defibrillation and

fragmentation has successfully undergone breaking of hydrogen bond and glycosidic bond thus exposing highly saturated hydroxyl group on the molecule surface.

4.5.3 Effect of Cs:H content

Notably, the role of Bronsted acid is less pronounce when the physical state of Bronsted acid changes from liquid to solid phase.

Table 4.16: The physical states of Bronsted acid for the heteropoly compounds.

Physical State of Bronsted Acid	Sample Code	Chemical formula
Liquid	CS01	$Cs_0H_3PW_{12}O_{40}$ (TPA)
	CS02	$Cs_1H_2PW_{12}O_{40}$
Solid	CS03	$Cs_2\ H_1PW_{12}O_{40}$
	CS04	$Cs_{2.5}H_{0.5}PW_{12}O_{40}$
	CS05	$Cs_{2.8}H_{0.2}PW_{12}O_{40}$
	CS06	$Cs_3H_0PW_{12}O_{40}$

There are two physical states of Bronsted acid introduced during the process of cellulose depolymerization. Table 4.16 differentiated phases of TPA, liquid phase of heteropoly compounds are accompanied by (CS01) $H_3PW_{12}O_{40}$ and (CS02) $Cs_1H_2PW_{12}O_{40}$ while the solid phase are (CS04) $Cs_{2.5}H_{0.5}PW_{12}O_{40}$ and (CS06) $Cs_3PW_{12}O_{40}$.

Table 4.17: Catalyzed depolymerization of cellulose by $Cs_xH_{3-x}PW_{12}O_{40}$ at different Cs:H ratio

Sample ID	Cs:H ratio	Physical appearance	Zeta potential (mv)	Surface tension (mN/m)	Yield (%)
Water	-	Clear liquid	n/a	72.00	n/a
Cellulose	-	White powder solid	-14.8	53.50	n/a
SN05	-	Whitish gel and viscous	-36.6	88.77	85
SN16	0:3.0	Whitish gel and viscous	-38.5	65.23	91
SN18	1.0:2.0	Whitish gel and viscous	-33.4	66.47	86
SN19	2.5:0.5	Whitish gel and viscous	-30.6	67.68	85
SN20	3.0:00	Whitish gel and viscous	-29.1	69.01	83

The application of $H_3PW_{12}O_{40}$ in nanocellulose production has showed an excellent yield. Introduction of cesium atom within the Keggin structure has tremendously effect the yield of nanocellulose. Increasing amount of cesium, has decreased the yield of nanocelluse. Region A shows an increase in yield when no subsituted cesium present in the reaction. Slope i is more steep compared to slope ii, this has explained that fibrils fragmentation occur under non substituted cesium in $H_3PW_{12}O_{40}$ is better compared to subsituted cesium. Eventhough both slopes do not represent the rate of reaction, but it still can be used as indicator for process efficiency. When higher cesium content is present within the Keggin network, the yield of nanocellulose dropped. The reaction is less pronounced and the production of nanocellulose is continued only via ultrasonication. This can be explained through the same yield of nanocellulose obtained when the ratio of Cs: H reached 2.5 with the uncatalyzed production of nanocellulose. It shows that the number of acid sites is higher than the acid strength and the process requires higher Bronsted acid strength for the depolymerization activity.

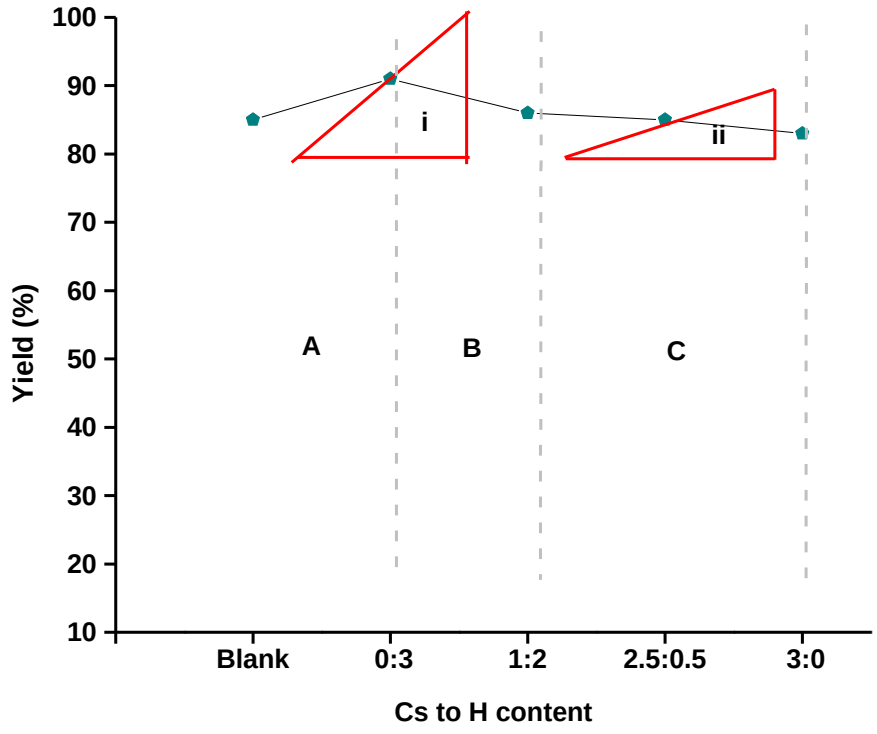

Figure 4.25: Yield of nanocellulose produced at different Cs : H ratio.

Both $H_3PW_{12}O_{40}$ and $Cs_1H_2PW_{12}O_{40}$ are soluble and ionize in water to generate highly concentrated acidic proton that hydrolyze β-linkages of cellulose microfibrils. On the other hand, solid phase of $Cs_{2.5}H_{0.5}PW_{12}O_{40}$ and $Cs_3PW_{12}O_{40}$ are insoluble in water and hardly ionize to produce acidic proton for cellulose hydrolysis. Low hydrolysis capacity posses by those catalysts are due to their low proximation between the cellulose molecules. It shows that, eventhough $Cs_{2.5}H_{0.5}PW_{12}O_{40}$ and $Cs_3PW_{12}O_{40}$ catalyst posses' high surface area which is 115 and 138 m^2g^{-1} respectively, the values obtained seem insignificant in cellulose depolymerization to nanocellulose.

Conventionally, mineral acid especially sulfuric acid was used to assist the process of cellulose depolymerization. Therefore, the process type involved was solid – liquid reaction. Nevertheless, it was clearly known that catalyst added to sample SN16 and SN18 were solid but have great interaction with aqueous solution due to low solvation energy. Whereas, catalyst catalyzed in SN19 and SN20 have low interaction with water molecules owing to its hydrophobicity thus creates low hydronium ion concentration. Consequently, depolymerization of cellulose in SN19 and SN20 are less effective due to lack of interaction of solid catalyst with cellulose molecules. Eventhough both catalysts used to catalyze the reaction posses excellent porosity and surface area, but those elements were less pronounce when solid bio-polymer was used as a raw materials. Therefore, good zeta potential values obtained from the reaction are mainly due to the ultrasonication effect that creates good dispersibility of colloidal in aqueous medium.

4.6 Nanocellulose product assay

4.6.1 Crystallinity Index by X-ray Diffraction (XRD)

Cellulose crystallinity is very significant in determining the thermal and mechanical properties of NCC generated. The crystalline structure of cellulose has been extensively been studied through XRD method. Generally, cellulose I is the most abundant form found in nature, with cellulose I_β (monoclinic) form being dominant in higher plants. XRD patterns in Figure 4.26 exhibits the diffraction signals at 2θ of 15 °, 16 ° , and 22.8 ° (PDF –File 050- 2241)

Table 4.18: Main diffractions peak of cellulose I.

No	d-spacing (Å)	2θ (°C)	Intensity (%)
1	5.90609	14.988	33
2	5.37240	16.487	33
3	3.90018	22.782	100

A parameter termed crystallinity index (CrI) has been extensively applied in order to illustrate the relative amount of crystalline portion in cellulose. To calculate CrI of cellulosic material from XRD spectra, peak height method was applied by using height ratio (Park, Baker, Himmel, Parilla, & Johnson, 2010) between the intensity of the crystalline peak (I_{002}-I_{am}) and the total intensity (I_{002}) as simplified into equation 4.3 whereby I_{002} represents both amorphous and crystalline region and I_{am} at 18 ° which signifies the amorphous region. This was done after subtraction of the background signal.

$$CrI = \frac{I002 - I\ am}{I002}\ x\ 100 \qquad \textbf{(Equation 4.3)}$$

Based on Figure 4.26 and Table 4.19, CrI of the raw material, microcrystalline cellulose (MCC) was measured to be 75.6 %. Introduction of ultrasonication on the cellulose fibers increases the CrI of the mechanically treated cellulose up to 87.5 %. Low sonication output power has significantly increased CrI about 6 % from the raw MCC. This value started to steadily grows when the output power were increased to 225 W. The increase in crystallinity was undoubtedly due to the decrease in compaction degree of cellulose polymer chain through delamination process. Powerful energy introduced also can lead to reduction and removal of amorphous section of cellulose during defibrillation. Unordered arrangement of amorphous domains in cellulose polymer chains make it more prone towards high energy treatment compared to crystalline region. The CrI of NCC was around 80 % and above, implying that ultrasonication subjected had greatly affected the crystallinity of NCC. Removal of amorphous region has successfully remained the crystalline region intact which reflects to better quality of NCC.

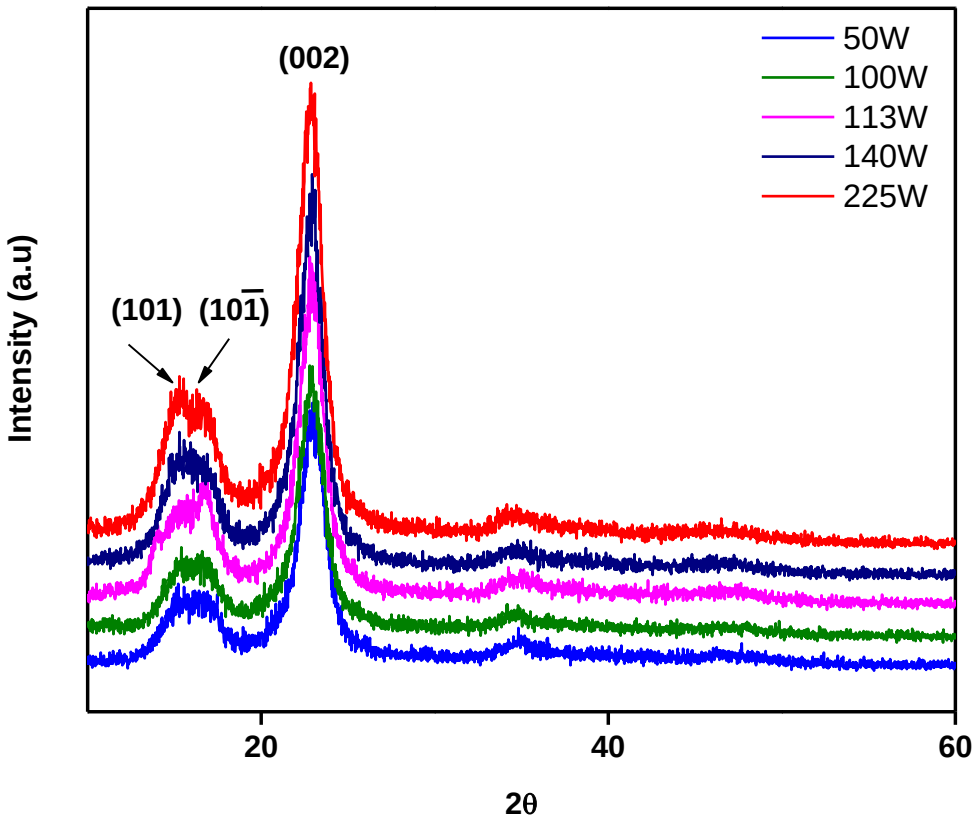

Figure 4.26: XRD diffractograms of on effect of sonication power.

Table 4.19: Crystallinity Index (CrI) values of NCC from effect of sonication power.

Sample ID	Power (W)	CrI (%)
MCC	-	75.6
SN01	50	80.1
SN02	100	84.5
SN03	113	85.1
SN04	140	86.0
SN05	225	87.5

Depolymerization of cellulose to NCC through ultrasonication treatment requires an appropriate amount of treatment time. Based on Table 4.20, 7 different time duration have been subjected for analysis in order to determine the best reaction times for obtaining NCC through the highest CrI values. As a result, SN12 with treatment duration of 15 minutes generates the best value of CrI with 88 %. Longer ultrasonication time introduced has created a great opportunity for the system to

generate adequate energy for cellulose fiber defibrillation. During the cellulose defibrillation, cellulose macrofibril tends to delaminate itself using the sono –energy created by the ultrasonication. The delamination process involves breaking of hydrogen bond leaving the cellulose fibrils intact. Sufficient time introduced has given an opportunity to the fibrils for undergoing fibrils fragmentation thus cleaving the amorphous domain. Therefore, high percentage of amorphous region diminished within the cellulose fibrils has significantly increased the CrI illustrated in Figure 4.27.

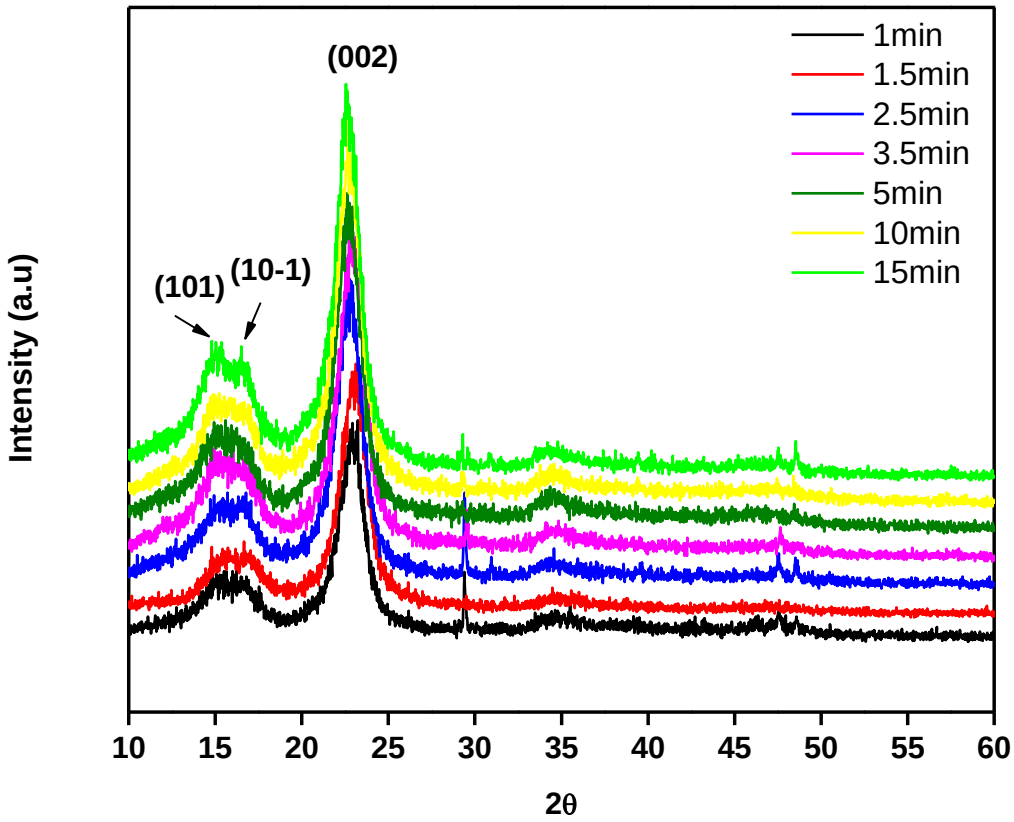

Figure 4.27: XRD diffractograms of on effect of sonication time.

Table 4.20: Crystallinity Index (CrI) values of NCC from effect of sonication time.

Sample ID	Duration time (Min)	CrI (%)
MCC	-	75.6
SN08	1	85.6
SN09	1.5	85.7
SN10	2.5	86.0
SN11	3.5	86.3
SN12	5	87.0
SN13	10	87.5
SN14	15	88.0

Hydrolysis of cellulose via sulfuric acid is a classical method in obtaining NCC. Minerals acid such sulfuric acid, nitric acid, hydrochloric acid and others act as a proton donor that hydrolyzed ether linkages present within the cellulose polymer chain. Amorphous regions that are more susceptible toward low pH environment are hydrolyzed, leaving the crystalline region intact. The removal of amorphous domain has increased the crystallinity values of the NCC generated which can be shown in Figure 4.28.

However, uncontrolled hydrolysis reaction can cause the reduction of CrI of NCC. Highly concentrated of hydronium ion were able to penetrate into the crystalline region, thus promoting the hydrolytic cleavage of glycosidic bond which decrease the crystalline crystallites. Same effect has been adopted in studying the CrI generated from NCC catalyzed by Heteropolyacid (HPA). Based on Table 4.21 the CrI of NCC increases from 75.6 % to 86.5 % when the hydrolysis reaction was catalyzed by 2 g of TPA. TPA has caused such transformation because of its Bronsted acid properties that dissolves the amorphous region of cellulose polymer chain.

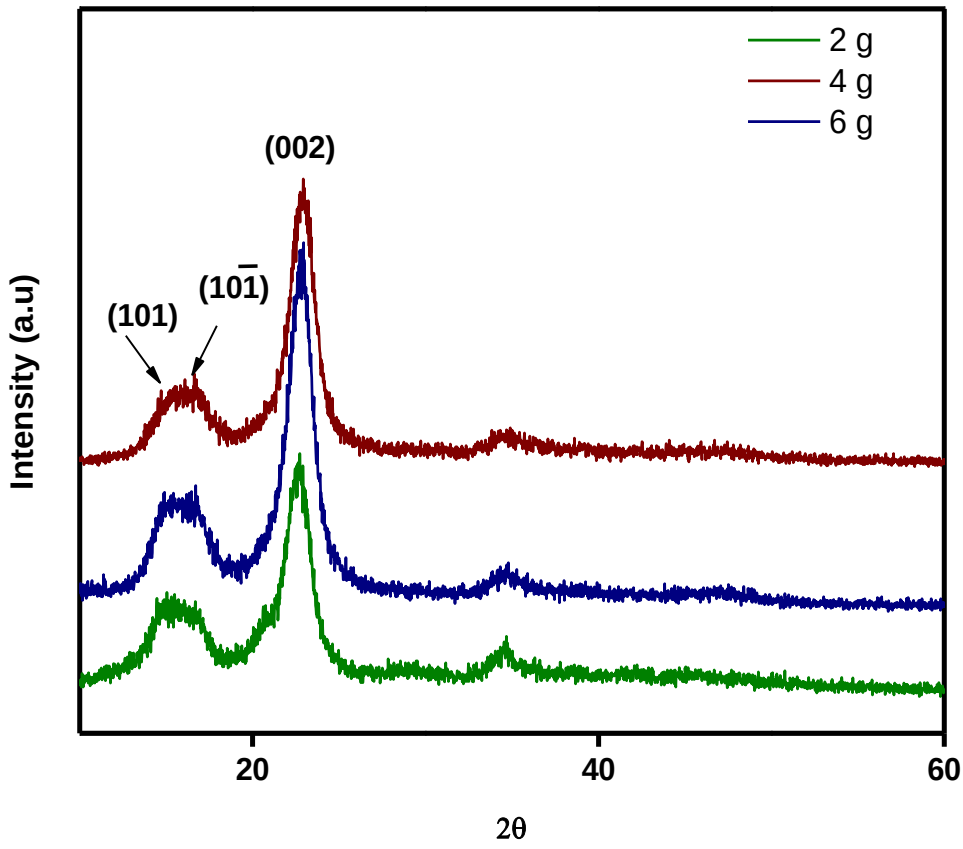

Figure 4.28: XRD diffactograms on effect amount of TPA catalyst.

Table 4.21: Crystallinity Index (CrI) values of NCC from effect of TPA's amount.

Sample ID	TPA's amount (g)	CrI (%)
SN05	-	87.5
SN15	2	87.8
SN16	4	88.0
SN17	6	85.4

However, by increasing the amount of TPA to 6 g, the CrI of NCC produced was reduced while 4 g of TPA gave the best value of CrI. As a result, 4 g of TPA is the optimum weight to get the best CrI of NCC produced. The value obtained was similar with SN14. This is because, application of TPA as a catalyst has reduced the activation energy for depolymerization of cellulose thus lesser time is required to obtain such CrI. It shows that TPA acts as an excellent catalyst in producing NCC.

Depolymerization or hydrolysis of cellulose requires an acidic environment in order to diminish the amorphous region present. Substitution of proton with a larger monovalent cation such as cesium cation reduced the acidity of the Heteropoly compound. This is because introduction of cesium ion within the Keggin network has increase the alkalinity of the compound plus alteration of its hydrophilicity.

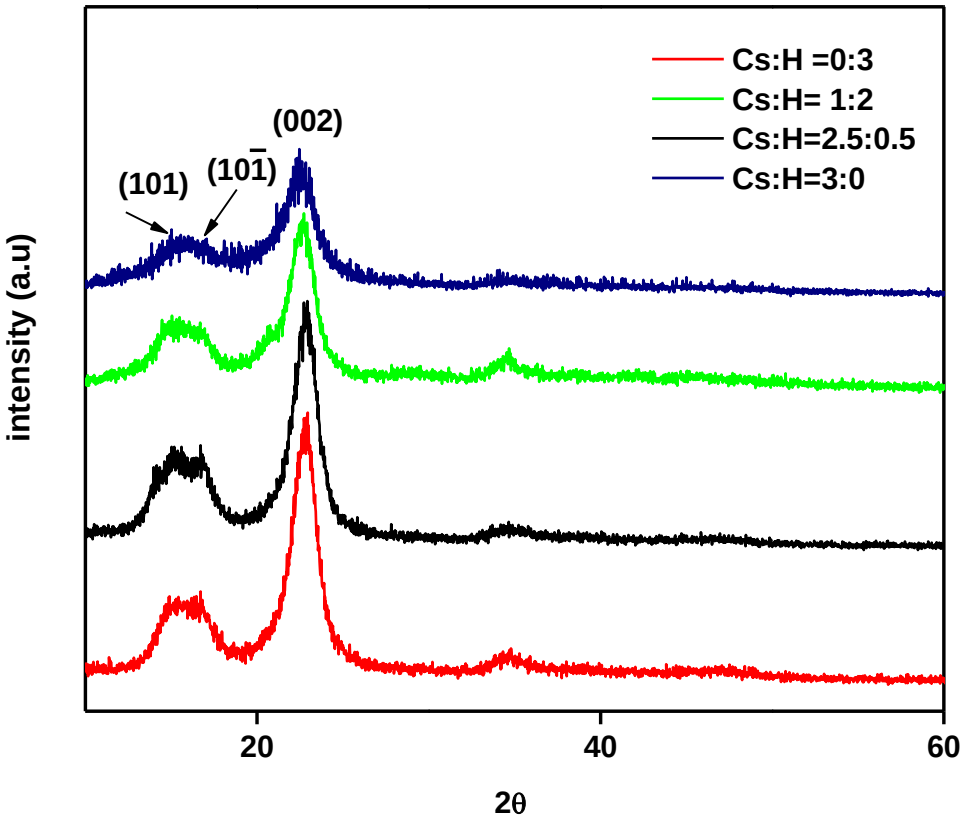

Figure 4.29: XRD diffactograms of NCC catalyzed by $Cs_xH_{3-x}PW_{12}O_{40}$ at different Cs:H ratio

Table 4.22: Crystallinity Index (CrI) values of NCC at different Cs: H ratio

Sample ID	Catalyst ID	Cs:H ratio	CrI (%)
SN16	CS01	0: 3	88.0
SN18	CS02	1:2	84.2
SN19	CS03	2.5 :0.5	80.4
SN20	CS04	3:0	80.1

It has been mentioned in Section 4.2 that CS03 and CS04 were insoluble in water. Therefore, both of th catalysts does not ionize in water to produce hydrogen ions. As a result, the hydrolysis effectiveness drops through the reduction of CrI. Based on Figure 4.29 and Table 4.22, the highest CrI is 88.0% and the lowest is 80.1 %. The number of titratable acid sites decreases with increase of Cs content. Hence, CS01 has the greatest protonic acid sites, thus showing excellent catalytic performance in terms of higher value of CrI. Among the 3 catalysts that have Cs substituted, CS02 catalyzed reaction has shown good CrI compared to the reaction catalyzed by CS04 and CS06. Despite, CS04 and CS06 has high surface area and porosity, low CrI of nanocellulose are obtained from the depolymerization process catalyzed by them. This can be credited to mass transport in solid –solid reaction. High porosity and surface area of CS04 and CS06 are most favorable in liquid or gas reaction system (Tian et al., 2011).

4.6.2 Chemical structure by Fourier Transform Infrared (FTIR) spectroscopy

FTIR spectroscopy is one of the most important analytical techniques available to researches. FTIR was carried out using KBr method. This is crucial for determining the chemical characteristic and compositions of cellulose biopolymer. Any changes occurred which involving the bond breaking or forming can be illustrated through FTIR spectra. Therefore, for depolymerization of cellulose to NCC, this characterization was done to observe the changes happening at β - linkages of cellulose polymer chain. The intensity of transmittance (%) generated will give an information about the adjustment that has taken place during the process. Alteration of the crystalline domains offers a guide towards a significant generalization through the reduction of intensity of the crystalline domains characteristic bands. Therefore, FTIR spectroscopy method is important in giving rapid information about the efficiency of the process commenced. Table 4.23 displays the general characteristic bands for the cellulosic material.

Table 4.23: Common band assignments for cellulose through FTIR spectroscopy.

Wavenumber (cm^{-1})	Band assignments	References
3400	O-H stretching	(Fan, Dai, & Huang, 2012)
2800	C-H stretching	(Mohamad Haafiz et al., 2013)
1640	O-H bending of absorbed water	(Johar et al., 2012)
1425	CH_2 bending	(Kumar, de la Luz Reus-Medina, & Yang, 2002)
1054	C-O-C pyranose ring stretching vibration	(Mandal & Chakrabarty, 2011)
1151	Asymmetric vibration of C-O-C bonds	(Fan et al., 2012)
1043	Stretching of C-O-C bond	(Fan et al., 2012; Halib & Amin, 2012; R. Li et al., 2009)
896	Glycosidic $^4C_1$ deformation of β-linkages	(Ciolacu, Ciolacu, & Popa, 2011; Jiang & Hsieh, 2013)

Generally, broad band at 3500 – 3200 cm^{-1} are due to the existence of hydroxyl group through free O-H stretching in cellulose polymer, hydrogen bonded gives broader bands. Based on Figure 1.2 (Chapter 1), there are three different hydroxyl groups present which in C2, C3 and C6. Their presences have allowed the formation of different kinds of intra and inter- molecular hydrogen bonds (Habibi et al., 2010). 2894 – 2911 cm^{-1}, bands are assigned for C-H stretching vibration. Peaks at 1641- 1650 cm^{-} are mainly related to O-H bending properties associated to absorbed water, the peak exists in every cellulose's spectra. Absorption band at 1430 cm^{-1} is related with to intermolecular hydrogen attraction at C6 group. Meanwhile, peaks at 1043 cm^{-1} and 896 cm^{-1} correspond to glycosidic ether bonds and glycosidic $^4C_1$ deformation of β- linkages respectively are very important in determining the effectiveness of cellulose depolymerization. Based on Figure 4.30, it can be clearly observed that there are no distinct changes in chemical structure of cellulose shown in the FTIR spectra. However, if the figure was further focused, there is some small changes in transmittance (%) has

taken place at peak 896 cm^{-1}. The changes in transmittance (%) reading are recorded in Table 4.24. The transmittance (%) of peaks 896 cm^{-1} gradually reduced in intensity when the sonication powers were increased from 50 W to 225 W. The changes happen due to the defibrillation process that has taken places. It has been mentioned in Ciolacu et al., (2011) that absorption band at 896 cm^{-1} is designed as an "amorphous absorption band". The decrease in its intensity indicates the increase in crystallinity of the samples due to the loss of glycosidic linkages through hydrolysis process in amorphous domain. Peak 896 cm^{-1} was used as a reference because removal of amorphous domain is much easier compared to crystalline domain. Disordered crystallites of cellulose molecules present in amorphous region were easily diminished when high ultrasonication energy was introduced which also contribute to the increase in NCC crystallinity.

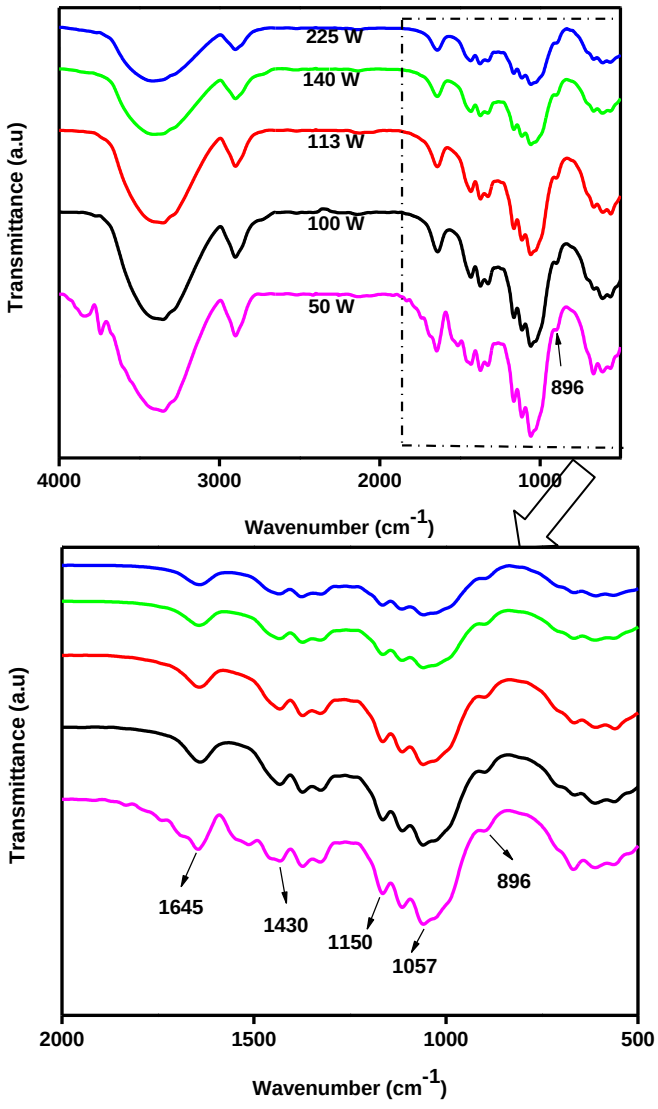

Figure 4.30: FTIR spectra of NCC from effect of sonication power.

Table 4.24: Relationship between sonication powers (W) with transmittance's intensity at absorption bands 896 cm^{-1}.

Sample ID	Power (W)	Wavenumber (cm^{-1})	Transmittance
SN01	50	896.74	0.96
SN02	100	896.74	0.94
SN03	113	896.74	0.91
SN04	140	896.74	0.89
SN05	225	896.74	0.79

The patterns of FTIR spectra in Figure 4.31 were almost identical for all time duration, but the intensity of each peak was different to some extent. The broadness of peak 3400 cm^{-1} was reduced into small area when the reaction time was longer. Longer treatment time has broken the hydrogen bonds that are connected through intra and intermolecular attraction. Furthermore, peak 896 cm^{-1} (Table 4.25) also shows reduction in intensity when the treatment time was increased to 15 minute. The decrease in intensity was the indication of increasing crystallinity of NCC which can be related to fiber fragmentation due to breaking of glycosidic bond in amorphous region. Amorphous regions are consists of disordered cellulose crystallite while crystalline region are consists of ordered cellulose crystallite. The amorphous amount was being used as the indicator for the determination of crystallinity index. This is because the removal of amorphous domain is easier compared to crystalline region. Removal or lacking of crystalline region has shown that the reaction time subjected to reaction is too long thus caused the crystallinity index to decrease.

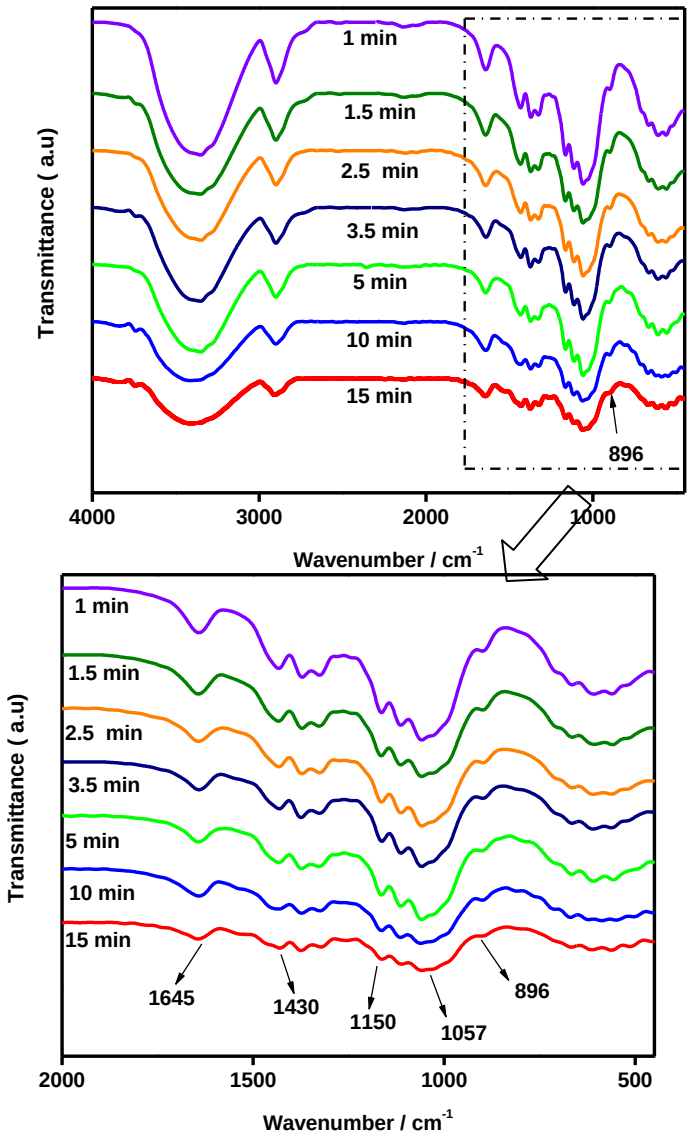

Figure 4.31: FTIR spectra of NCC from effect of sonication time.

Table 4.25: Relationship between sonication time (min) with transmittance's intensity at absorption bands 896 cm^{-1}.

Sample ID	Time (min)	Wavenumber (cm^{-1})	Transmittance
SN07	1	896.74	0.95
SN08	1.5	896.74	0.88
SN09	2.5	896.74	0.87
SN10	3.5	896.74	0.86
SN12	5	896.74	0.80
SN13	10	896.74	0.79
SN14	15	896.74	0.77

Infrared absorption bands around 900 cm $^{-1}$ to 1100 cm^{-1} is found to be very sensitive to the amount of crystalline structure against amorphous structure (Janardhnan & Sain, 2011). Therefore, any broadening of the band reflects to higher degree of disordered crystallite structures. Increasing the amount of acidic TPA in the reaction reduced the intensity of peaks 896 cm^{-1} from 0.79 to 0.78. The relative absorbance of β - 1, 4-linkages between glucose units were drastically decreased by adding CS01 catalyst similar to acid hydrolysis (Nada, El-Kady, El-Sayed, & Amine, 2009). The collaboration between ultrasonication and acid hydrolysis has increased the possibility in obtaining NCC. CS01 produces hydronium ions which can easily penetrate the defibrillated fiber after the ultrasonication process. As a result, enhanced removal of amorphous region can be accomplished.

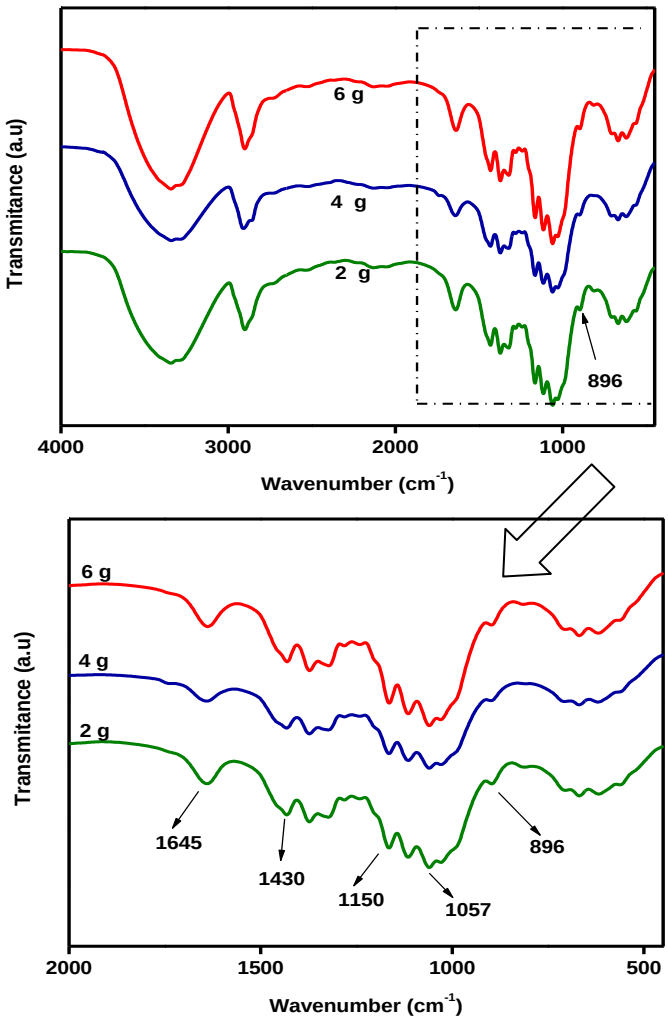

Figure 4.32: FTIR spectra of NCC from effect of TPA's amounts.

Table 4.26: Relationship between TPA's amount with transmittance's intensity at absorption bands 896 cm^{-1}.

Sample ID	TPA's amount (g)	Wavenumber (cm^{-1})	Transmittance
SN15	2	896.74	0.78
SN16	4	896.74	0.75
SN17	6	896.74	0.71

Based on Figure 4.33, it shows that high Cs content in TPA posess high intensity of 896 cm^{-1} absorption band. It can be explained by the low acidity displayed by CS02, CS04 and CS06. Low acidity and high hydrophobicity of CS04 and CS06 did not cause any increment in crystallinity degree of nanocellulose. Low interaction of CS04 and CS06 in water medium makes them less ionizable thus producing lesser numbers of hydronium ion. Low concentration of proton makes the penetration and rupture of amorphous region less pronounced. As a result, the production of nanocellulose was fully developed from ultrasonication energy through defibrillation and fragmentation process. The breaking activities of hydrogen bond network were higher compared to the breaking of glycosidic linkages. This has undoubtedly maintained the high percentage of amorphous domain in the nanocellulose produced since the breaking of ether bond in amorphous region was less pronounced. Additionally, infrared spectroscopy above shows no trace of HPA left which means that the nanocellulose purification has been successful.

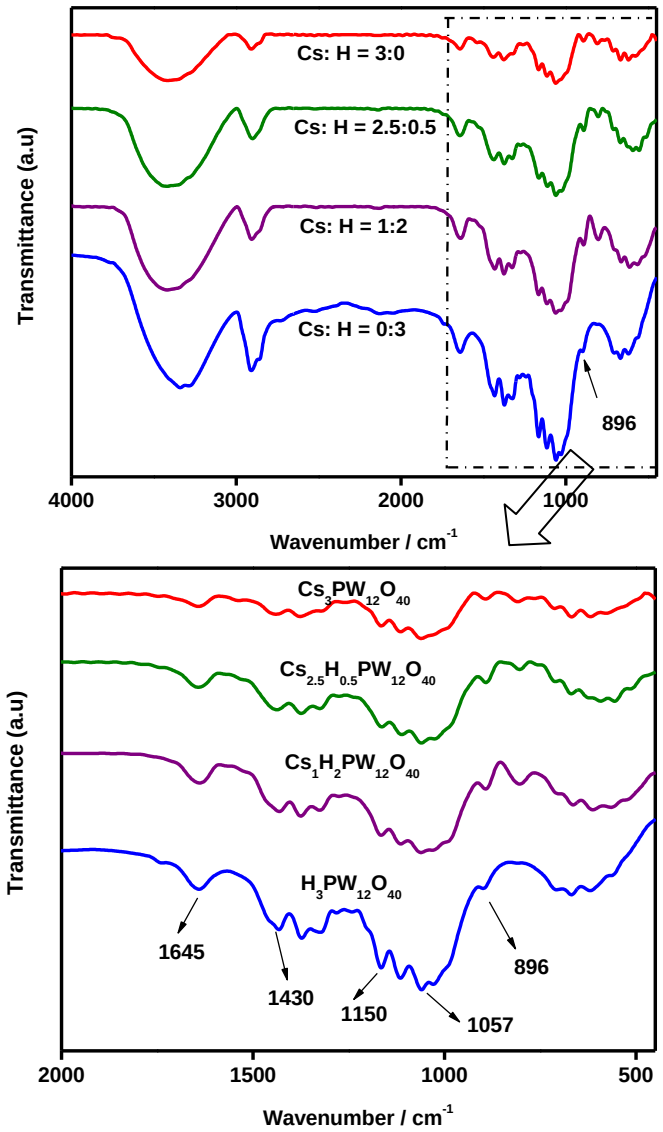

Figure 4.33: Chemical structure of nanocellulose catalyzed by $Cs_xH_{3-x}PW_{12}O_{40}$ at different Cs:H ratio.

Table 4.27: Relationship between Cs: H ratio with transmittance's intensity at absorption bands 896 cm^{-1}.

Sample ID	Catalyst ID	Cs: H ratio	Wavenumber (cm^{-1})	Transmittance
SN16	CS01 (TPA)	0:3	896.74	0.75
SN18	CS02	1:2	896.74	0.78
SN19	CS04	2.5:0.5	896.74	0.79
SN20	CS06	3:0	896.74	0.84

4.6.3 Raman Spectroscopy.

Raman spectroscopy technique is important and effective method for investigating the vibrational spectra of cellulose, pulp as well as cellulose derivatives. Ease of sample preparation and short analysis time make it a popular characterization technique besides FTIR spectroscopy. Moreover, Raman spectra also contributed to further conformation and examination on the NCC generated which has been analyzed by FTIR spectroscopy. Furthermore, Raman spectroscopy is a useful tool in evaluating the degree of crystallinity of the cellulose other than XRD. Therefore, in this section, CrI through Raman intensity data will not be calculated since the CrI values of NCC has been calculated in section 4.5.3. This section will be focusing more in supporting the CrI values gained in the previous section.

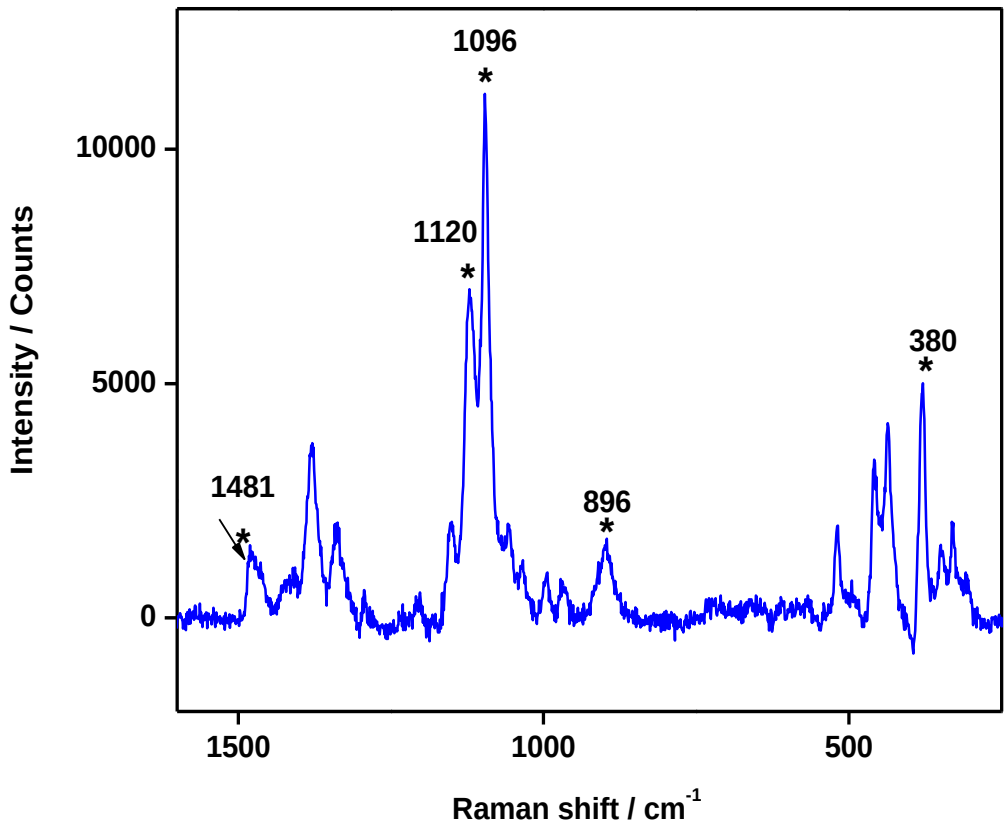

Figure 4.34: Raman spectra of microcrystalline cellulose (MCC) in the range of 250 – 1600 cm^{-1}.

Cellulose is a complex bio-molecule that possesses high vibrational degree of freedom that can be illustrated in Raman spectra, but some modes are probably degenerated. Cellulose is composes of C, H and O atoms and the main bonds is ether bond through β-1, 4- linkages. Therefore, the skeletal stretching and bending modes of C-C-C, C-O-C, and O-C-C are dominant, and located at region below than 600 cm^{-1} (Kavkler & Demšar, 2012). However, stretching of C-C and C-O in pyranose compounds was dominated at region of 800 to 1200 cm^{-1} (Wiley & Atalla, 1987). While asymmetric vibration signal specifically at 1150 cm^{-1} (Zhang, Feldner, & Fischer, 2011). Moreover, it has been mentioned previously that peak 896 cm^{-1} associates to cellulose crystallinity, whereby higher and narrower peak were related to low crystallinity and the value will shift to higher frequencies around 900 – 913 cm^{-1} when the crystallinity is higher (Szymańska-Chargot, Cybulska, & Zdunek, 2011).

The notable peak at 1096 cm^{-1} is a characteristic peak of cellulose which represents the symmetric ring vibration of C-O-C group. This peak was usually related to peak at signal 380 cm^{-1}, where the relationship between these two intensity values gives a CrI of a cellulose material (Agarwal, Reiner, & Ralph, 2010; Agarwal, Reiner, Filpponen, Isogai & Argyropouos, 2010). Peaks at 1481 cm^{-1} and 1462 cm^{-1} are an assignment band for H-C-H scissoring bending in cellulose I. Both peaks will appear at crystalline cellulose while lacking of peak at 1481 cm^{-1} is a confirmation of amorphous cellulose (Schenzel, Fischer, & Brendler, 2005). Therefore, through mercerization process the loss of peak 1481 cm^{-1} will be replaced with broad 1462 cm^{-1} which indicates the transformation of cellulose I to cellulose II. As a result it can be concluded that high degree of crystallinity corresponds to higher peaks at 1481 cm^{-1} (Szymańska-Chargot et al., 2011). The main purpose of introducing ultrasonication in the production of NCC is to help defibrillation of cellulose polymer chain.

It has been mentioned, that peak 1481 cm^{-1} is use qualitatively to indicate whether the NCC contain highly crystalline structure or not. Based on Table 4.28, the intensity of peak 1481 cm^{-1} has increase from 1158 to 2340 counts when being subjected to powerful sonication power. Raman spectroscopy was done in order to strengthen as well as to support the statement that higher sonication power increases the degree of crystallinity. That statement has been already proven quantitatively in section 4.6.1. The extensive energy generated from cavitation process has significantly disintegrated the fiber into less compact form. The complex multilayers of cellulose polymer chain was later reduced and create better probability in revealing or exposing highly crystalline cellulose crystallite. The embedded crystalline region in the matrix of amorphous domain has reduced the exposure of cellulose's crystalinity. Appropriate amount of energy can also lead to fiber defragmentation which increases the crystallinity of NCC. The intramolecular forces hydrogen bond present in flexible amorphous region was broken revealing the rigid crystalline region unharmed.

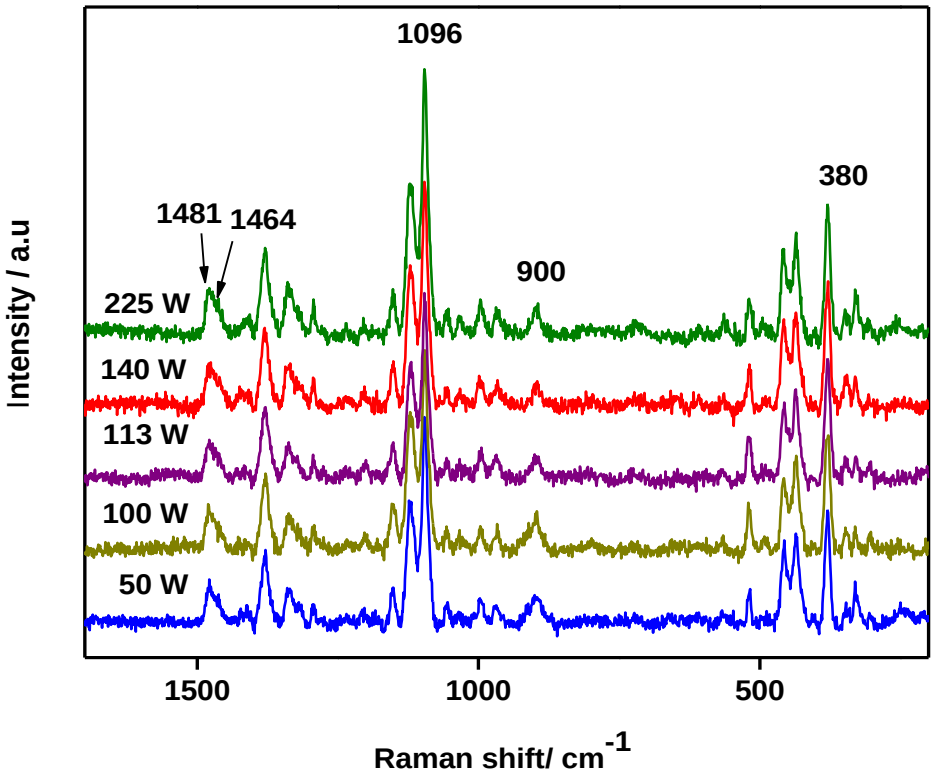

Figure 4.35: Raman shift for NCC generated on effect of sonication power

Table 4.28: Intensity of peaks 1481 and 1464 cm^{-1} on effect of sonication power.

Sample ID	Power (W)	Raman shift of 1481 cm^{-1}	Raman shift of 1464 cm^{-1}
SN01	50	1158	801
SN02	100	1472	1072
SN03	113	1956	1466
SN04	140	2126	165
SN05	225	2340	1975

Based on previous description about Raman spectroscopy, the Raman spectra will give a lot of information about the skeletal stretching of the main bonds present in cellulose molecules. Longer treatment time of sonication toward cellulose fibers has significantly affected some of the original skeletal backbone of cellulose molecules. Different treatment time at higher energy of sonication has caused some changes in the vibrational properties of cellulose fibers. The difference can be illustrated in Figure 4.36. A specifically characteristic band at 1481 cm-1 was further focused, and the intensity was tabulated in Table 4.29. It can be clearly observed that all the spectra exhibit similar patterns. Peak 1481 cm^{-1} is assigned to $–CH_2$ bending, the peak intensity increase when longer treatment time is introduced. This peak indicates the difference in crystallinity degree in the NCC samples. Higher intensity of this peaks is corresponds to high crystallinity index (CrI). Moreover, peak at 896 cm^{-1} displayed in Figure 4.36 is shifted to higher frequencies around 900 cm^{-1}, which signifies an increment in crystallinity. Therefore, the information given creates a good correlation with section 4.6.1 thus support the hypothesis of longer sonication time increases the CrI of NCC produced.

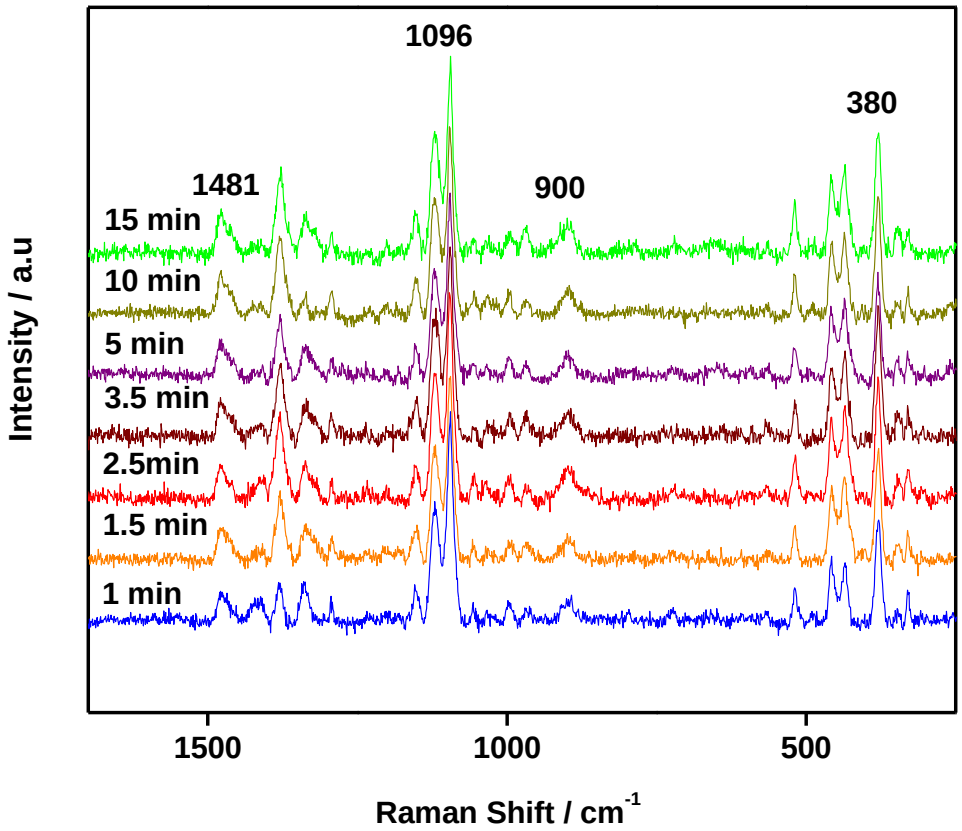

Figure 4.36: Raman shift for NCC generated under effect of time

Table 4.29: Intensity of peaks 1481 and 1464 cm^{-1} on effect of sonication time.

Sample ID	Time (min)	Raman shift of 1481 cm^{-1}	Raman shift of 1464 cm^{-1}
SN08	1	986	754
SN09	1.5	1137	869
SN10	2.5	1389	912
SN11	3.5	1532	1144
SN12	5	1798	1474
SN13	10	2340	1975
SN14	15	2513	2137

HPA plays an important task in facilitating the depolymerization of cellulose through hydrolyzing the unordered crystallites that constitutes the amorphous domain. The presence of Keggin anion of TPA can be detectable through the existence of peak at 1010 cm^{-1} (Figure 4.37(b)). The peak was assigned as the characteristics band for the phosphate group (Mioč, Stojadinović, & Nedić, 2009) presence in the main backbone of Keggin's TPA. However, the peak disappears after the purification process were accomplished leaving only the main characteristic peaks of cellulose as shown in Figure

4.37. As discussed earlier, the peak at 1481 cm^{-1} is an indicator peak for degree of crystallinity and it was measured quantitatively using the intensity (counts). Moreover, the control for this reaction was SN05 and addition of 2 g of TPA in catalyzing the reaction has caused an increment of intensity from 1145 counts to 1258 counts. Thus, this demonstrates and proofs the catalyst effectiveness in catalyzing the depolymerization process. The value continues to increase up to 2114 counts when 4 g of TPA was added but lowered when the amount reached 6 g. This phenomenon was seen earlier in evaluating CrI using XRD method. Higher concentration of hydronium ion in the reaction medium has caused excessive hydrolysis to the ether bond present in the crystalline region. As a result, less amount or content of crystalline region present in each of the polymer chain.

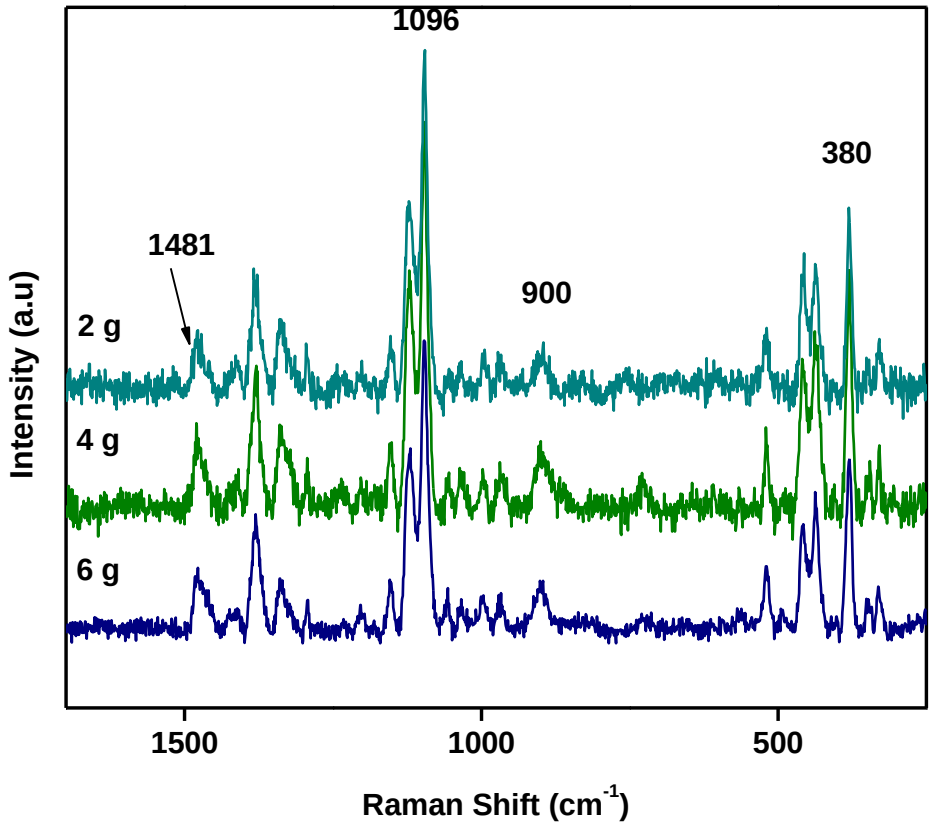

Figure 4.37(a): Raman shift of NCC generated under effect of TPA's amount after purification process.

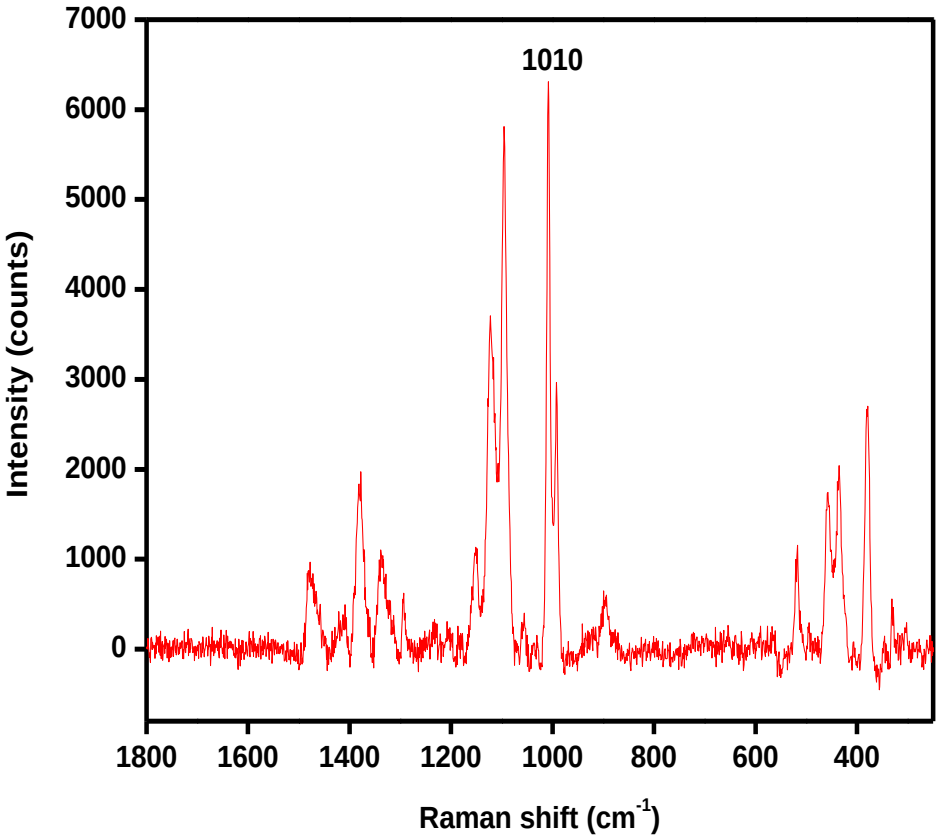

Figure 4.37 (b): Raman shift of NCC generated under effect of TPA's amount before purification process.

Table 4.30: Intensity of peaks 1481 and 1464 cm^{-1} on effect of TPA's amount.

Sample ID	TPA's amount (g)	Raman shift of 1481 cm^{-1}	Raman shift of 1464 cm^{-1}
SN15	2	2390	2116
SN16	4	2599	2066
SN17	6	2321	2122

Acidic cesium salts of TPA are common in many organic synthesis reactions especially in liquid – liquid phase reaction (Kozhevnikov, 1995). Increasing the cesium content in the Keggin network has caused an alteration on the physical and chemical properties of the catalyst. The critical effects of the TPA transformation during the substitution process are the hydrophobicity and decreasing acidity. Those effects have tremendously reduced the crystallinity of NCC produced through the reduction of crystallinity characteristic band at 1481 cm^{-1}. From SN16 to SN18, 40 % intensity reduction has taken place, and the biggest reduction occurred from SN19 to SN20 where it causes

about 50 % of intensity reduction. This is because when the cesium content increased until the ratio of Cs: H reaches 2.5: 0.5, the concentration of proton present in the reaction media is limited due to the hydrophobicity of the catalyst. As a result, the hydrolysis efficiency dropped due to low interaction between the two compounds. The same effects and explanations can be implemented when the ratio of Cs: H reaches 3:0. It can be clearly observed that the area under the curves at peak 1481 cm^{-1} were very small compared to the other three spectra and peak at 903 cm^{-1} is shifted to lower frequencies when the cesium content increased to the maximum. The shifting indicates an increasing amount of unordered crystallites in the NCC produced. This can be concluded that the cellulose depolymerization through acid hydrolysis process becomes less pronounce when being catalyzed with acidic cesium salt of TPA compared to TPA alone.

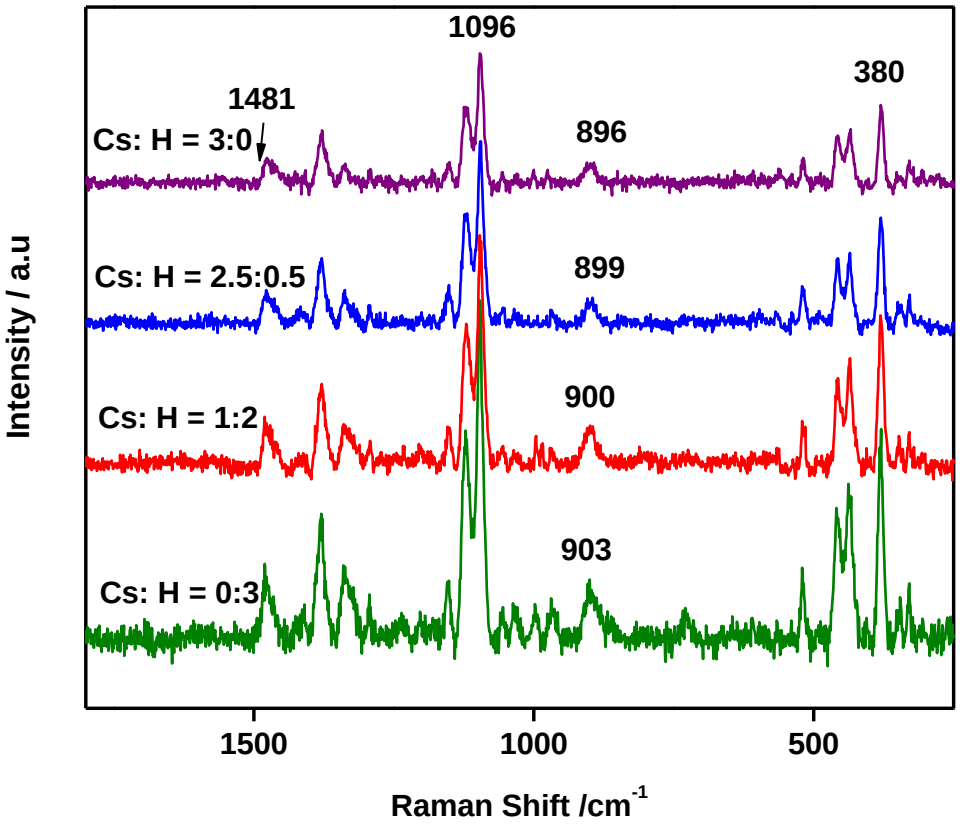

Figure 4.38: Raman shift of NCC catalyzed by $Cs_xH_{3-x}PW_{12}O_{40}$ at different Cs:H ratio

Table 4.31: Intensity at peaks 1481 and 1464 cm^{-1} at effect of Cs: H ratio

Sample ID	Ratio Cs: H	Raman shift of 1481 cm^{-1}	Raman shift of 1464 cm^{-1}
SN16	0:3	2114	2066
SN18	1:3	1313	1035
SN19	2.5:0.5	1278	1112
SN20	3:0	1149	943

4.5.4 Particle Size Distribution (PSD)

Particle size distribution (PSD) or size dispersion analysis was accomplished to discover the statistical distribution of NCC particles in water dispersant (Zhou, Fu, Zheng, & Zhan, 2012). Generally, Dynamic Light Scattering (DLS) or sometimes referred as Quasi –Elastic Light Scattering (QELS) is an established method designed for measuring size of particles that has a dimension lower than 1 nm. DLS has the advantage of less time consuming compared to microscopy- based method.

Basically, applications of DLS are for determining particles sizes which have been successfully dissolved in a liquid (dispersant). The Brownian motion of freely moving NCC particles in water dispersant causes the laser light to be scattered at different intensities. Three measurements were taken with each reading takes 120 s, and the standard deviations of the reading are stated. The PSD values range from 37.84 nm to 91.26 nm were tabulated in Table 4.32 until Table 4.35, and the histogram of the values listed are illustrated in Figure 4.39 until Figure 4.42.

PSD analysis reveals an average particle size of less than 100 nm for almost 90 % number of particles. However, a small percentage of particles size larger than 100 nm also existed in the colloidal mixtures.

When the lowest ultrasonication power was subjected to the process, large proportion of particles size is 68.09 nm with 24.9 % was measured with 10.6 % of particles size were larger than 100 nm. Increasing sonication power from 50 W to 225 W has narrowed the size distribution curves with almost 100 % number of particles posses size less than 100 nm. By introducing high sonication power the hydrogen bonds interconnected within the cellulose polymer chain was harshly destroyed thus resulting in narrowing NCC size distribution. Therefore, when the highest sonication power was applied to the cellulose mixture, defragmentation of cellulose fiber also occurred through intramolecular hydrogen bonding breakage which caused 88.5 % of NCC particles sizes ranging from 58.77 nm to 79.92 nm were gained obtained compared to NCC generated at 100 W with only 67.3 %. Besides that raising the sonication power from 50 W to 225 W has decreased the amount of particles having size bigger than 100 nm.

Table 4.32: PSD values of NCC prepared from effect of sonication power.

Size	**Number (%)**				
	SN01	**SN02**	**SN03**	**SN04**	**SN05**
	50W	**100W**	**113W**	**140W**	**225W**
50.75	9.1	9.10	2.0	-	6.2
58.77	23.2	23.20	22.1	1.0	26.4
68.06	24.9	24.90	42.2	25.5	38.9
79.92	19.2	19.20	27.3	48.2	23.2
91.26	13	-	4.5	23.6	4.6
Total	89.4	76.40	98.1	98.3	99.3

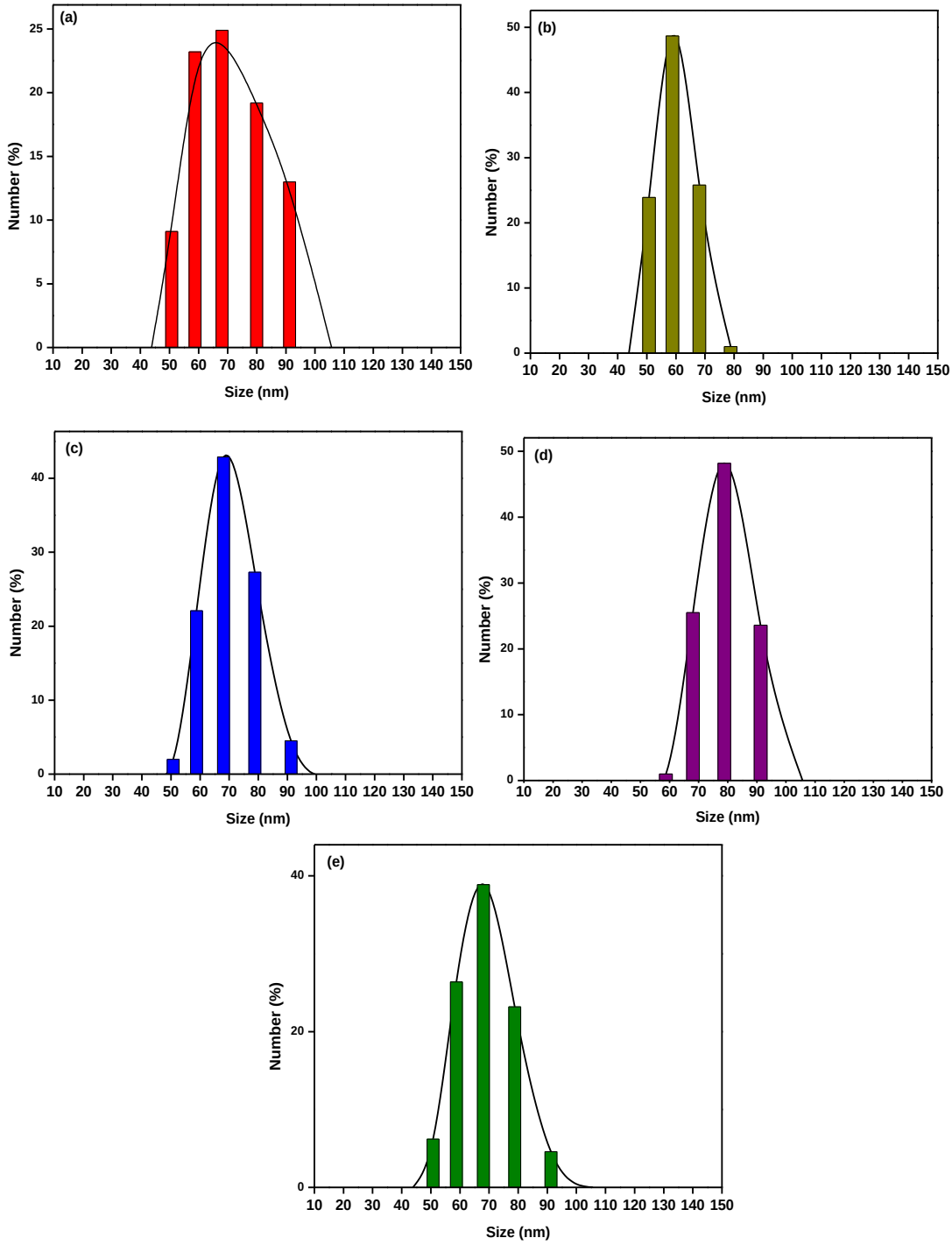

Figure 4.39: PSD of NCC prepared from effect of sonication, a) 50W, b) 100W, c) 113W, d) 140 W and e) 225W.

Ideal treatment time in depolymerization of cellulose through ultrasonication is crucial in producing a good distribution of particles size. Short sonication time produced only 29.8 % of particles with size less than 100 nm with the smallest size obtained were 68.06 nm. However, when 15 minutes of treatment time was applied, a wider range of particles size was obtained with the smallest size is 37.84 nm. Table 4.33 shows that the percentage of particles size smaller than 100 nm increases when longer sonication time was introduced. Despite the fact that the particles exhibit wider size distribution in 15 minutes reaction, the treatment managed to obtain size of 37.84 nm. This proves that, longer treatment time can create higher possibility in defibrillating and fragmenting the cellulose fibers.

Table 4.33: PSD values of NCC prepared from effect of sonication time

Size	**Number (%)**						
	SN08	**SN09**	**SN10**	**SN11**	**SN12**	**SN13**	**SN14**
	1min	**1.5 min**	**2.5 min**	**3.5 min**	**5 min**	**10 min**	**15 min**
37.84	-	-	-	-	-	-	8.3
43.82	-	-	-	-	4.4	-	16.2
50.75	-	-	-	-	12.6	6.2	23.4
58.77	-	-	3.3	6.6	12.1	26.4	31.6
68.06	3.5	3.7	10.2	19.8	11.0	38.9	18.2
79.92	10.4	11.4	16.1	21.1	15.6	23.2	1.7
91.26	15.9	20.2	20.2	14.2	16.3	4.6	-
Total	29.8	35.3	49.8	61.7	72.0	99.3	99.4

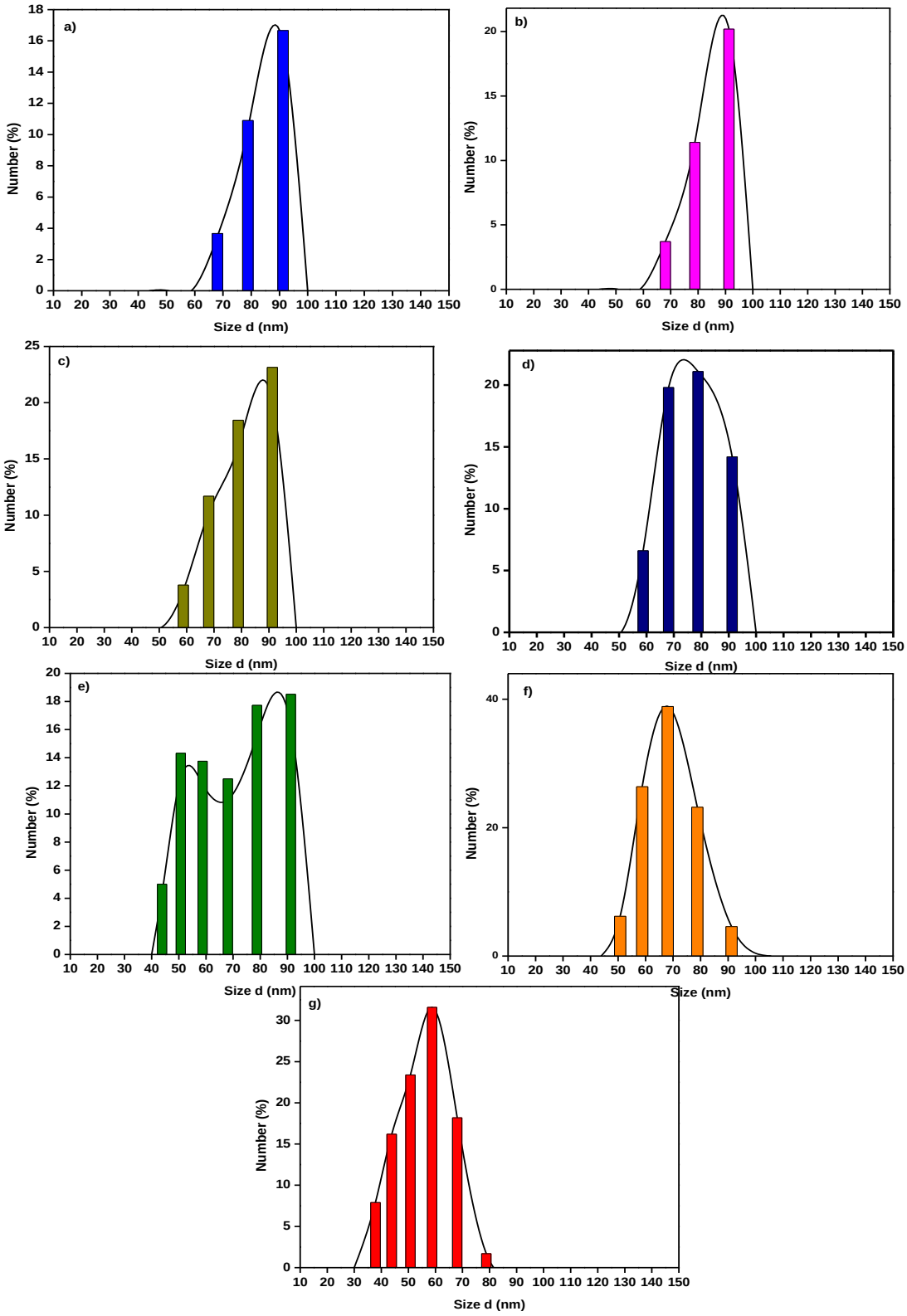

Figure 4.40: PSD of NCC prepared from effect of time; a) 1 min, b) 1.5 min, c) 2.5 min, d) 3.5 min, e) 5 min, f) 10 min, and g) 15 min.

Depolymerization of cellulose through TPA catalyzed reaction creates excellent particles size distribution with almost 100 % of particles exhibit size less than 100 nm. The results obtained indicated that TPA is one of the best catalysts in hydrolyzing cellulose fibers other than sulfuric acid. SN05 was the blank used for these reactions. The addition of TPA has produced NCC with the smallest size of 43.82 nm with 5.5 %, however the smallest size for SN05 was only 50.75 nm with 6.2 %. When TPA amount was increased from 4 g (SN16) to 6 g (SN17), the difference in number of particle size obtained was only 0.3 %. This shows higher amount of TPA has generated higher concentration of hydronium ion in reaction media. The concentrated hydronium ion present has consequently boosted up the probability of proton in hydrolyzing the cellulose fiber thus allowing the rupture of β - linkages.

Table 4.34: PSD values of NCC prepared from effect TPA's amount

Size	**Number (%)**		
	SN15	**SN16**	**SN17**
	2 g	**4 g**	**6 g**
37.84	-	10.0	14.6
43.82	5.5	17.1	18.2
50.75	9.6	23.4	24.0
58.77	16.4	33.2	30.7
68.06	22.1	15.4	11.9
79.92	27.3	-	-
91.26	15.2	-	-
Total	96.1	99.1	99.4

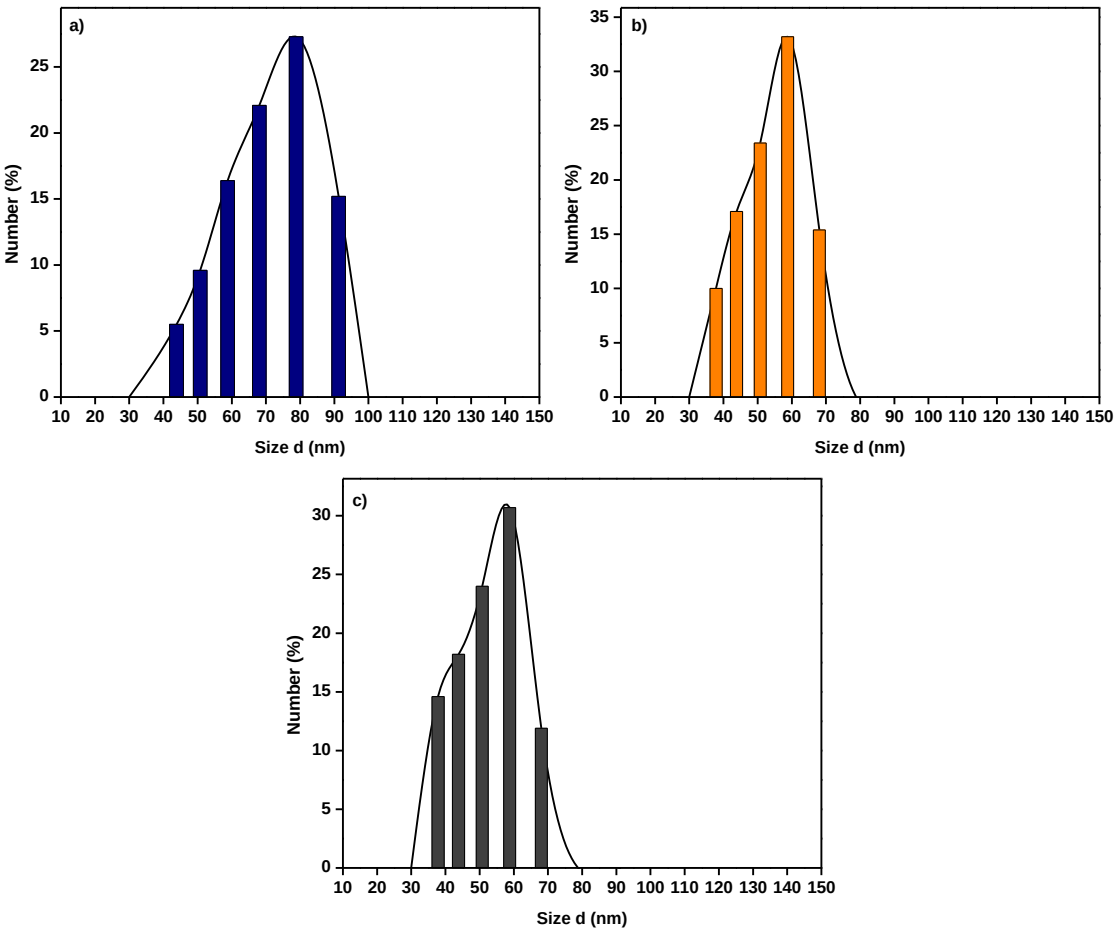

Figure 4.41: PSD of NCC prepared from effect of TPA's amount; a) 2 g, b) 4 g and c) 6 g.

Depolymerization process catalyzed by high cesium content catalyst has reduced the number of particles size in nano-size dimensions. This was clearly shown in Table 4.35 that by increasing Cs: H ratio fewer NCC with particles size less than 100 nm was obtained. Furthermore, when no cesium was present, the particles size of NCC produced were almost 100 % with only 0.9 % particles displayed sizes more than 100 nm. The best size obtained was 37.84 nm (10.0 %). Presence of cesium atom extensively reduced the number of NCC particles size with none of particles exhibit sizes less than 50 nm. Catalyst in reaction SN19 to SN20 displayed low acidity with limited solubilization in water media. This has consequently limits the acid hydrolysis process during the defibrillation process.

Table 4.35 PSD values of NCC catalyzed by $Cs_xH_{3-x}PW_{12}O_{40}$ at different Cs:H ratio

Size	Number (%)			
	SN16	**SN18**	**SN19**	**SN20**
	0:3	**1:2**	**2.5:0.5**	**3:0**
37.84	10.0	-	-	-
43.82	17.1	-	-	-
50.75	23.4	7.6	-	-
58.77	33.2	22.5	-	-
68.06	15.4	23.1	2.1	1.6
79.92	-	9.2	9.1	6.4
91.26	-	3.9	17.8	10.0
Total	99.1	66.3	29.0	18.0

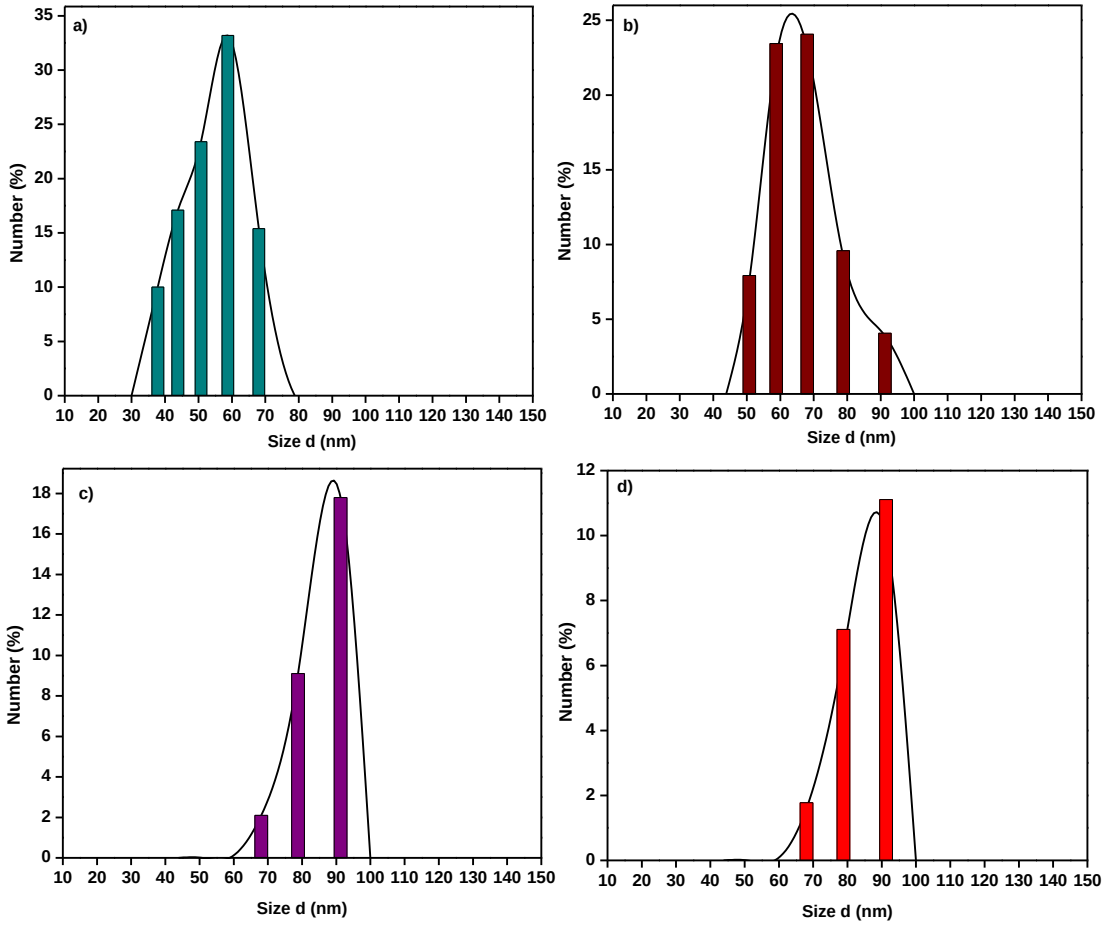

Figure 4.42: PSD of NCC catalyzed by $Cs_xH_{3-x}PW_{12}O_{40}$ at different Cs:H ratio ; a) Cs: H = 0:3, b) Cs: H = 1:2, c) Cs: H = 2.5:0.5 and d) Cs: H = 3:0.

4.6.5 Morphological analysis (SEM, TEM and AFM)

Optical microscope is generally used for observing micron level materials with reasonable resolution. Further magnification becomes less practical through common optical microscope due to aberrations and limit in wavelength of light. Hence the imaging using transmission electron microscope (TEM), scanning electron microscope (SEM) and atomic force microscopy (AFM) have been developed to observe the sub-micron size materials. Though the principles of all the techniques are different, they generate a highly magnified image of the surface.

SEM, TEM and AFM were widely utilized to characterize the NCC morphology and dimensions. This method can provide information on NCC width and length. Although these techniques are able to provide that information, aggregations of cellulose nanofibers have caused difficulty in examining the edges of individual NCC. The nanofibers aggregation are theoretically due to high density free hydroxyl groups present on the nanofibers surface which allowed them to strongly interact and resemble thus lead to aggregation especially after drying.

Therefore, this section will explain thoroughly the visual explanation that occurs from microcrystalline cellulose (MCC) to cellulose nanocrystals (NCC) via images captured from SEM, TEM and AFM. Generally, SEM micrographs and AFM images displayed three-dimensional (3D) images while TEM can only illustrate two-dimensional (2D) images. Low magnification power capability inhibits in the imaging process from SEM techniques which make TEM and AFM the most favorable tools in viewing nano-scaled cellulose.

Raw material used for depolymerization process of cellulose was MCC originated from cotton linters. The non- conductive cellulose specimen was coated with a layer of gold by low vacuum sputter coating prior to SEM analysis. The action was taken in order to prevent accumulation of static electric charge on the specimen during electron irradiation (Joshi, Bhattacharyya, & Ali, 2008).

Figure 4.43, shows five different SEM images of MCC captured at various magnifications. It clearly shows the irregular shape and size distribution of the microfibrils in MCC. It can be clearly observed in Figure 4.43(a-c) that MCC are non – fibrous and appears as big clumped particles. The SEM images (Figure 4.43 (d-e)) of one individual macrofiber at larger magnification shows that the surface of the fiber is uneven and rough with presence of pores. Each particle shows a compact structure exhibiting an alignment on the fiber surface.

Generally, MCC particles consist of non – fibrous component with width of 20 to 40 μm and length more than 50 μm. The non –fibrous component are scattered over the surface, displaying variation of size. The agglomeration prevents us from correctly measuring the length and diameter of corresponding fibers. MCC can be easily obtained through hydrolysis of cellulose using dilute mineral acids.

The treatment applied has effectively converted MCC into NCC. Figure 4.44 to Figure 4.47 shows the TEM micrographs of dilute nanocellulose suspension generated through depolymerization process. The main mechanisms applied in the production of NCC were defibrillation and fiber fragmentation. The analysis has revealed that the aqueous suspensions of NCC consist of whisker like particles rather than rod like structure. Based on Figure 4.43, the big cluster of cellulose present in the micro- range scale has been successfully transformed into smaller dimensions with nano-range scale. The non –fibrous MCC cluster particles was destroyed and transformed into small irregular

shape of nanowhisker (Figure 4.44). The help of mechanical treatment itself has actively transformed big chunky agglomerated cellulose into less thick nano –whisker under appropriate condition. By adding Bronsted acid (TPA) into the reaction process, the particles generated were thinner and appear as needle-like shape (Figure 4.45). The presence of proton donated from Bronsted acid activity has increased the fibrils fragmentation activities thus reducing the thickness of the particles. Figure 4.46 has strongly illustrated the defibrillation process that occurs during the production of NCC. The detachment of the fibrils from the fiber was being enhanced by the cavitation process resulting from the high intensity ultrasonication. The energy generated from the ultrasonication process has forced the fibrils to appear freely from the fiber attachment. Prolonged sonication activity has given extra energy to break free the fibrils and undergo fragmentation which causes the fibrils to be shorter.

Some of the nanoparticle were agglomerated and aggregated in the forms of cluster particles, clumped in the form of bundle, though some of them are well separated. The agglomeration that happens between the particles shows that NCC particle were attracted via Van der Waals forces due to intermolecular hydrogen bonding and strong hydrophilic hydroxyl group on the NCC surface. The NCC dimension illustrated through TEM micrograph can be measurable. It was found that the diameter of NCC was in the range of 10 – 30 nm while the length was larger than 30 nm. Based on Figure 4.47 (4 g of $Cs_1H_2PW_{12}O_{40}$) a clear demonstration of defibrillation process can also be monitored. By comparing the images from Figure 4.45 (4 g of $H_3PW_{12}O_{40}$), the main difference between the two images is the configuration of the fibrils. The fibril in Figure 4.47 is longer compared to fibril in Figure 4.45. The interconnected fibrils illustrated in Figure 4.47 have proven that fibril fragmentation through breaking of B-linkages is crucial. Low concentration of hydrogen ions led to less breakage of fibrils which can lead to longer and entangled fibrils.

AFM of all NCC (Figures 4.48 to 4.51) show the aggregation and accumulation of the particles. Transition from 10 min to 15 min has changed the larger fibrils (20 nm in diameter) into a smaller fibril (10 nm in diameter). The aggregation of the particles makes it difficult to calculate the whole particles present in the image. However, a big difference has been illustrated in Figure 4.51 compared to other AFM images where the diameter of the NCC is much thinner. The application of HPA as a solvent and proton donor has successfully gives better quantity of nanocellulose compared to classical sulfuric acid. Sulfuric acid is a strong oxidizing agent which can lead to uncontrolled depolymerization of cellulose which causes the yield of NCC to decrease.

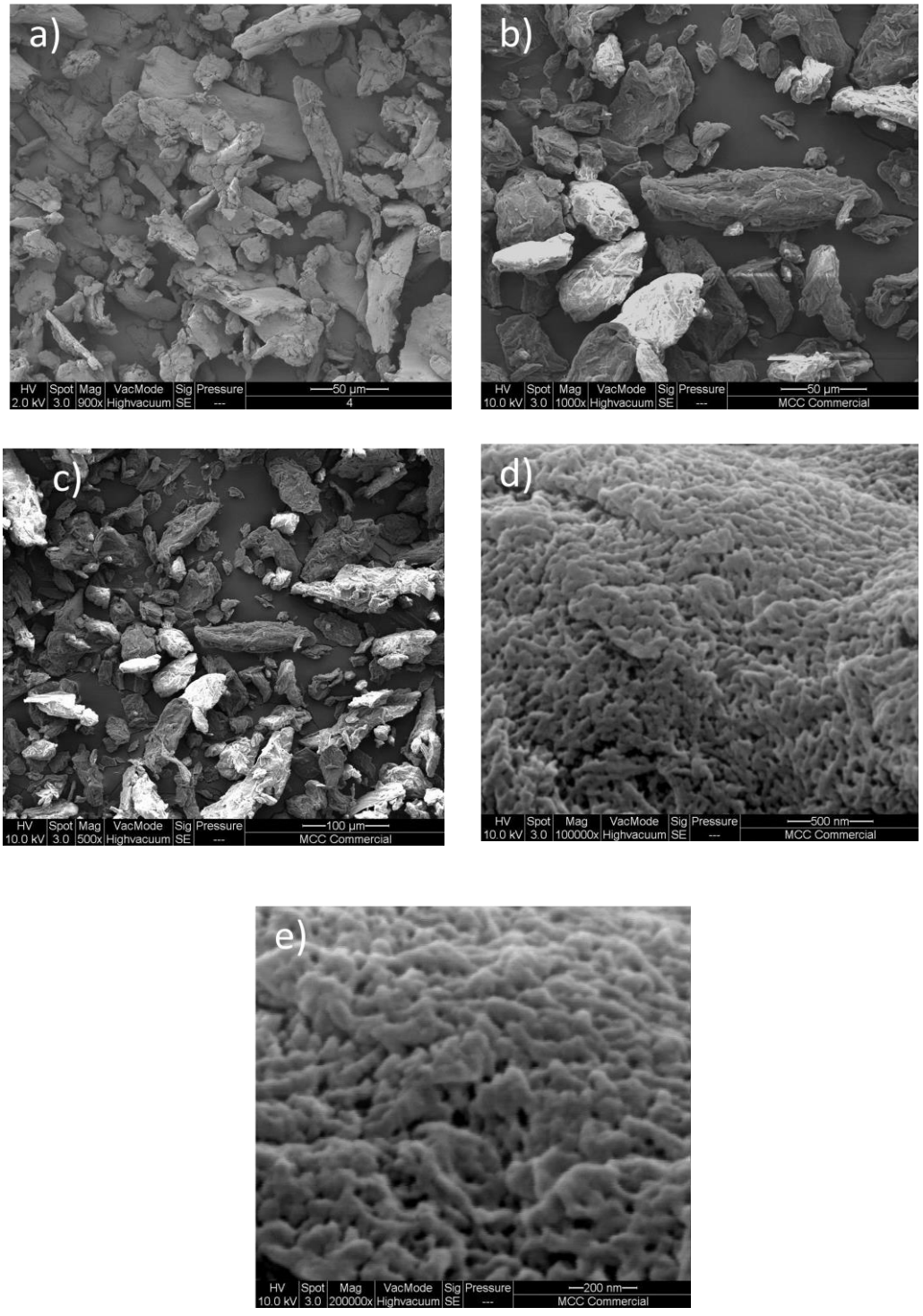

Figure 4.43: SEM micrographs for microcrystalline cellulose (MCC); a) MCC at 900x magnification, b) MCC at 900x magnification, c) MCC at 500x magnification, d) MCC at 100 000x magnification and e) MCC at 200 000x magnification.

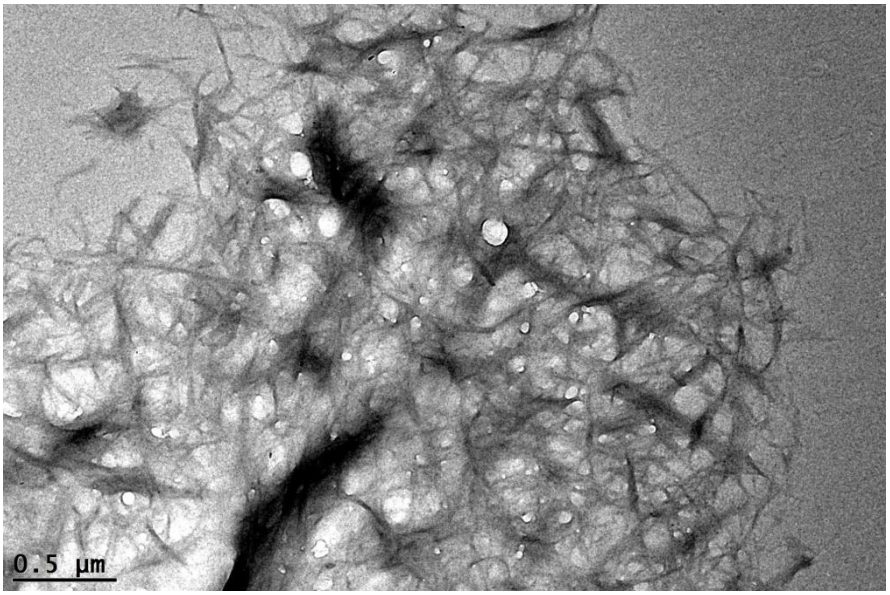

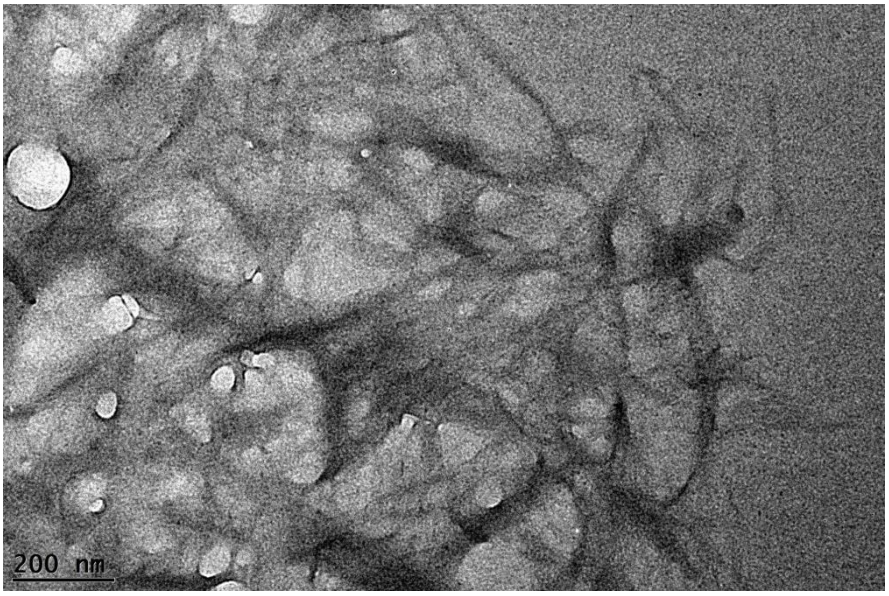

Figure 4.44: TEM images of NCC generated at 225 W for 15 min with absence of catalyst (SN14

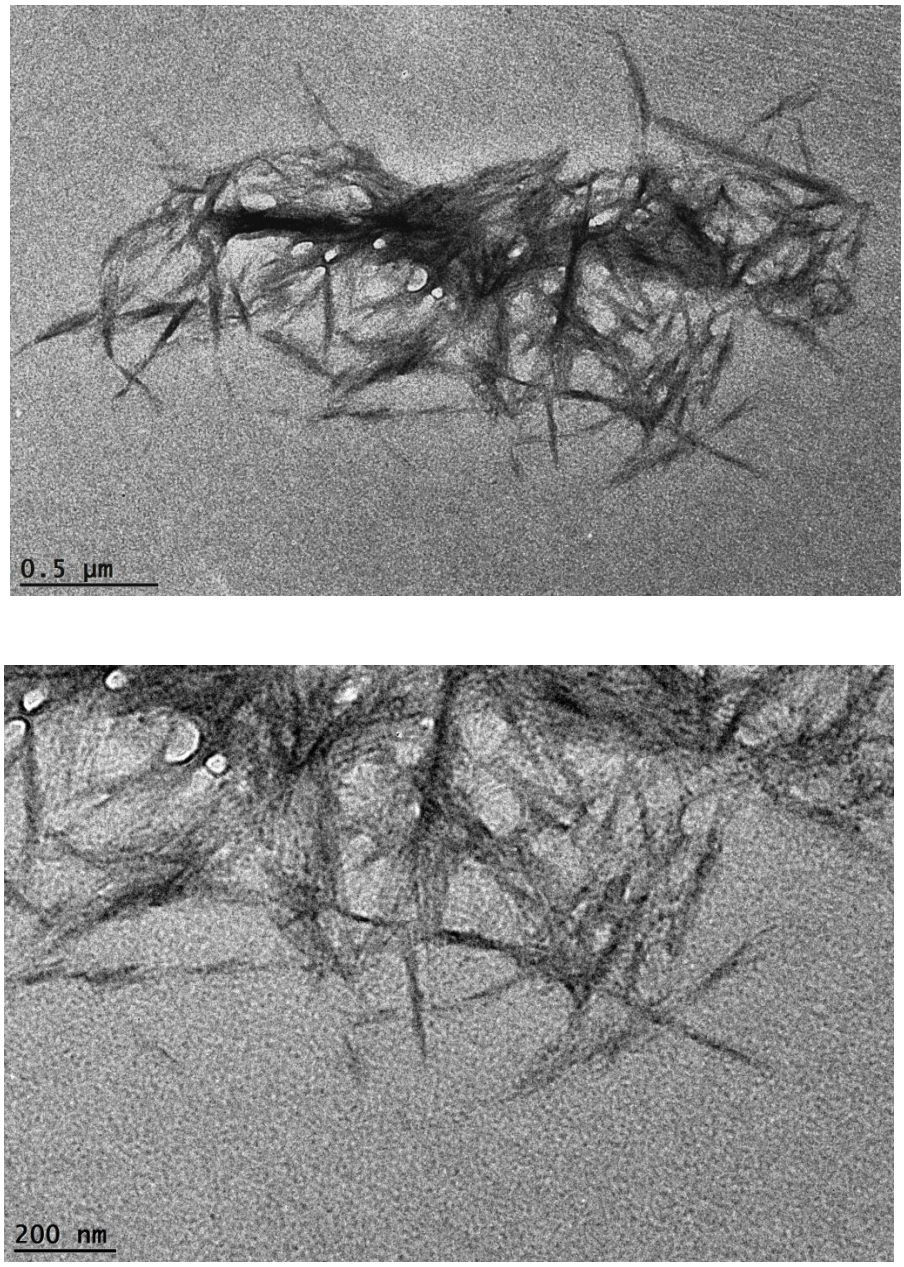

Figure 4.45: TEM images of NCC generated at 225 W at 10 min with 4 g of TPA (SN16)

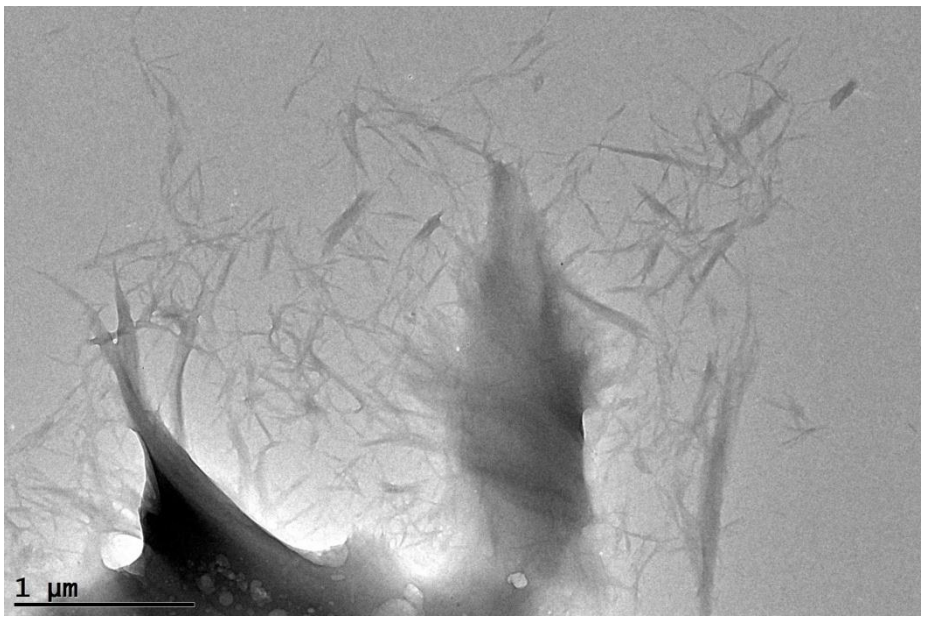

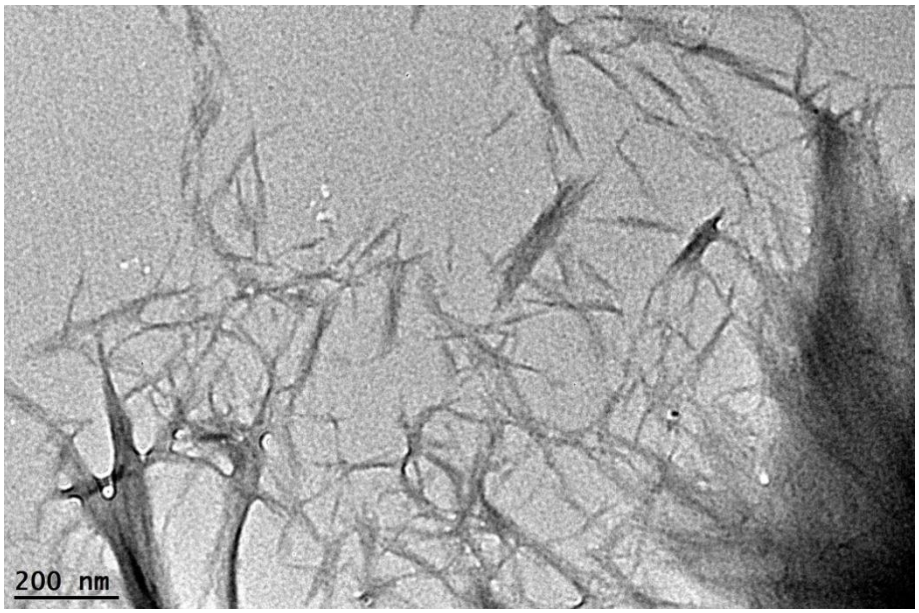

Figure 4.45 (continued): TEM images of NCC generated at 225 W for 10 min with 4g of TPA (SN16).

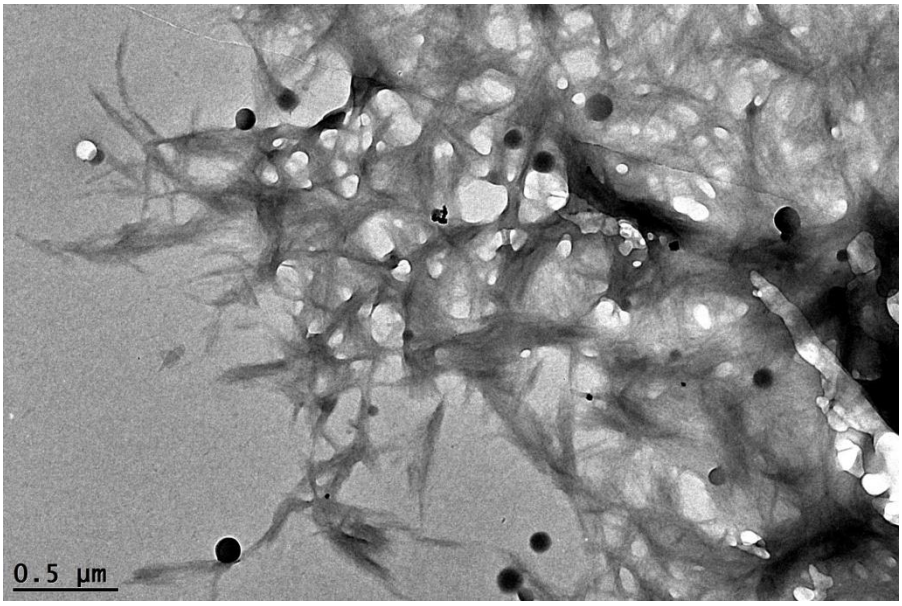

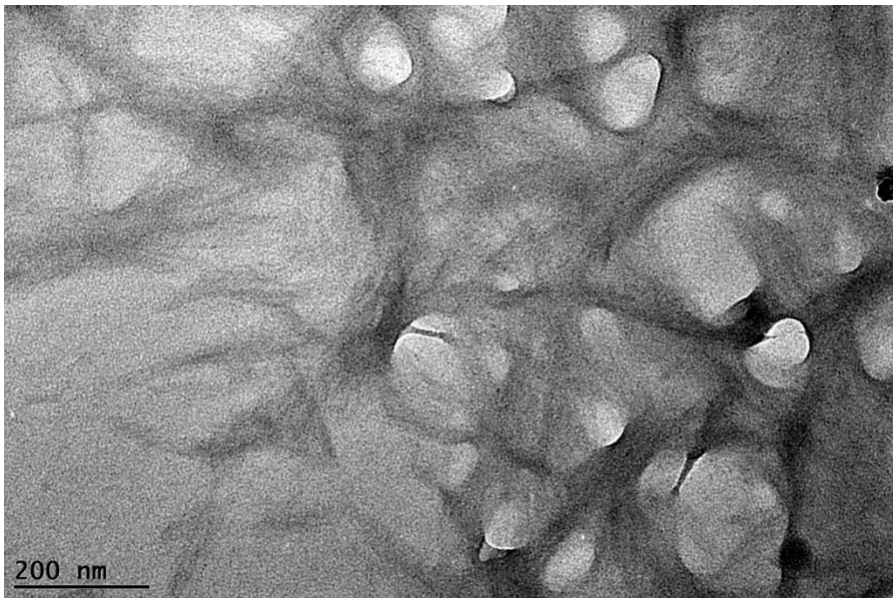

Figure 4.46: TEM images of NCC generated at 225 W for 10 min with absence of catalyst (SN13).

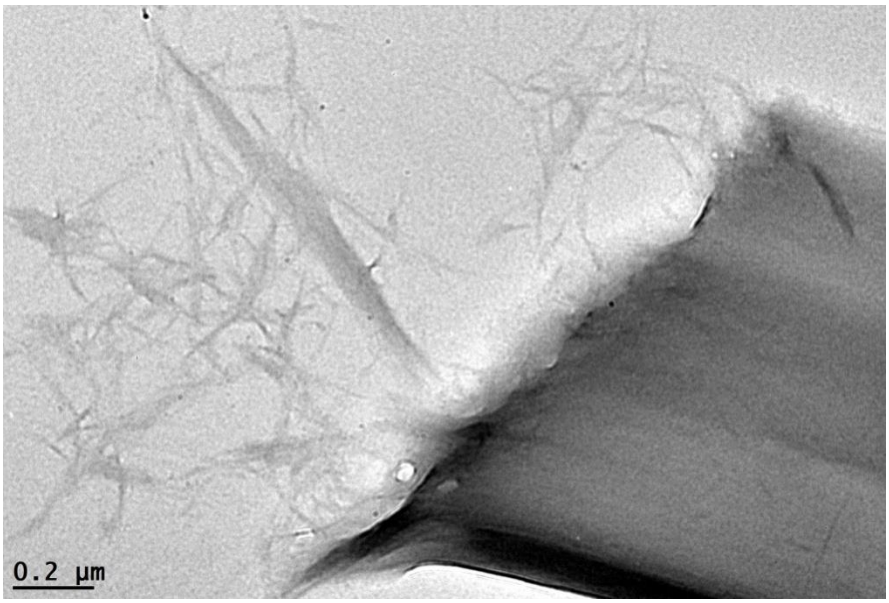

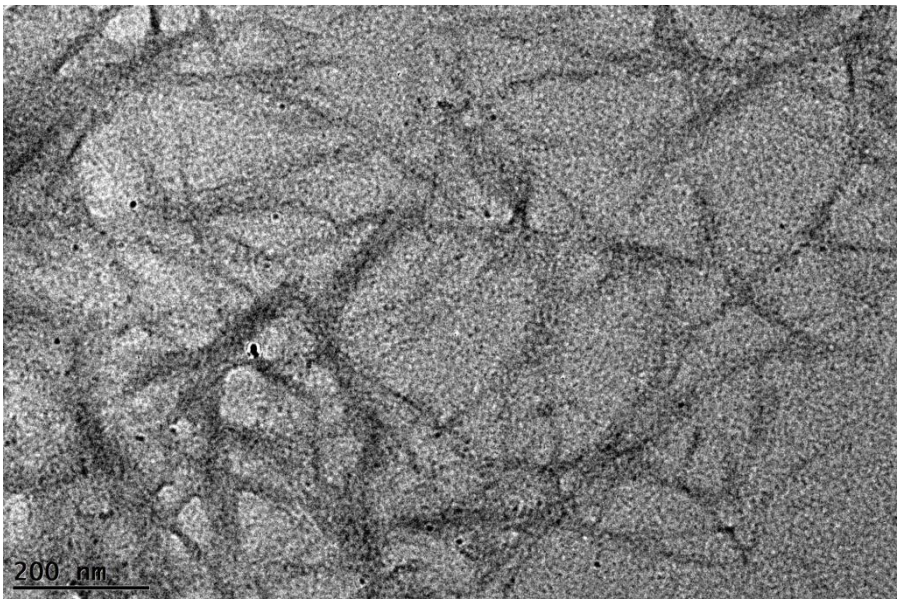

Figure 4.46 (continued): TEM images of NCC generated at 225 W for 10 min with absence of catalyst (SN13)

-

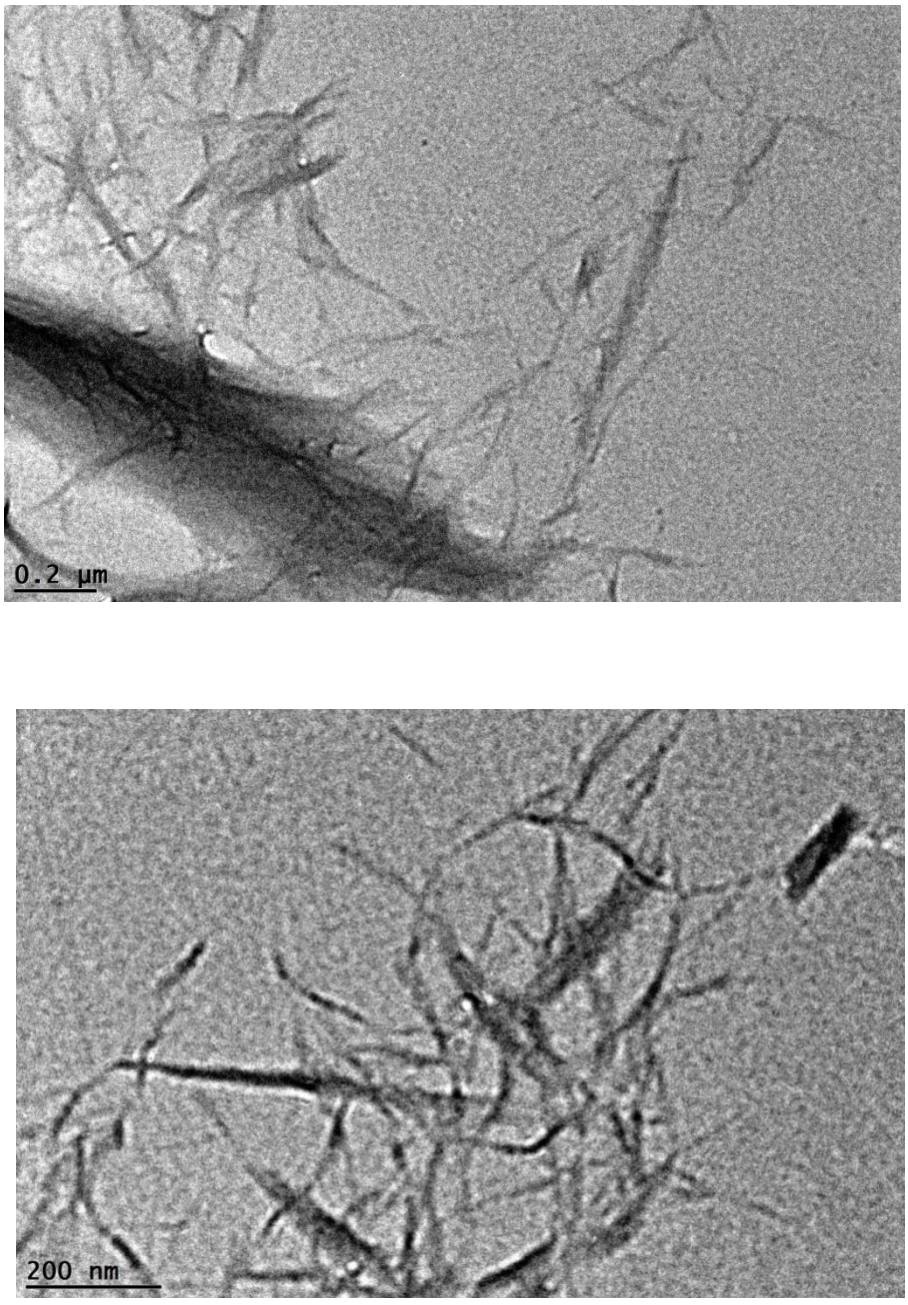

Figure 4.47: TEM images of NCC generated at 225 W for 10 min with 4 g of $Cs_1H_2PW_{12}O_{40}$ (SN18).

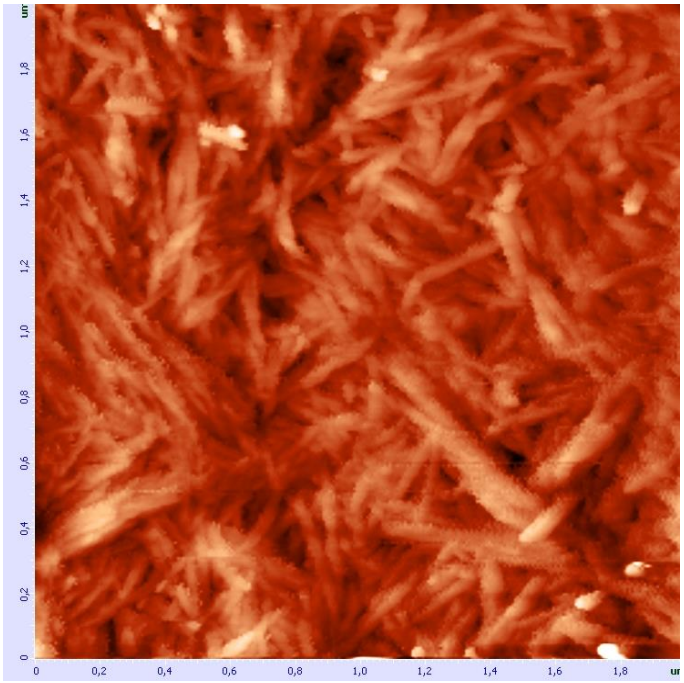

Figure 4.48: AFM images of NCC produced at 225 W for 10 min with absence of catalyst (SN13).

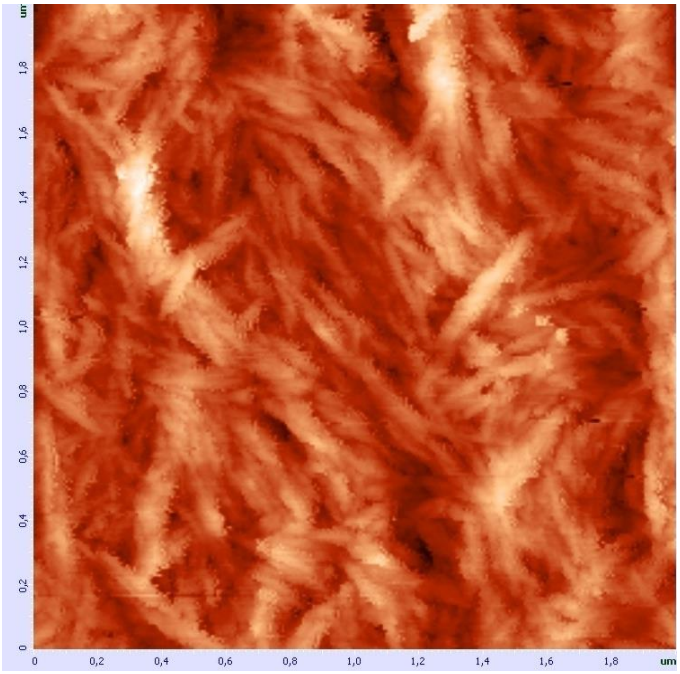

Figure 4.49: AFM images of NCC produced at 225 W for 15 min with absence of catalyst (SN14)

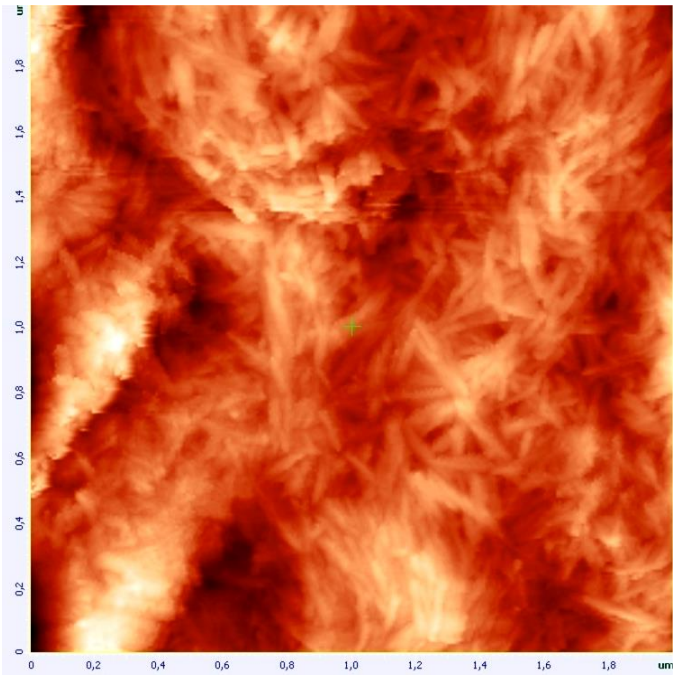

Figure 4.50: AFM images of NCC produced at 225 W for 10 min with 4 g of TPA (SN16)

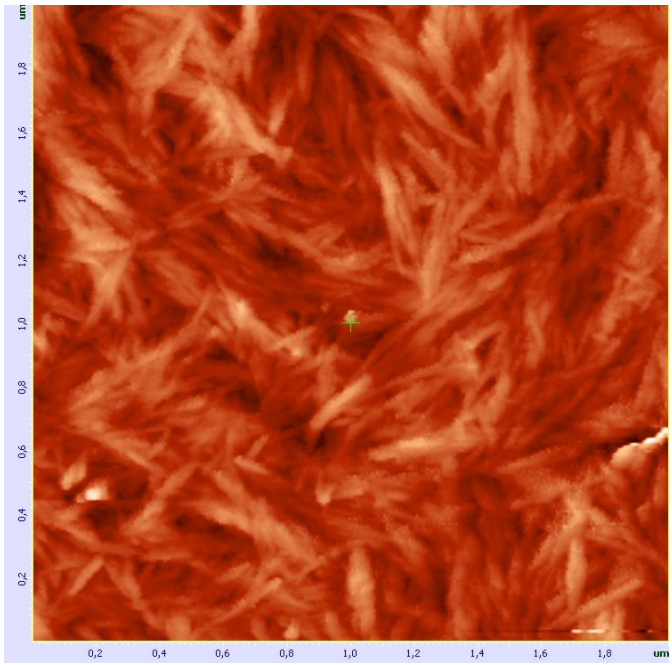

Figure 4.51: AFM images of NCC produced at 225W for 10 min with 6 g of TPA (SN17).

4.6.6 Thermal stability by Thermogravimetric Analysis (TGA)

Thermal stability of NCC can be identified using information given through Thermogravimetric (TG) curves and differential curves plotted below in Figure 4.52. The samples were burned under oxidizing environment that comprised mainly of oxygen gas through dynamic heating process. The flow rate of oxygen gas was controlled to 40 ml /min when entering the combusted chamber with specific heating rate subjected. The mass loss or the weight loss was recorded against temperature. Identification of thermal steadiness is important in identifying the highest temperature for NCC can withstand. Beyond that temperature, NCC will be oxidized into its simplest and low energy form that result the formation of tar, char and incombustible gases.

Table 4.36: Weight losses at various steps and temperature as obtained from thermal analysis data.

Sample	Step 1		Step 2		Residue (%)
	T_R (°C)	%	T_R (°C)	%	
SN05	25-130	6.35	290-488	93.65	0.00
SN14	25-130	6.16	281-467	91.77	2.07
SN16	25-130	4.33	282-462	94.71	2.96
SN18	25-130	2.14	301-422	85.62	12.24

TG and DTG curves of a) SN14; NCC generated at 225 W, 15 min with absence of catalyst, b) SN16; NCC generated at 225 W, 10 min with present of 4 g of TPA catalyst, c) SN05; NCC generated at 225 W, 10 min with absent of catalyst, and d) SN18; NCC generated at 225 W, 10 min with 4 g of $Cs_1H_2PW_{12}O_{40}$ catalyst. The weight loss was recorded upon continuous heating up to 1000 °C. The initial weight loss occurred at ~ 25 °C for all analyzed NCC. Based on Table 4.52, the first weight loss happen at temperature range 25 °C – 130 °C for almost all samples. The early weight loss recorded are maybe due to evaporation of moisture and loosely bound water that are

physically absorbed on the surface of NCC. It is remarkable to see that degradation of SN14 and SN16 are almost identical. However, both SN14 and SN16 undergo thermal decomposition at 281 °C. While for SN05 and SN18, the thermal degradation occurred at 290 °C and 301 °C respectively. Plus, the highest rate of degradation reported for SN05 and SN18 are 337 °C and 347 °C (revealed by DTG curve) correspondingly. Nevertheless, the rate of degradation of SN14 is 335 °C (revealed by DTG curve) and almost identical with SN16 with only 1 °C different which is 336 °C (revealed by DTG curve).

Through the information discovered above, SN 14 and SN16 have the lowest thermal stability while SN18 has the highest thermal stability. Early onset of degradation happens due to the high CrI posses by both SN14 and SN16. Both type of NCC posses 88.0 % degree of crystallinity. Higher content of crystalline domain of cellulose crystallite has reduced the thermal stability of NCC. This is because, the compactness of cellulose fiber has been broken down together with the collapse of highly connected hydrogen bonding that are responsible in enhancing the thermal stability of cellulose fiber. Plus, TPA catalyzed reaction has further disintegrated the fibers plus facilitate the defibrillation process thus increase the probability to have an early thermal decomposition.

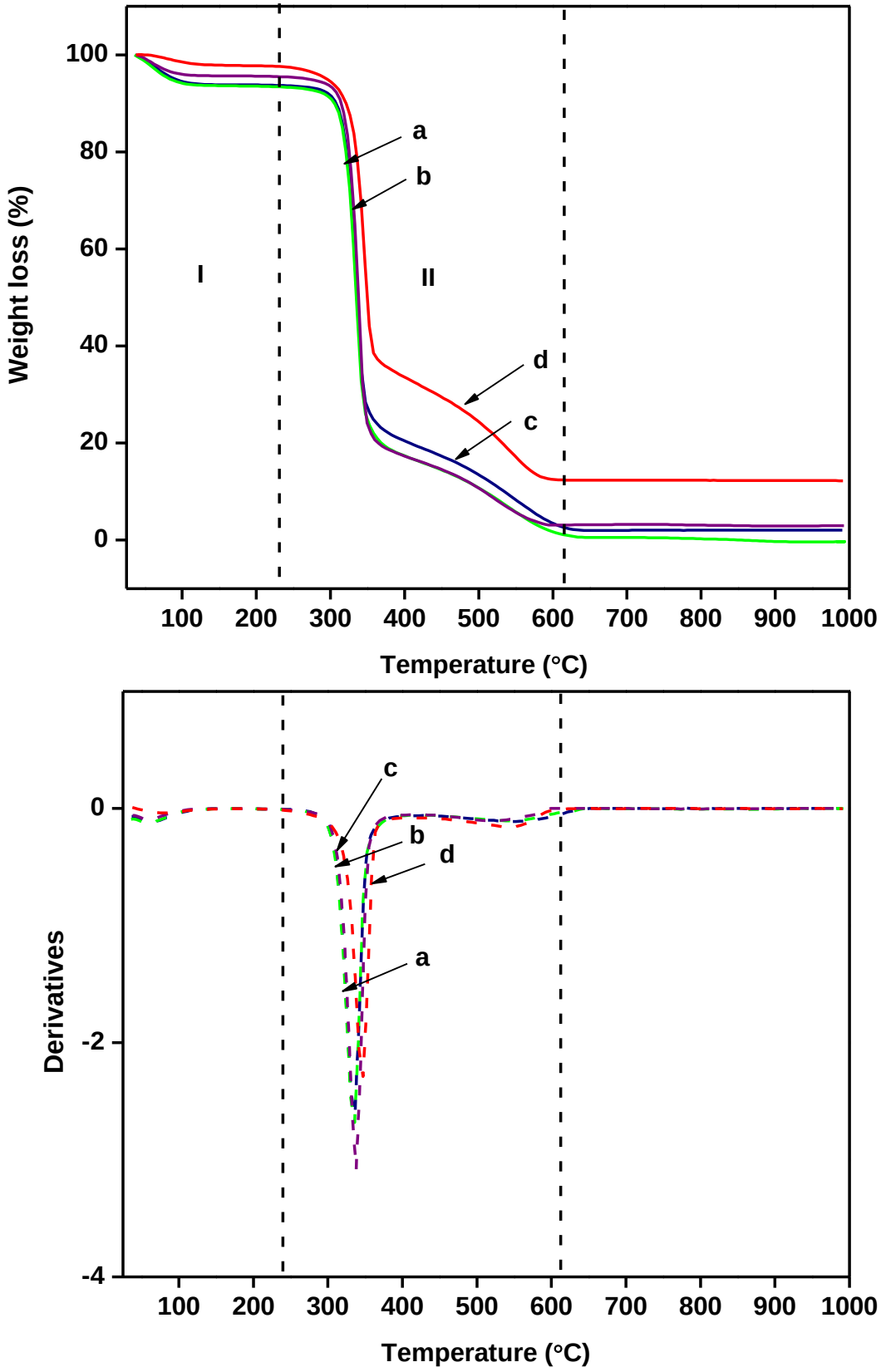

Figure 4.52: TG and DTG curve of a) SN14; b) SN 16; c) SN05; and d) SN18

4.7 Summary and discussion

New and advanced properties and functions, including biodegradability and sustainability, are required for the next generation of cellulose based products and their engineering applications. Nanocellulose is a novel material that has been gaining a lot of attentions due to their low cost, abundance and other excellent properties. Cellulose which is the skeletal components in all plants has been extensively utilized as the major feedstock for nanocellulose production.

The main constituent of cellulose starts in the cell wall, the extracytoplasmic matrices of plant cells, consist of a planned array of cellulose fibrils. Cell wall forms a continuous and dynamic network through the whole body of the plant (Kubicek & Christian, 2012). Cellulose that is a linear polymer is predominantly located in the secondary wall. The 3 group of hydroxyl group (Figure 4.54) of the monomer and their ability to form networking of hydrogen bonds play a major role in establishing the crystalline packing which governs the cellulose physical properties.

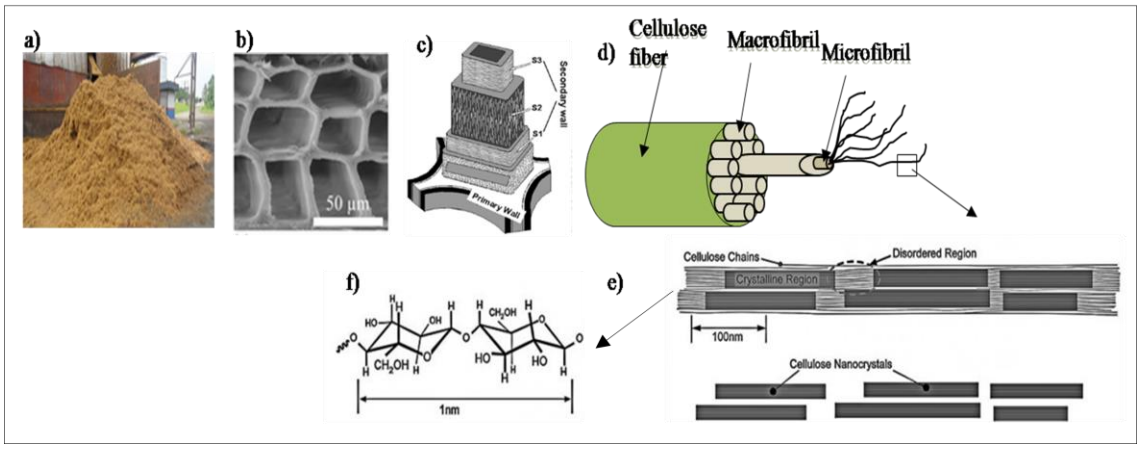

Figure 4.53: Wood hierarchical from biomass to cellulose; a) biomass, b) cellular structure, c) cell wall structure, d) fibril structure, e) elementary fibril, f) cellobiose.

The defibrillation and fragmentation of nanocellulose needs intensive mechanical treatment. It is worth noting that appropriate treatment on the cellulose fibers help to promote the accessibility of hydroxyl groups, increase the inner surface, alter the crystallinity and break the hydrogen networking to boost the reactivity of the fibers. Mechanical approaches help to diminish cellulosic fibers into nanofibers. A mechanical enhancement through mechanical shearing actions was applied on the cellulose fibers in order to release more individual cellulose microfibrils. The action has significantly increased the accessible area for the hydrolysis reaction to take place. The production route is normally associated with high energy utilization for example high intensity ultrasonication.

Ultrasonication energy introduced helps in delamination or defibrillation of cellulose fiber into a less complex cellulose microfibril. The energy generated from the ultrasonication process is through cavitation and the output energy is approximately 10 - 100 kJ/mol. The value obtained can significantly destroy the hydrogen bonding present, since it is within the hydrogen bond energy scale (Tischer, Sierakowski, Westfahl, & Tischer, 2010). As a result, the actions has broken the inter and intra hydrogen bond (Figure 4.54) present within the cellulose polymer chains thus exposing the individual fibrils of cellulose fiber. There are 3 types of hydrogen bonding network present in cellulose I, two intramolecular bonding involving O(2)---O(6) bonding and O(3)---O(5) and one intermolecular bonding O(6)---O(3). Application of ultrasonic energy will contribute a lot in breaking the intermolecular bond of O(6)---O(3) within the cellulose polymer chain. This has consequently generated high density of freely O-H group of O (6)-H and O (3)-H on the fibrils surface (Gardner et al., 2008).

Breakage of glycosidic bond by acids leads to the cellulose depolymerization which can cause the formation of nano-scaled cellulose. Minerals acids, such as H_2SO_4 have been extensively applied in hydrolysis of cellulose. However, they suffer from problems of

product separation, reactor corrosion and the need for treatment of waste influent. The use of solid acid catalyst can solve some of these problems through ease of separation and good catalyst recyclability. The acid strength, acid site density, adsorption of the substances and the micropore of the solid material are all key factors for effective depolymerization processes. HPAs are a type of solid acid, consisting of early transition metal oxygen anion clusters. The most common HPAs used are Keggin type acids. It has gained much attention due to the fascinating architectures and excellent physicochemical properties such as high proton mobility, Bronsted acidity and good stability. They dissolve and ionize in polar solvents and release H^+ whose acid strength is stronger than typical mineral acids.

Zeta potential gives information about the colloidal stability systems. The DVLO theory suggests that the stability of a colloidal system is determined by the sum of Van der Waals attractive and electric double layer repulsive forces that exist between particles as they approach each other (Horinek, 2014). Therefore to maintain the colloidal stability, the repulsive forces should be dominant. The negative value of zeta potential obtained is due to the dissociation of OH^- and $PW_{12}O_{40}^{3-}$ ions on the surface of the particles. The presence of Keggin anion has introduced the steric repulsion and electrostatic stabilization that help to separate the nanoparticle effectively. From the previous reported results, the surface charge increase when the sonication power, time and amount of TPA catalyst added increase. These increasing values were resulted from the good stability of NCC colloidal suspension. By referring to Figure 4.55, ultrasonication process creates high hydrophilicity on the microfibrils surface through polar hydroxyl group. The hydrophilicity was further enhanced through the formation of more exposed hydroxyl group through breakage of intramolecular hydrogen bonding.

As is known, cellulose depolymerization is always restricted by the poor contact between a catalyst and cellulose. The process might require higher catalyst/substrate

mass ratios and longer time to achieve maximum conversion. Extensive work has been focused on developing effective approaches or technologies for the cellulose depolymerization. By using HPAs under ultrasonication treatment, the yield of nanocellulose obtained is almost to 90 %.

The formation of smaller diameter nanocellulose was not only accompanied by ultrasonication activity but also through introduction of proton donor type solvent such as mineral acids. This is because, the application of acidic proton has led to fiber fragmentation which shorten the defibrillated fibrils and turns it into NCC and led to higher crystallinity degree at lower duration time. The dramatic morphology changes on cellulose microfiber were observed at increased depolymerization level with changing in crystallinity index calculated from the XRD patterns. The XRD patterns shows that the ordered structure of the crystalline domain on the cellulose is disrupted by ultrasonication and also acid hydrolysis. The large difference in reactivity between amorphous and crystalline region within cellulose results in fast removal of amorphous domain near the macrofibril surface, which leads to exposure of microfibrils cellulose. The loss of amorphous surface has significantly changed the apparent cellulose crystallinity.

Both FTIR and Raman spectroscopy have further confirmed the reduction of amorphous amount in that particular NCC samples. FTIR and Raman show changes in band and peak intensity at 896 cm^{-1} and 1481 cm^{-1} respectively. The particle size distribution (PSD) of NCC under effect of sonication power has successfully produced NCC with the smallest size of 50.75 nm. Prolongation of sonication time from 10 min to 15 min has increased the yield of nano-sized cellulose to 0.01 % with the smallest size of 37.84 nm. The application of TPA in catalyzing the reaction has increased the particle size (number %) of 37.84 nm from 8.3 % to 10 %. This shows that the yield of the smallest particle size (37.84 nm) can be increased at lower duration with the presence of TPA

catalyst. Eventhough the yield of SN16 (NCC at 10 min, 225 W with 4 g of TPA) is 0.02 % less than SN 13 (NCC at 10 min, 225 W with absent of TPA), SN 16 and SN13 posses PSD ranging from 37.84 to 68.06 nm and 50.75 to 91.26 nm respectively. Introduction of the cesium atom within Keggin structure has reduced the Bronsted acid sites of the catalyst, as a result the PSD in nano –scaled ranged decreased from 99.1 % to 18.0 % when the entire acidic proton being substituted with alkaline monovalent cation. Bronsted acid strength is very important in order to obtain good quality NCC in terms of size. The process has illustrated that the number of acid sites is more important rather than the acid strength in order to obtain the NCC by using solid acid catalysts.

All the quantitative clarification of NCC through zeta potential, surface tension, crystallinity index and particle size were further proven through their morphological examination. TEM of dilute colloidal suspension of NCC has shown the formation nano –scale cellulose in the range of less than 30 nm. Some images has also shown better illustration on the defibrillation process (Figure 4.46), where the loosen bond has allowed the formation of microfibrils. Introduction of TPA as a proton donor has caused the fibril fragmentation to occur efficiently thus giving smaller fibrils dimension. AFM image of NCC (Figure 4.53) has illustrated smaller diameter compared to NCC image (Figure 4.52) when mixture acidity was increased from 4 g to 6 g. This has proven that heteropoly acid is also a suitable option in producing NCC rather mineral acids.

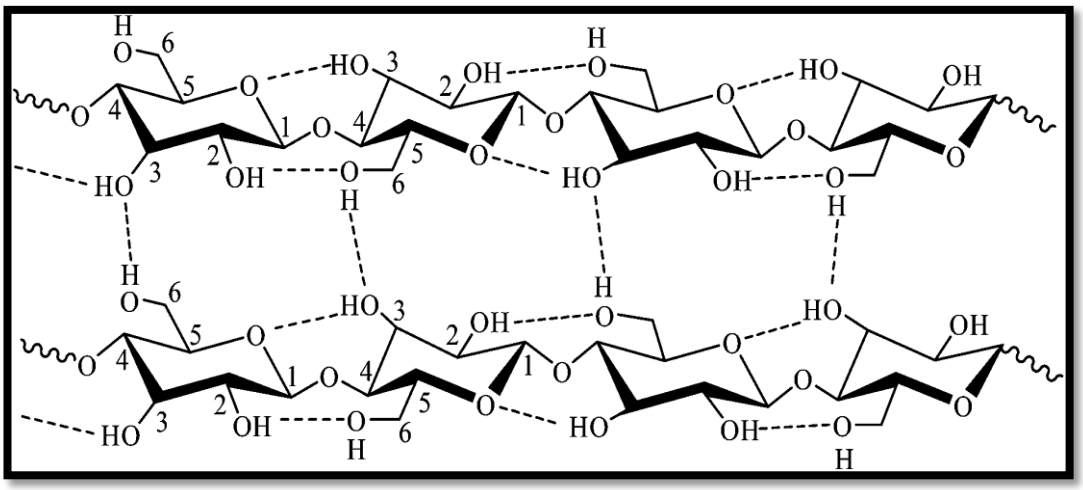

Figure 4.54: Inter-intramolecular hydrogen bonding network of cellulose.

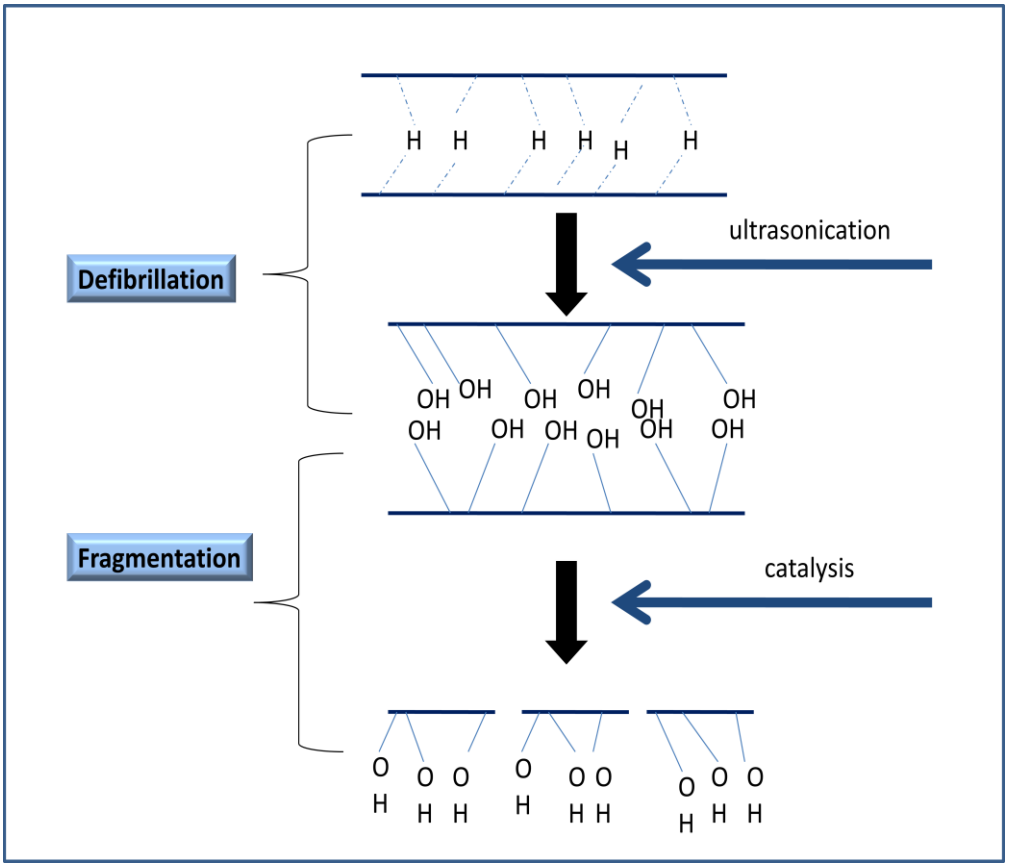

Figure 4.55: The reaction scheme for depolymerization of cellulose.

CONCLUSION AND RECOMMENDATION

5.1 Overall conclusion

This study was mainly focused in investigating the new method of producing Nanocrystalline cellulose (NCC) with the help of ultrasonication. Tungstophosphoric acid (TPA) which is the selected Heteropoly acid (HPA) was applied in replacing conventional mineral acids. Eventhough, TPA is the best candidate for catalyzing the hydrolysis process; the substitution process was also being accomplished by exchanging the proton with bigger cation such as cesium ion. This process was preceded so that the relationship between cesium content in Keggin structure of TPA with hydrolysis of cellulose can be studied. The process has extremely transformed smooth surface of TPA into highly porosity surface. Eventhough high porosity and high surface area are very crucial and important factor in some catalytic reaction, for depolymerization of cellulose, those elements are less pronounce. This is because; high cesium content has lead to the modification of Keggin structure which transforms TPA into higher hydrophobic character. As a result, less ionizable hydronium ions were produced in hydrolyzing cellulose bio-polymer.

The application of ultrasonication during the catalytic reaction helps to enhance the fiber defragmentation. The ultrasonication itself has contributed a lot in defibrillation and delamination of cellulose polymer chain through breaking of intra –molecular hydrogen bonding of cellulose polymer. Therefore, the introduction of TPA as catalyst and solvent has ease and facilitated the depolymerization process.

Effect of cesium content, effect of sonication power, duration time and amount of catalyst has been applied in order to study and understand the relationship between chemical treatments using a mechanical assisted.

The Infrared and Raman spectroscopy have discovered that, the intensity of β -linkages of cellulose fiber has weaken and reduced due to the depolymerization process. That was the first indication of increasing degree of crystallinity of NCC when certain effect was applied. The statement was further support with XRD quantitative analysis through CrI measurement. The highest CrI obtained was 88.0 % indicating that only 12 % of the amorphous domain remains in the cellulose crystallite. Eventhough, uncatalyzed process managed to get 88 .0 % of NCC crystallinity when 225 W and 15 minutes of ultrasonication procedure was introduced, the application of TPA catalyst on the other hand has suppressed the activation energy for that particular process. As a result, the chemical reaction has taken place at shorter time with similar value of CrI. Therefore, the introduction of TPA in catalyzing the process is one step closer towards green chemistry.

The evident was further confirmed through PSD where 10 % of the NCC particles posses size of 37.84 nm. While in the absence of TPA catalyst, only 7.4 % of NCC particles with size bigger than 50 nm were generated. Depolymerization of cellulose has broken down the larger aggregation of micro-sizes cellulose into nano-scale cellulose whisker. The diameter of NCC measured by TEM has revealed the size at average of 25 nm with high degree of agglomeration. Most of the NCC viewed under TEM and AFM shows agglomeration and accumulation of NCC at certain place due to stronger attraction between polar hydroxyl groups present on the NCC‘s surface. Therefore, from this research the best condition for producing NCC is at 225 W sonication power output for 10 min with the presence of 4 g of TPA.

5.2 Recommendations

The catalytic depolymerization of cellulose through ultrasonication process focused on verifying the effect of sonication power, sonication time, amount of catalyst and cesium content in TPA catalyst toward the production of NCC. This methodology has greatly contributed in identifying the ideal treatment condition for generating NCC with present and absence of catalyst. From the process, it has identified that TPA is an active catalyst in replacing conventional sulfuric acid.

Therefore, next phases of the research can be proceeded by using different type of Heteropoly acid (HPA) catalyst together with other solid acid catalyst for the production of NCC. Plus the research can also be widen by investigating the effect of temperature during the treatment and effect of solvent to fiber ratio in generating NCC.

On the basis, positive rules for producing cellulose nanocrystals (NCC) would be:

- Use smaller size cellulose especially MCC as raw material in obtaining NCC, since smaller size posses bigger surface area.
- Determination of NCC decomposition temperature using TGA helps us in understanding the highest temperature NCC can withstand.
- More sophisticated tools like Gel Permeation Chromatography (GPC) with suitable column and dissolving solvent could be useful in obtaining the molecular weight of NCC obtained in future research.

REFERENCES

Abdul Khalil, H.P.S., Bhat, A.H., & Ireana Yusra, A.F. (2012). Green composites from sustainable cellulose nanofibrils: A review. *Carbohydrate Polymers, 87*(2), 963-979. doi: 10.1016/j.carbpol.2011.08.078

Abdul Khalil, H.P.S., Davoudpour, Y., Islam, M.N., Mustapha, A., Sudesh, K., Dungani, R., & Jawaid, M. (2014). Production and modification of nanofibrillated cellulose using various mechanical processes: A review. *Carbohydrate Polymers, 99*(0), 649-665.

Abraham, E., Deepa, B., Pothan, L.A., Jacob, M., Thomas, S., Cvelbar, U., & Anandjiwala, R. (2011). Extraction of nanocellulose fibrils from lignocellulosic fibres: A novel approach. *Carbohydrate Polymers, 86*(4), 1468-1475.

Agarwal, U., Reiner, R., & Ralph, S. (2010). Cellulose i crystallinity determination using ft–raman spectroscopy: Univariate and multivariate methods. *Cellulose, 17*(4), 721-733. doi: 10.1007/s10570-010-9420-z

Agarwal, U.P., Reiner, R.S., Filpponen, I., Isogai, A., & Argyropoulos, D.S. (2010). *Crystallinities of nanocrystalline and nanofibrillated celluloses by ft-raman spectroscopy.* Paper presented at the TAPPI international conference on nanotechnology for the forest product industry, Helsniki.

Amirinejad, M., Madaeni, S.S., Rafiee, E., & Amirinejad, S. (2011). Cesium hydrogen salt of heteropolyacids/nafion nanocomposite membranes for proton exchange membrane fuel cells. *Journal of Membrane Science, 377*(1–2), 89-98.

Amirinejad, M., Madaeni, S.S., Rafiee, E., & Amirinejad, S. (2011). Cesium hydrogen salt of heteropolyacids/nafion nanocomposite membranes for proton exchange membrane fuel cells. *Journal of Membrane Science, 377*(1-2), 89-98. doi: 10.1016/j.memsci.2011.04.014

Angles, M.N., & Dufresne, A. (2000). Plasticized starch/tunicin whiskers nanocomposites. 1. Structural analysis. *Macromolecules, 33*(22), 8344-8353.

Astimar, A.A., Anis , M., Kamaruddin, H., Ridzuan, R., Rosnah, M.S., & Wan Hasamudin, W.H. (2011). Development in oil palm biomass utilization *Further advances in oil palm research, 2000-2010* (Vol. 2): Malaysian Palm Oil Board, Ministry of Plantation Industries and Commodities.

Azizi Samir, M.A.S., Alloin, F., & Dufresne, A. (2005). Review of recent research into cellulosic whiskers, their properties and their application in nanocomposite field. *Biomacromolecules, 6*(2), 612-626. doi: 10.1021/bm0493685

Bai, W., Holbery, J., & Li, K. (2009). A technique for production of nanocrystalline cellulose with a narrow size distribution. *Cellulose, 16*(3), 455-465. doi: 10.1007/s10570-009-9277-1

Bardin, B.B., Bordawekar, S.V., Neurock, M., & Davis, R.J. (1998). Acidity of keggin-type heteropolycompounds evaluated by catalytic probe reactions, sorption

microcalorimetry, and density functional quantum chemical calculations. *The Journal of Physical Chemistry B, 102*(52), 10817-10825. doi: 10.1021/jp982345y

Berglund, L. (2005). Cellulose-based nanocomposites: CRC Press: Boca Raton, FL.

Bond, G.C., Frodsham, S.J., Jubb, P., Kozhevnikova, E.F., & Kozhevnikov, I.V. (2012). Compensation effect in isopropanol dehydration over heteropoly acid catalysts at a gas–solid interface. *Journal of Catalysis, 293*, 158-164. doi: 10.1016/j.jcat.2012.06.021

Bruckman, K., Haber, J., Lalik, E., & Serwicka, E. (1988). Heteropolysalt-supported heteropolyacids as a new class of acid-base and redox catalysts. *Catalysis letters, 1*(1-3), 35-40.

Cao, X., Ding, B., Yu, J., & Al-Deyab, S.S. (2012). Cellulose nanowhiskers extracted from tempo-oxidized jute fibers. *Carbohydrate Polymers, 90*(2), 1075-1080.

Chorkendorff, I., & Niemantsverdriet, J.W. (2005). Introduction to catalysis *Concepts of modern catalysis and kinetics* (pp. 1-21): Wiley-VCH Verlag GmbH & Co. KGaA.

Ciolacu, D., Ciolacu, F., & Popa, V.I. (2011). Amorphous cellulose—structure and characterization. *Cellulose chemistry and technology, 45*(1), 13.

de Mesquita, J.o.P., Donnici, C.L., & Pereira, F.V. (2010). Biobased nanocomposites from layer-by-layer assembly of cellulose nanowhiskers with chitosan. *Biomacromolecules, 11*(2), 473-480. doi: 10.1021/bm9011985

Dias, A.S., Lima, S., Pillinger, M., & Valente, A.A. (2006). Acidic cesium salts of 12-tungstophosphoric acid as catalysts for the dehydration of xylose into furfural. *Carbohydrate Research, 341*(18), 2946-2953.

Dias, J.A., Caliman, E., & Loureiro Dias, S.C. (2004). Effects of cesium ion exchange on acidity of 12-tungstophosphoric acid. *Microporous and Mesoporous Materials, 76*(1–3), 221-232.

Dufresne, A., & Belgacem, M.N. (2013). Cellulose-reinforced composites: From micro- to nanoscale. *Polímeros, 23*(3), 277-286.

Eichhorn, S.J. (2011). Cellulose nanowhiskers: Promising materials for advanced applications. *Soft Matter, 7*(2), 303-315. doi: 10.1039/C0SM00142B

Essayem, N., Holmqvist, A., Gayraud, P.Y., Vedrine, J.C., & Ben Taarit, Y. (2001). In situ ftir studies of the protonic sites of h3pw12o40 and its acidic cesium salts mxh3−xpw12o40. *Journal of Catalysis, 197*(2), 273-280.

Fagerlund, G. (1973). Determination of specific surface by the bet method. *Matériaux et Construction, 6*(3), 239-245. doi: 10.1007/BF02479039

Fahma, F., Iwamoto, S., Hori, N., Iwata, T., & Takemura, A. (2010). Isolation, preparation, and characterization of nanofibers from oil palm empty-fruit-bunch (opefb). *Cellulose, 17*(5), 977-985.

Fan, M., Dai, D., & Huang, B. (2012). Fourier transform infrared spectroscopy for natural fibres. *Fourier Transform–Materials Analysis. intech.*

Fengel, & Dietrich, W. (2011). *Wood : Chemistry, ultrastructure, reactions*. Berlin, DEU: Walter de Gruyter.

Frone, A.N., Panaitescu, D.M., Donescu, D., Spataru, C.I., Radovici, C., Trusca, R., & Somoghi, R. (2011). Preparation and characterization of pva composites with cellulose nanofibers obtained by ultrasonication. *BioResources, 6*(1), 487-512.

Gamelas, J.A., Couto, F.A.S., Trovão, M.C.N., Cavaleiro, A.M.V., Cavaleiro, J.A.S., & de Jesus, J.D.P. (1999). Investigation of the thermal decomposition of some metal-substituted keggin tungstophosphates. *Thermochimica Acta, 326*(1–2), 165-173.

Gardner, D.J., Oporto, G.S., Mills, R., & Samir, M.A.S.A. (2008). Adhesion and surface issues in cellulose and nanocellulose. *Journal of Adhesion Science and Technology, 22*(5-6), 545-567. doi: 10.1163/156856108X295509

Ghaffar, S.H., & Fan, M. (2014). Lignin in straw and its applications as an adhesive. *International Journal of Adhesion and Adhesives, 48*(0), 92-101.

Habibi, Y., & Lucia, L.A. (2012). *Polysaccharide building blocks : A sustainable approach to the development of renewable biomaterials*. Hoboken, NJ, USA: Wiley.

Habibi, Y., Lucia, L.A., & Rojas, O.J. (2010). Cellulose nanocrystals: Chemistry, self-assembly, and applications. *Chemical Reviews, 110*(6), 3479-3500. doi: 10.1021/cr900339w

Habibi, Y., Mahrouz, M., & Vignon, M.R. (2009). Microfibrillated cellulose from the peel of prickly pear fruits. *Food Chemistry, 115*(2), 423-429.

Halib, N., & Amin, M.C.I.M. (2012). Physicochemical properties and characterization of nata de coco from local food industries as a source of cellulose. *Sains Malaysiana, 41*(2), 205-211.

Horinek, D. (2014). Dlvo theory. In G. Kreysa, K.-i. Ota & R. Savinell (Eds.), *Encyclopedia of applied electrochemistry* (pp. 343-346): Springer New York.

Huang, Y.-B., & Fu, Y. (2013). Hydrolysis of cellulose to glucose by solid acid catalysts. *Green Chemistry, 15*(5), 1095.

Ioelovich, M. (2012). Optimal conditions for isolation of nanocrystalline cellulose particles. *Nanoscience and Nanotechnology, 2*(2), 9-13.

Izumi, Y. (1997). Hydration/hydrolysis by solid acids. *Catalysis Today, 33*(4), 371-409.

Janardhnan, S., & Sain, M.M. (2011). Targeted disruption of hydroxyl chemistry and crystallinity in natural fibers for the isolation of cellulose nano-fibers via enzymatic treatment. *BioResources, 6*(2), 1242-1250.

Jiang, F., & Hsieh, Y.-L. (2013). Chemically and mechanically isolated nanocellulose and their self-assembled structures. *Carbohydrate Polymers, 95*(1), 32-40.

Johar, N., Ahmad, I., & Dufresne, A. (2012). Extraction, preparation and characterization of cellulose fibres and nanocrystals from rice husk. *Industrial Crops and Products, 37*(1), 93-99.

Joshi, M., Bhattacharyya, A., & Ali, S.W. (2008). Characterization techniques for nanotechnology applications in textiles. *Indian Journal of Fibre and Textile Research, 33*(3), 304-317.

Kavkler, K., & Demšar, A. (2012). Application of ftir and raman spectroscopy to qualitative analysis of structural changes in cellulosic fibres. *Tekstilec, 55*(1).

Klemm, D., Schmauder, H.-P., & Heinze, T. (2005). Cellulose *Biopolymers online*: Wiley-VCH Verlag GmbH & Co. KGaA.

Koyano, G., Ueno, K., & Misono, M. (1999). Three types of acid catalysis in liquid phase of metal salts of 12-tungstophosphoric acid, mn+xh3−nxpw12o40. *Applied Catalysis A: General, 181*(2), 267-275.

Kozhevnikov, I. (2002). *Catalysts for fine chemical synthesis, catalysis by polyoxometalates*: Wiley.

Kozhevnikov, I.V. (1995). Heteropoly acids and related compounds as catalysts for fine chemical synthesis. *Catalysis Reviews, 37*(2), 311-352. doi: 10.1080/01614949508007097

Kozhevnikov, I.V. (1998). Catalysis by heteropoly acids and multicomponent polyoxometalates in liquid-phase reactions. *Chemical Reviews, 98*(1), 171-198. doi: 10.1021/cr960400y

Kubicek, & Christian, P. (2012). *Fungi and lignocellulosic biomass*. Somerset, NJ, USA: Wiley.

Kumar, V., de la Luz Reus-Medina, M., & Yang, D. (2002). Preparation, characterization, and tabletting properties of a new cellulose-based pharmaceutical aid. *International journal of pharmaceutics, 235*(1), 129-140.

Lavoine, N., Desloges, I., Dufresne, A., & Bras, J. (2012). Microfibrillated cellulose - its barrier properties and applications in cellulosic materials: A review. *Carbohydr Polym, 90*(2), 735-764.

Li, J., Wei, X., Wang, Q., Chen, J., Chang, G., Kong, L., . . . Liu, Y. (2012). Homogeneous isolation of nanocellulose from sugarcane bagasse by high pressure homogenization. *Carbohydrate Polymers, 90*(4), 1609-1613.

Li, R., Fei, J., Cai, Y., Li, Y., Feng, J., & Yao, J. (2009). Cellulose whiskers extracted from mulberry: A novel biomass production. *Carbohydrate Polymers, 76*(1), 94-99.

Liu, Y., Wang, H., Yu, G., Yu, Q., Li, B., & Mu, X. (2014). A novel approach for the preparation of nanocrystalline cellulose by using phosphotungstic acid. *Carbohydrate Polymers, 110*(0), 415-422.

Lombardo, S.J., & Bell, A.T. (1991). A review of theoretical models of adsorption, diffusion, desorption, and reaction of gases on metal surfaces. *Surface Science Reports, 13*(1–2), 3-72.

Lu, P., & Hsieh, Y.-L. (2012). Preparation and characterization of cellulose nanocrystals from rice straw. *Carbohydrate Polymers, 87*(1), 564-573.

Mandal, A., & Chakrabarty, D. (2011). Isolation of nanocellulose from waste sugarcane bagasse (scb) and its characterization. *Carbohydrate Polymers, 86*(3), 1291-1299.

Mioč, U., Stojadinović, S., & Nedić, Z. (2009). Characterization of bronze surface layer formed by microarc oxidation process in 12-tungstophosphoric acid. *Materials, 3*(1), 110-126.

Misono, M. (2013). Chapter 4 - catalysis of heteropoly compounds (polyoxometalates). In M. Makoto (Ed.), *Studies in surface science and catalysis* (Vol. Volume 176, pp. 97-155): Elsevier.

Misono, M., & Nojiri, N. (1990). Recent progress in catalytic technology in japan. *Applied Catalysis, 64*(0), 1-30.

Mohamad Haafiz, M.K., Eichhorn, S.J., Hassan, A., & Jawaid, M. (2013). Isolation and characterization of microcrystalline cellulose from oil palm biomass residue. *Carbohydrate Polymers, 93*(2), 628-634.

Morais, J.P., Rosa Mde, F., de Souza Filho Mde, S., Nascimento, L.D., do Nascimento, D.M., & Cassales, A.R. (2013). Extraction and characterization of nanocellulose structures from raw cotton linter. *Carbohydr Polym, 91*(1), 229-235.

Morán, J., Alvarez, V., Cyras, V., & Vázquez, A. (2008). Extraction of cellulose and preparation of nanocellulose from sisal fibers. *Cellulose, 15*(1), 149-159.

Morin, P., Hamad, B., Sapaly, G., Carneiro Rocha, M.G., Pries de Oliveira, P.G., Gonzalez, W.A., . . . Essayem, N. (2007). Transesterification of rapeseed oil with ethanol: I. Catalysis with homogeneous keggin heteropolyacids. *Applied Catalysis A: General, 330*(0), 69-76.

Nada, A.-A.M., El-Kady, M.Y., El-Sayed, E.S.A., & Amine, F.M. (2009). Preparation and characterization of microcrystalline cellulose (mcc). *BioResources, 4*(4), 1359-1371.

Nakagaito, A., & Yano, H. (2004). The effect of morphological changes from pulp fiber towards nano-scale fibrillated cellulose on the mechanical properties of high-strength plant fiber based composites. *Applied Physics A, 78*(4), 547-552.

Park, S., Baker, J.O., Himmel, M.E., Parilla, P.A., & Johnson, D.K. (2010). Cellulose crystallinity index: Measurement techniques and their impact on interpreting cellulase performance. *Biotechnol Biofuels, 3*, 10.

Pizzio, L.R., & Blanco, M.N. (2003). Isoamyl acetate production catalyzed by $H_3PW_{12}O_{40}$ on their partially substituted cs or k salts. *Applied Catalysis A: General, 255*(2), 265-277.

Rafiee, E., Joshaghani, M., Tork, F., Fakhri, A., & Eavani, S. (2008). Esterification of mandelic acid catalyzed by heteropoly acid. *Journal of Molecular Catalysis A: Chemical, 283*(1–2), 1-4.

Rinaldi, R., & Schüth, F. (2009). Design of solid catalysts for the conversion of biomass. *Energy & Environmental Science, 2*(6), 610-626.

Sadeghifar, H., Filpponen, I., Clarke, S., Brougham, D., & Argyropoulos, D. (2011). Production of cellulose nanocrystals using hydrobromic acid and click reactions on their surface. *Journal of Materials Science, 46*(22), 7344-7355.

Sano, K.i., Uchida, H., & Wakabayashi, S. (1999). A new process for acetic acid production by direct oxidation of ethylene. *Catalysis Surveys from Asia, 3*(1), 55-60.

Santos, J.S., Dias, J.A., Dias, S.C.L., Garcia, F.A.C., Macedo, J.L., Sousa, F.S.G., & Almeida, L.S. (2011). Mixed salts of cesium and ammonium derivatives of 12-tungstophosphoric acid: Synthesis and structural characterization. *Applied Catalysis A: General, 394*(1–2), 138-148.

Sasca, V.Z., Verdes, O., Avram, L., Popa, A., Erdőhelyi, A., & Oszko, A. (2013). The $Cs_{3-x}H_xPW_{12}O_{40}$ catalysts microstructure model. *Applied Catalysis A: General, 451*(0), 50-57.

Scheller, H.V., & Ulvskov, P. (2010). Hemicelluloses. *Annual Review of Plant Biology, 61*(1), 263-289. doi: doi:10.1146/annurev-arplant-042809-112315

Schenzel, K., Fischer, S., & Brendler, E. (2005). New method for determining the degree of cellulose i crystallinity by means of ft raman spectroscopy. *Cellulose, 12*(3), 223-231.

Serwicka, E., Bruckman, K., Haber, J., Paukshtis, E., & Yurchenko, E. (1991). Acid—base properties of $H_{3+n}PV_nMo_{12}O_{40}$ heteropolyacids, pure and supported on $K_3PMo_{12}O_{40}$. *Applied catalysis, 73*(2), 153-163.

Sheltami, R.M., Abdullah, I., Ahmad, I., Dufresne, A., & Kargarzadeh, H. (2012). Extraction of cellulose nanocrystals from mengkuang leaves (pandanus tectorius). *Carbohydrate Polymers, 88*(2), 772-779.

Shiju, N.R., Williams, H.M., & Brown, D.R. (2009). Cs exchanged phosphotungstic acid as an efficient catalyst for liquid-phase beckmann rearrangement of oximes. *Applied Catalysis B: Environmental, 90*(3–4), 451-457.

Shobeiri, Z., Pourayoubi, M., Heydari, A., Percino, T.M., & Ramírez, M.A.L. (2011). Ultrasound assisted synthesis of cs2.5h0.5pw12o40: An efficient nano-catalyst for preparation of β-amino ketones via aza-michael addition reactions. *Comptes Rendus Chimie, 14*(6), 597-603.

Silvério, H.A., Flauzino Neto, W.P., Dantas, N.O., & Pasquini, D. (2013). Extraction and characterization of cellulose nanocrystals from corncob for application as reinforcing agent in nanocomposites. *Industrial Crops and Products, 44*, 427-436.

Siró, I., & Plackett, D. (2010). Microfibrillated cellulose and new nanocomposite materials: A review. *Cellulose, 17*(3), 459-494.

Spence, K.L., Venditti, R.A., Habibi, Y., Rojas, O.J., & Pawlak, J.J. (2010). The effect of chemical composition on microfibrillar cellulose films from wood pulps: Mechanical processing and physical properties. *Bioresour Technol, 101*(15), 5961-5968.

Srilatha, K., Sree, R., Prabhavathi Devi, B.L.A., Sai Prasad, P.S., Prasad, R.B.N., & Lingaiah, N. (2012). Preparation of biodiesel from rice bran fatty acids catalyzed by heterogeneous cesium-exchanged 12-tungstophosphoric acids. *Bioresource Technology, 116*(0), 53-57.

Szymańska-Chargot, M., Cybulska, J., & Zdunek, A. (2011). Sensing the structural differences in cellulose from apple and bacterial cell wall materials by raman and ft-ir spectroscopy. *Sensors, 11*(6), 5543-5560.

Texter, J. (2011). *Reactions and synthesis in surfactant systems*: CRC Press.

Tian, J., Fang, C., Cheng, M., & Wang, X. (2011). Hydrolysis of cellulose over csxh3–xpw12o40 (x = 1–3) heteropoly acid catalysts. *Chemical Engineering & Technology, 34*(3), 482-486.

Tian, J., Wang, J., Zhao, S., Jiang, C., Zhang, X., & Wang, X. (2010). Hydrolysis of cellulose by the heteropoly acid h3pw12o40. *Cellulose, 17*(3), 587-594.

Timofeeva, M.N. (2003). Acid catalysis by heteropoly acids. *Applied Catalysis A: General, 256*(1–2), 19-35.

Tischer, P.C.S.F., Sierakowski, M.R., Westfahl, H., & Tischer, C.A. (2010). Nanostructural reorganization of bacterial cellulose by ultrasonic treatment. *Biomacromolecules, 11*(5), 1217-1224.

Tsukuda, E., Sato, S., Takahashi, R., & Sodesawa, T. (2007). Production of acrolein from glycerol over silica-supported heteropoly acids. *Catalysis Communications, 8*(9), 1349-1353.

Uma Maheswari, C., Obi Reddy, K., Muzenda, E., Guduri, B.R., & Varada Rajulu, A. (2012). Extraction and characterization of cellulose microfibrils from agricultural residue – cocos nucifera l. *Biomass and Bioenergy, 46*, 555-563.

Weissermel, K., & Arpe, H.-J. (2008). *Industrial organic chemistry*: John Wiley & Sons.

Wertz, J.L., Bédué, O., & Mercier, J.P. (2010). *Cellulose science and technology*: EFPL Press.

Wiley, J.H., & Atalla, R.H. (1987). Band assignments in the raman spectra of celluloses. *Carbohydrate Research, 160*, 113-129.

Xian-e, C., Daichun, D., Jianping, N., Youming, J., Jing, Z., & Yixiang, Q. (1997). Enthalpies of formation and dsc and tg results of heteropoly acids containing tungsten and molybdenum. *Thermochimica Acta, 292*(1–2), 45-50.

Xiong, R., Zhang, X., Tian, D., Zhou, Z., & Lu, C. (2012). Comparing microcrystalline with spherical nanocrystalline cellulose from waste cotton fabrics. *Cellulose, 19*(4), 1189-1198.

Zaini, L.H., Jonoobi, M., Tahir, P.M., & Karimi, S. (2013). Isolation and characterization of cellulose whiskers from kenaf (hibiscus cannabinus l.) bast fibers. *Journal of Biomaterials and Nanobiotechnology, 4*, 37.

Zhang, K., Feldner, A., & Fischer, S. (2011). Ft raman spectroscopic investigation of cellulose acetate. *Cellulose, 18*(4), 995-1003.

Zhou, Y., Fu, S., Zheng, L., & Zhan, H. (2012). Effect of nanocellulose isolation techniques on the formation of reinforced poly (vinyl alcohol) nanocomposite films. *Express Polymer Letter, 6*(10), 794-804.